

Supporting Information for  
*Environ. Sci. Technol.*

## A Proteomics Approach to Trace Site-specific Damage in Extracellular Enzymes During Photoinactivation

Christine M. Egli<sup>1,2</sup> and Elisabeth M.L. Janssen<sup>2,\*</sup>

<sup>1</sup>Institute of Biogeochemistry and Pollutant Dynamics (IBP), ETH Zürich

<sup>2</sup>Eawag, Swiss Federal Institute of Aquatic Science and Technology

\*Corresponding author: [elisabeth.janssen@eawag.ch](mailto:elisabeth.janssen@eawag.ch)  
phone: +41 58 765 54 28, fax +41 58 765 58 02

[73](#) Pages, 16 Figures, 6 Tables

## Contents

<b>S1 Tryptophan-mediated Intramolecular Reaction Pathways</b>	<b>4</b>
<b>S2 Chemicals</b>	<b>6</b>
<b>S3 PNA-Pyr Actinometry</b>	<b>6</b>
<b>S4 Indirect Photoactivation</b>	<b>7</b>
<b>S5 Michaelis-Menten-Kinetics of Model Enzymes</b>	<b>7</b>
<b>S6 UPLC-based Activity Assays</b>	<b>8</b>
<b>S7 Log-linear and Shoulder-log-linear Decay Model</b>	<b>9</b>
<b>S8 Proteomics Workflows</b>	<b>10</b>
<b>S9 Peptide Analysis with LC-HRMS</b>	<b>10</b>
<b>S10 Peptide Tables and Colormaps</b>	<b>12</b>
<b>S11 Loss of Model Enzyme and Biofilm Activities</b>	<b>20</b>
<b>S12 Peptide Degradation and Inactivation</b>	<b>22</b>
<b>S13 Solvent Accessibility of Trp Residues and external antioxidant effect</b>	<b>23</b>
<b>S14 Change in Activity Compared to Loss of Trp-like Fluorescence</b>	<b>23</b>
<b>S15 Reactivity of Peptides Containing Photolabile Amino Acids</b>	<b>24</b>
<b>S16 Chromatograms with Mass Spectra</b>	<b>26</b>

## List of Figures

S1.1 Trp-mediated intramolecular reaction pathways . . . . .	4
S5.1 Michaelis-Menten-kinetics of model enzymes . . . . .	8
S10.1 Color maps of aminopeptidase viridis . . . . .	15
S10.2 Color maps of alkaline phosphatase . . . . .	16
S10.3 Color maps of alkaline phosphatase viridis . . . . .	17
S10.4 Color maps of $\alpha$ -glucosidase . . . . .	18
S10.5 Color maps of $\alpha$ -glucosidase viridis . . . . .	19
S11.1 Photoactivation in sunlight . . . . .	20
S11.2 Original data photoactivation model enzymes . . . . .	20
S12.1 Peptide degradation rate constants normalized to inactivation rates . . . . .	22
S13.1 Solvent accessibility of Trp residues and external antioxidant effect . . . . .	23
S14.1 Loss of inactivation and Trp-like fluorescence . . . . .	23
S15.1 Distance dependency of Tyr- and His-containing peptides . . . . .	24
S15.2 Relative reaction rate constants for all quantified peptides . . . . .	25
S16.1 View and information about the software Skyline . . . . .	26

## List of Tables

S4.1	Result table for indirect photoinactivation experiments with singlet oxygen . . . . .	7
S10.1	Information on aminopeptidase peptides . . . . .	12
S10.2	Information on phosphatase peptides . . . . .	13
S10.3	Information on glucosidase peptides . . . . .	14
S11.1	Photoinactivation rate constants for all model enzymes . . . . .	21
S15.1	Reaction rate constants for Cys-containing peptides . . . . .	25

## S1 Tryptophan-mediated Intramolecular Reaction Pathways

In the context of protein damage by exposure to light, we investigated five major processes that can be responsible for site-specific damage in this study. We briefly outline these reaction pathways below.

**A. Photoionization of Tryptophan.** Within amino acid-based molecules, tryptophan residues present the major chromophores and therefore targets of direct photochemical damage. In the following Trp refers to the neutral and  $\text{Trp}(-\text{H})^\bullet$  to the deprotonated indole amine in the residue. Upon absorbing light in the UVB range, Trp is excited and undergoes intersystem crossing to the excited triplet state,  ${}^3\text{Trp}^*$ . From the  ${}^3\text{Trp}^*$  the molecule can either relax back to ground state Trp or undergo further reactions. One of the possible oxidation reactions is photoionization, where a tryptophan radical cation intermediate,  $\text{Trp}^\bullet+$ , is formed that can further deprotonate ( $\text{pK}_a = 4.3$ )<sup>1</sup> to the neutral radical,  $\text{Trp}(-\text{H})^\bullet$  (see Figure S1.1 and 1A).<sup>2-6</sup> Overall, this process of direct photoionization leads to the photodecay of Trp-containing peptides. In the following paragraphs known secondary photochemical pathways initiated by tryptophan photooxidation, relevant to this study, are presented.

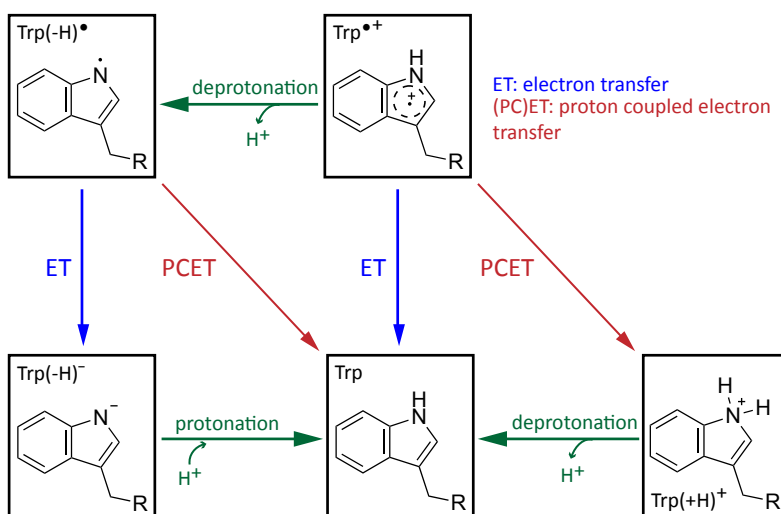


**Figure S1.1** In presence of an antioxidant the reduction of  $\text{Trp}^\bullet+$  to Trp, can occur directly via an electron transfer (ET) or via a proton coupled electron transfer, (PC)ET, followed by an additional deprotonation step via a non-radical intermediate,  $\text{Trp}(+\text{H})^+$ . Additionally, the radical cation can undergo deprotonation and form a neutral radical,  $\text{Trp}(-\text{H})^\bullet$ , which converts back to Trp, either via (PC)ET or ET including an additional deprotonation step via  $\text{Trp}(-\text{H})^-$ .

**B. Decelerating Effect of Antioxidants and Tyrosine Oxidation.** Tryptophan radical intermediates,  $\text{Trp}^\bullet+$  and  $\text{Trp}(-\text{H})^\bullet$ , can be reduced to ground state tryptophan in the presence of suitable antioxidants. The radical cation,  $\text{Trp}^\bullet+$ , can be converted back to tryptophan by either direct electron transfer (ET) or proton coupled electron transfer (PCET) followed by a deprotonation step (see Figure 1B and S1.1), whereas the neutral radical,  $\text{Trp}(-\text{H})^\bullet$ , can undergo PCET or ET followed by a protonation step to form Trp. Phenolic moieties in natural organic matter such as hydroxylated coumaric acids and coumarins can participate in such

redox reactions.<sup>6</sup> Consequently, the presence of antioxidants in the bulk solution can decelerate the oxidation of the initial target tryptophan.

In proteins, tyrosine (Tyr) can function as an intramolecular antioxidant. Intramolecular (PC)ET reactions have been observed in proteins with inter-residue distances between tryptophan and tyrosine of less than 5.6 Å.<sup>7–9</sup> When tyrosine reduces Trp<sup>•+</sup> back to ground state Trp before further oxidation, the tryptophan residue is expected to decay slower compared to a tryptophan that does not have a tyrosine in close proximity. At the same time, the tyrosine residue that participates in the redox reaction shows an increased decay.

**C. Singlet Oxygen Formation.** The formation of proteinogenic <sup>3</sup>Trp<sup>\*</sup> can cause subsequent damage when it reacts directly with photolabile amino acids<sup>10</sup> or when it forms excited state singlet oxygen, <sup>1</sup>O<sub>2</sub>(see Figure 1C).<sup>11,12</sup> Major targets for reactions with <sup>1</sup>O<sub>2</sub> within the protein are tyrosine, tryptophan, cysteine, histidine, and methionine residues.<sup>10,13–16</sup> Although <sup>1</sup>O<sub>2</sub> is only formed from <sup>3</sup>Trp<sup>\*</sup> with a low quantum yield ( $\Phi_{1O_2} = 0.065$ )<sup>4</sup> it may mediate reactions that could enhance the degradation of these photolabile residues, especially in proteins with a high abundance of tryptophan.

**D. Disulfide Reduction.** An additional intramolecular pathway is presented by <sup>3</sup>Trp<sup>\*</sup> mediated disulfide (cystine) reduction (see Figure 1D). The photochemically excited <sup>3</sup>Trp<sup>\*</sup> can transfer an electron to a neighboring disulfide forming a Trp<sup>•+</sup> and reducing the disulfide to a thiolate, RS<sup>−</sup>, and thiyl radical, RS<sup>•</sup>.<sup>17–21</sup> Trp-mediated disulfide reduction has been demonstrated for several proteins including *Fusarium solani pisi* cutinase, goat and human α-lactalbumin and bovine somatotropin.<sup>22–25</sup> Authors found evidence for Trp-mediated disulfide reduction at inter-residue distances up to 8 Å.<sup>24,26</sup> The dissociation of a disulfide bond can change the conformational integrity of the protein and likely affects the enzymatic function. Overall, the reduction of disulfides by <sup>3</sup>Trp<sup>\*</sup> is expected to increase the decay of the involved Trp residue because the reaction competes with relaxation to ground state tryptophan. At the same time, the reduction of disulfides will result in faster decay of the involved cysteine-containing residues in the protein.

**E. Methionine Oxidation.** Previous studies observed methionine oxidation by charge transfer from triplet states such as of aromatic ketones and triplet state natural organic matter.<sup>10,11</sup> Oxidation of methionine (Met) by <sup>3</sup>Trp<sup>\*</sup> results in an unstable methionine radical cation intermediate, Met<sup>•+</sup>, and a tryptophan radical anion, Trp<sup>•−</sup> (see Figure 1E).<sup>15</sup> As a consequence, both residues would experience enhanced decay kinetics when the inter-residue distance allows such charge transfer.

## S2 Chemicals

*Escherichia coli* alkaline phosphatase (ECAP, PDB 1ED9, Sigma, 62.77 units mg<sup>-1</sup> protein, 3.25 mg mL<sup>-1</sup> in glycine buffer), *Aeromonas proteolytica* aminopeptidase (BLAP, PDB 1RTQ, Sigma, 116.51 units mg<sup>-1</sup>), *Bacillus stearothermophilus*  $\alpha$ -glucosidase (GLU, PDB 1MQP, Sigma, 117 units mg<sup>-1</sup> protein). From Sigma: 4-methylumbelliferyl phosphate, 4-methyl-umbelliferone, 7-hydroxy-4-methylcoumarin, 7-leucine-7-amido-4-methylcoumarin hydrochloride, 7-amino-4-methylcoumarin, p-nitrophenyl  $\alpha$ -D-glucopyranoside, p-nitrophenyl  $\beta$ -D-glucopyranoside, p-nitrophenol, acetic acid ( $\geq$ 99.99%), Rose Bengal, ethylenediaminetetraacetic acid disodium salt dihydrate (EDTA, BioUltra,  $\geq$ 99.5-101.5%), iodoacetamide (IAM,  $\geq$ 99%), DL-dithiothreitol (DTT,  $\geq$ 99%), ammonium bicarbonate (BioUltra,  $\geq$ 99.5%), tris(hydroxymethyl)aminomethane (Tris, ACS reagent,  $\geq$ 99.8%), potassium phosphate dibasic trihydrate (for molecular biology,  $\geq$ 99%), potassium phosphate monobasic (for molecular biology,  $\geq$ 98%), and 6,7-dihydroxy-coumarin (esculetin,  $\geq$ 98%). And acetonitrile (acros organics, HPLC grade), methanol (Fisher Scientific, OPTIMA LC/MS Grade), furfuryl alcohol (FFA, Merck, 98%), ProteaseMAX<sup>TM</sup> (Promega, lyophilized, V207A), sequencing grade modified trypsin (Promega, lyophilized, V511A), sequencing grade chymotrypsin (Promega, lyophilized, V106A), iRT peptides (iRT Kit, Biognosys). Suwannee River Fulvic Acid (SRFA, 2S101F), Nordic Lake Natural Organic Matter (1R108N) and Waskish Peat Organic Matter (1R107H) were purchased from the International Humic Substance Society (IHSS, St. Paul, MN) and Aldrich Humic Acid from Sigma-Aldrich.

## S3 PNA-Pyr Actinometry

In the UVB photoexperiments the photon fluence rate in the range of 300–400 nm was determined by p-nitroanisole (PNA)- pyridine (pyr) actinometry where p-nitroanisole has a known absorption and quantum yield.<sup>27,28</sup> The fluence rate was calculated at follows:

$$E_{p,250-400nm}^0 = \frac{k_{obs,PNA}}{2.303 \cdot \phi_{PNA/pyr} \cdot \sum_{\lambda=250nm}^{400nm} (f_{p,\lambda} \cdot \epsilon_{PNA,\lambda})} \quad (\text{S3.1})$$

where  $E_{p,250-400nm}^0$  [E m<sup>-2</sup>s<sup>-1</sup>] is the photon fluence rate between 250–400 nm,  $k_{p,PNA}$  [s<sup>-1</sup>], the observed reaction rate constant of PNA degradation,  $\phi_{PNA/pyr}$ , the quantum yield of PNA degradation with pyr ( $\phi_{PNA/pyr} = 0.29 \cdot [\text{pyr}] + 0.00029$ )<sup>28</sup>,  $f_{p,\lambda}$  the fraction of the relative light spectrum for each wavelength and  $\epsilon_{PNA}$  [m<sup>2</sup> mol<sup>-1</sup>] the molar absorption coefficient of PNA.

Photon fluence rate of 6 UVB bulbs was determined using 0.5 mM pyr and 8  $\mu$ M PNA ( $\phi_{PNA/pyr} = 0.00044$ ). The observed reaction rate constant was  $k_{p,PNA} = 1.26 \pm 0.01 \cdot 10^{-4}$  s<sup>-1</sup> and the respective fluence rate between 250–400 nm,  $E_{250-400nm}^0 = 1.78 \cdot 10^{-4}$  E m<sup>-2</sup>s<sup>-1</sup> using Equation S3.1. Here, we were especially interested in the irradiation in the UV range where Trp absorbs. Therefore, we calculated  $E_{270-320nm}^0 = 1.26 \cdot 10^{-4}$  E m<sup>-2</sup>s<sup>-1</sup> which refers to a 9.5-fold higher irradiance in the UV range compared to natural sunlight.

## S4 Indirect Photoinactivation

Steady-state  ${}^1\text{O}_2$  concentration was obtained using furfuryl alcohol (FFA) as a probe molecule. Indirect photochemical experiments were conducted with enzyme solutions containing FFA ( $40 \mu\text{M}$ ) and Rose Bengal ( $3 \mu\text{M}$ ) as  ${}^1\text{O}_2$  sensitizer using a Xenon lamp with 455 nm cut-off filter as the light source. Furfuryl alcohol was quantified with UPLC using the absorbance detector at 219 nm. The flow rate was  $1.00 \text{ mL min}^{-1}$  and the eluent composition 75% acetate buffer (pH 5.9,  $15.6 \text{ mM}$ ) and 25% acetonitrile. FFA followed a pseudo-first-order kinetics and steady state  ${}^1\text{O}_2$  concentrations,  $[{}^1\text{O}_2]_{\text{ss}}$ , were calculated using Equation S4.1 and the bimolecular reaction rate constant for FFA with  ${}^1\text{O}_2$  ( $k_{\text{rxn}}^{\text{FFA}} = 1.00 \cdot 10^8 \text{ M}^{-1}\text{s}^{-1}$ ).<sup>29</sup> Bimolecular reaction rates for enzyme inactivation,  $k_{\text{rxn}}^{\text{activity}}$ , were then calculated by dividing the observed inactivation rate,  $k_{\text{obs}}^{\text{activity}}$ , by  $[{}^1\text{O}_2]_{\text{ss}}$ . Table S11.1 shows the obtained and calculated results for indirect photoinactivation of the model enzymes.

$$[{}^1\text{O}_2]_{\text{ss}} = \frac{k_{\text{obs}}^{\text{FFA}}}{k_{\text{rxn}}^{\text{FFA}}} \quad (\text{S4.1})$$

**Table S4.1** Observed decay rate constants of FFA,  $k_{\text{obs}}^{\text{FFA}}$ , steady state singlet oxygen concentration,  $[{}^1\text{O}_2]_{\text{ss}}$ , and biomolecular reaction rate constant of enzyme inactivation,  $k_{\text{rxn}}^{\text{activity}}$ , for the model enzymes ECAP, BLAP and GLU.

enzyme	$k_{\text{obs}}^{\text{FFA}}$ [ $10^{-3} \text{ s}^{-1}$ ]	$[{}^1\text{O}_2]_{\text{ss}}$ [ $10^{-11} \text{ M}$ ]	$k_{\text{rxn}}^{\text{activity}}$ [ $10^7 \text{ M}^{-1}\text{s}^{-1}$ ]
ECAP	$0.37 \pm 0.04$	0.37	$3.10 \pm 0.01$
BLAP	$3.07 \pm 0.55$	3.07	$2.39 \pm 0.46$
GLU	$1.25 \pm 0.01$	1.25	$11.21 \pm 0.05$

## S5 Michaelis-Menten-Kinetics of Model Enzymes

For activity measurements we first determined required substrate concentrations to achieve maximum hydrolysis rates,  $V_{\text{max}}$ , using Michaelis-Menten-Kinetics. At maximum rates the reaction is not limited by substrate availability, assuming reversible formation of the enzyme-substrate complex and single kinetically significant step for product formation. We determined activities with substrate dilution series at constant enzyme concentration by bulk fluorescence measurements (see Figure S5.1). Maximum rates,  $V_{\text{max}}$ , and concentration at which half-maximal rate is obtained,  $K_m$ , were determined by least square method (using Excel 2011 Solver). The derived minimal substrate concentration equates to  $2 \cdot K_m$  or higher for ECAP and BLAP. For GLU 1

- $K_m$  was chosen because of high substrate requirements.

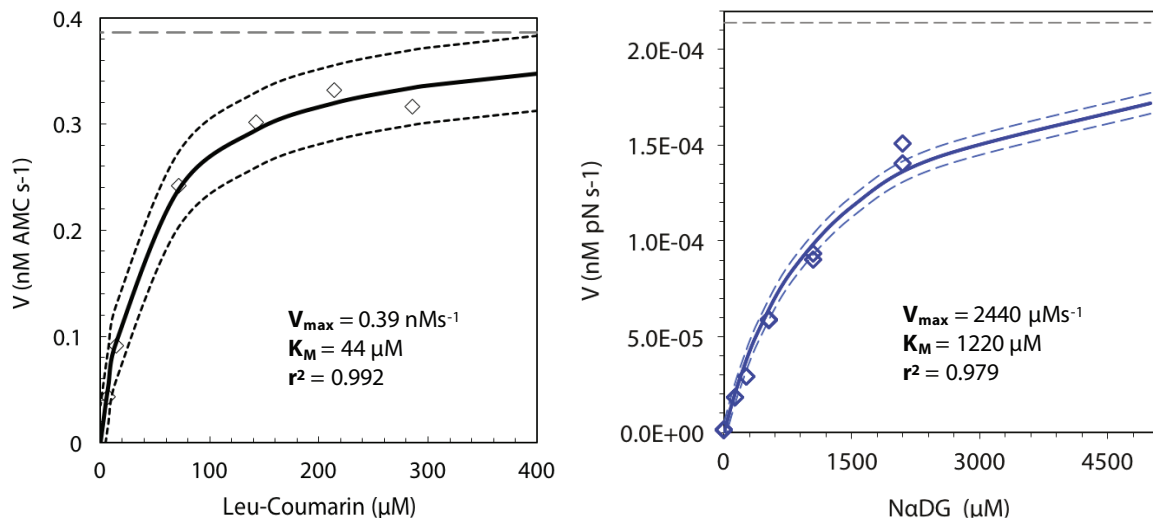


**Figure S5.1** Kinetic characterisation of aminopeptidase, BLAP, (left) and  $\alpha$ -glucosidase,  $\alpha$ -GLU, (right) with  $V_{max}$  (horizontal dashed line) and 95% confidence intervals (dashed lines). For BLAP L-leucine-7-amido-4-methyl coumarin (LeuC) and for GLU p-Nitrophenol  $\alpha$ -D-glucopyranoside ( $\text{NaDG}$ ) was used as a substrate. Results for phosphatase, ECAP, have been published previously.<sup>30</sup>

## S6 UPLC-based Activity Assays

The development of the activity assays included the determination of the Michaelis-Menten kinetics of each enzyme (see Text S5) and conducted at the substrate concentrations for maximum rates,  $V_{max}$ . We further ensured that the substrates and formed products were stable after the activity assay was stopped until the sample was analysed by UPLC with reference standards.

Phosphatase activity was quantified by hydrolysis of 4-methylumbellifluorone phosphate (MUP, 0.1 mM final concentration) to 4-methylumbellifluorone (MUOH). Therefore, 20  $\mu$ L MUP solution (0.5 mM in Tris buffer at pH 7.5) was added to 80  $\mu$ L sample and vortexed. The incubation was stopped sharply after 20 min with 20  $\mu$ L phosphate buffer (10 mM, pH 3.0) and vortexed. Within 30 min after stopping the incubation, MUOH was analyzed by UPLC using 50% phosphate buffer (10 mM, pH 7.5) and 50% methanol isocratically at a flow rate of 0.25 mL min<sup>-1</sup> and detected by fluorescence at an excitation/emission wavelength of 320/450 nm. Aminopeptidase activity was quantified by the hydrolysis of L-leucine-7-amido-4-methylcoumarin (LeuC, 0.114 mM final concentration) to 7-amino-4-methylcoumarin (AMC). Therefore, 20  $\mu$ L LeuC (0.8 mM in nanopure water) was added to 120  $\mu$ L sample and vortexed. The incubation was stopped sharply after 10 min by adding 20  $\mu$ L 0.1 M HCl and vortexed. Within 30 min AMC was analyzed by UPLC with 65% phosphate buffer (10 mM, pH 7.5) and 35% acetonitrile and its fluorescence detected at 320/450 nm. AMC formation from LeuC in biofilm was stopped with 50 mM 0.1 M HCl otherwise the same protocol as for synthetic aminopeptidase was applied (isocratic, 0.2 mL<sup>-1</sup>). Glucosidase activities were measured by the formation of p-Nitrophenol

(pNP) from p-Nitrophenol  $\alpha$ -D-glucopyranoside ( $\text{NaDG}$ , 2 mM final concentration) and  $\beta$ -D-glucopyranoside ( $\text{N}\beta\text{DG}$ , 2 mM final concentration, in biofilm only). Therefore, 10  $\mu\text{L}$  dithiothreitol (DTT, 10 mM, in nanopure water) and 20  $\mu\text{L}$   $\text{NaDG}$  (10 mM in nanopure water) or  $\text{N}\beta\text{DG}$  (10 mM in nanopure water) was added to 70  $\mu\text{L}$  sample and vortexed. Formation of pNP was stopped sharply after 15 min (and 60 min for biofilm samples) by adding 10  $\mu\text{L}$  HCl (0.5 M). Within 30 min pNP was analyzed by UPLC with 70% A (MQ, 10% ACN, 0.1% FA) and 30% B (ACN, 0.1% FA) and detected by absorbance at 320 nm (isocratic, 0.2  $\text{mLmin}^{-1}$ ).

The detected peak areas of the products were converted to concentrations by external calibration (see Figure S6.1). The activity,  $A$ , ( $\text{Ms}^{-1}$ ) was obtained by dividing the product concentration by the respective incubation time of enzyme and substrate. To determine inactivation in our time series experiments, each rate was normalized to the initial rate (at time zero,  $A/A_0$ ). As inactivation followed pseudo-first-order kinetics, a linear regression was performed from log-normalized rates,  $\ln(A/A_0)$  versus time, and the slope corresponded to the inactivation rate constant ( $\text{s}^{-1}$ ). Where suitable a shoulder-log-linear model was used to determine inactivation rate constants (see text S7).

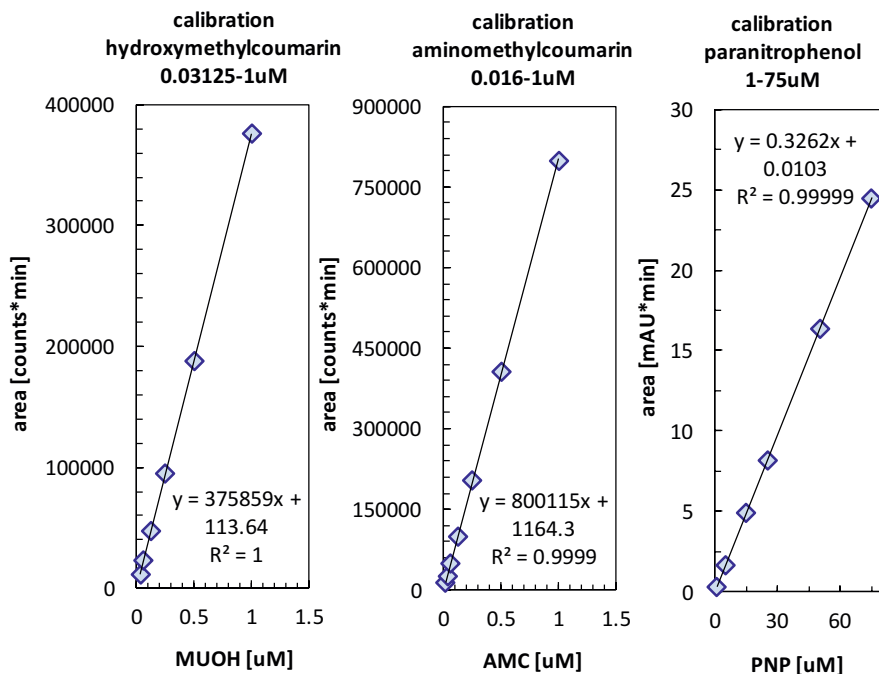


**Figure S6.1** Calibration series of all activity assay products (MUOH for ECAP, AMC for BLAP and PNP for GLU) measured by UPLC.

## S7 Log-linear and Shoulder-log-linear Decay Model

Inactivation rate constants were determined from linear regression of the log-normalized areas of the hydrolysis product peaks in the UPLC analysis over time. To fit inactivation data and determine inactivation rate constants of aminopeptidase the Geeraerd and Van Impe shoulder-log linear model was used.<sup>31,32</sup>

$$A(t) = A_0 e^{-kt} \cdot \left( \frac{e^{-kS}}{1 + (e^{kS} - 1)e^{-kt}} \right) \quad (\text{S7.1})$$

where A is the area of the quantified hydrolysis product, k the first-order inactivation rate constant, t the reaction time and S the lag time. If the enzyme does not show lag phase behaviour (S=0), Equation S7.1 simplifies to  $A(t) = A_0 e^{-kt}$ . This was the case for all inactivation experiments except the model BLAP (see Figure S11.2).

## S8 Proteomics Workflows

The sample preparation work flow for ECAP consisted of (1) metal chelation with 2.97  $\mu\text{L}$  500  $\mu\text{M}$  EDTA solution to 45  $\mu\text{L}$  irradiated sample (0.13  $\mu\text{g } \mu\text{L}^{-1}$  ECAP) prior to incubation for 40 min at RT, (2) reduction of the disulfide bridges by addition of 0.63  $\mu\text{L}$  100 mM DTT (in Ambic 50 mM, pH 8) and 60 min sonication at 60  $^{\circ}\text{C}$ , (3) alkylation of thiols with 3.69  $\mu\text{L}$  200 mM IAM during 60 min at 37  $^{\circ}\text{C}$ , and (4) addition of 2  $\mu\text{L}$  trypsin (0.1  $\mu\text{g } \mu\text{L}^{-1}$ , S/E of 25:1) to 42.2  $\mu\text{L}$  of the denatured sample prior to 10 min microwave-assisted digestion (standard program mode, 100 W, 50  $^{\circ}\text{C}$ ). After 15 min cooling of the digestion was stopped with 2.7  $\mu\text{L}$  glacial acetic acid.

Sample preparation work flow for BLAP was altered from the above described one for ECAP. Workflow consisted of (1) addition of 2.2  $\mu\text{L}$  EDTA to 60  $\mu\text{L}$  irradiated sample (0.13  $\mu\text{g } \mu\text{L}^{-1}$  BLAP) and incubation for 30 min, an additional denaturation step where the samples were heated up to 95  $^{\circ}\text{C}$  in a water bath during 10 min, (2) addition of 0.72  $\mu\text{L}$  200 mM DTT and sonication for 30 min at 85  $^{\circ}\text{C}$ , (3) addition of 2.01  $\mu\text{L}$  of 1% ProteaseMAX detergent and 4.21  $\mu\text{L}$  400 mM IAM before 60 min incubation at 37  $^{\circ}\text{C}$ , and (4) over night digestion with 1  $\mu\text{L}$  of chymotrypsin (0.25  $\mu\text{g } \mu\text{L}^{-1}$ , S/E of 25:1), which was stopped with 3.7  $\mu\text{L}$  glacial acetic acid.

Sample preparation of GLU samples consisted of (2) addition of 1.37  $\mu\text{L}$  DTT 50 mM to 50  $\mu\text{L}$  irradiated sample (0.12  $\mu\text{g } \mu\text{L}^{-1}$  GLU) and sonication during 60 min at 85  $^{\circ}\text{C}$ , (3) addition of 1.66  $\mu\text{L}$  1% ProteaseMAX with 15 min of sonication and addition of 4.04  $\mu\text{L}$  200 mM IAM with 60 min incubation at 37  $^{\circ}\text{C}$ , and (4) over night digestion with 2  $\mu\text{L}$  trypsin (0.1  $\mu\text{g } \mu\text{L}^{-1}$ , S/E of 25:1), which was again stopped with 3.0  $\mu\text{L}$  glacial acetic acid.

## S9 Peptide Analysis with LC-HRMS

Digested phosphatase (ECAP) samples (5  $\mu\text{L}$ ) were injected to a nUPLC (nanoAcuity Waters) equipped with a 5  $\mu\text{L}$  sample loop, a C18 trap column (Waters Nano Acuity UPLC, 2G-VMTrap, 5  $\mu\text{m}$ , 180  $\mu\text{m} \times 20 \text{ mm}$ ) and a C18 column (Nano Acuity UPLC, BEH130, 1.7  $\mu\text{m}$ , 300  $\mu\text{m} \times 150 \text{ mm}$ , Waters) at a flow rate of 5  $\mu\text{L}/\text{min}$ . Peptide separation was obtained with a gradient of A (95% MQ, 5% acetonitrile, 0.1% formic acid) and B (95% acetonitrile, 5% MQ, 0.1% formic acid). With the following gradient: 0 to 3.5 min, 5% B; 3.5-20 min, 5-10% B; 20-55 min, 10-30% B; 55-60 min, 30-70% B; 60-63 min, 70% B; 63-70 min, 70-5% B.

The nUPLC (nanoAcuity Waters) was coupled to an Orbitrap mass spectrometer (Exactive, Thermo Scientific, Bremen) and data was obtained with electron spray ionization (ESI) source, 3.8 kV spray voltage, 275°C capillary temperature, sheat gas of 10.00 and auxiliary gas of 5.00. Data was acquired in full scan mode (*m/z* range: 150–2'500, resolution: 50'000 (@400m/z), maximum injection time: 100 ms, balanced automatic gain control (AGC), profile mode).

Digested aminopeptidase (BLAP) and glucosidase (GLU) samples (5  $\mu$ L) were injected to a  $\mu$ UPLC (Ultimate 3000 RSLCnano, Dionex) with the same setting as the nUPLC. Peptide separation was obtained with the same eluents and with the following gradients: 0 to 53 min, 5-30% B; 53-62 min, 30-99% B; 62-66 min, 99% B; 66-70 min, 99-5% B; and 0 to 3 min, 1-13% B; 3-50 min, 13-34% B; 50-60 min, 34-99% B; 60-62 min, 99% B; 62-70 min, 99-1% B for BLAP and GLU, respectively.  $\mu$ UPLC was coupled to to a quadrupole-Orbitrap mass spectrometer (Q-Exactive-Plus, Thermo Scientific, Bremen). Q-Exactive-Plus was operated with an electron spray ionization (ESI) source at a spray voltage of 3 kV, capillary temperature of 275°C, sheat gas of 15.00 and auxiliary gas of 5.00. Data was acquired in full scan mode (*m/z* range: 150–2'000, resolution: 140'000 (@400m/z), maximum injection time: 200 ms, automatic gain control (AGC) target: 10<sup>6</sup>, profile mode).

## S10 Peptide Tables and Colormaps

**Table S10.1** Information on aminopeptidase (BLAP) peptides used for the colormap. Table contains sequence information, observed reaction rate constants ( $k_{obs}$ ) with standard deviation (stdev) and  $R^2$ , relative reaction rate constant ( $k_{rel}$ ), most intense charge state (M+nH) and according mass to charge ratio (m/z).

from <sup>a</sup>	to <sup>a</sup>	sequence	$k_{obs}$ [ $10^{-4}s^{-1}$ ]	stdev	$R^2$	$k_{rel}$	M+nH	m/z
1	32	MPPITQQATVTAWLPQVDASQ– ITGTTISSLESF	8.47	0.58	0.98	0.74	3	1139.9131
33	37	TNRFY	2.78	0.36	0.81	0.24	2	350.6743
38	56	TTTSGAQASDWIASEWQAL	11.37	0.41	0.98	1.00	2	1011.9738
57	73	SASLPNASVKQVSHSGY	4.61	0.38	0.91	0.41	3	577.9602
74	80	NQKSVVM	8.36	1.02	0.92	0.73	2	403.2155
81	91	TITGSEAPDEW	6.73	0.64	0.89	0.59	2	603.2697
92	132	IVIGGHLDSTIGSHTNEQSVAPG– ADDDASGIAAVTEVIRVL	5.24	1.27	0.74	0.46	3	1362.3644
133	145	SENNFQPKRSIAF	2.12	0.43	0.64	0.19	3	513.2634
146	165	MAYAAEEVGLRGSQDLANQY	8.60	0.41	0.97	0.76	3	729.3443
166	183	KSEGKNVVSALQLDMTNY	11.11	0.86	0.92	0.98	3	666.3385
184	205	KGSAQDVVFITDYTDNSNFTQYL	4.23	0.47	0.85	0.37	3	838.0675
206	208	TQL	0.72	0.25	0.62	0.06	1	361.2082
210	218	DEYLPSLTY	2.95	0.32	0.86	0.26	2	550.7610
234	244	HNAGYPAAMPF	7.36	0.62	0.91	0.65	2	588.2688
245	262	ESKFNDYNPRIHTTQDTL	4.17	0.44	0.88	0.37	3	727.0187
263	275	ANSDPTGSHAKKF	5.33	0.71	0.82	0.47	3	453.8932
276	299	TQLGLAYAIEMGSATGDTPTPGNQ	5.50	0.63	0.86	0.48	3	798.3812

<sup>a</sup> number of the amino acid in the sequence

**Table S10.2** Information on phosphatase (ECAP) peptides used for the colormap. Table contains sequence information, observed reaction rate constants ( $k_{obs}$ ) with standard deviation (stdev) and  $R^2$ , relative reaction rate constant ( $k_{rel}$ ), most intense charge state (M+nH) and according mass to charge ratio (m/z).

from <sup>a</sup>	to <sup>a</sup>	sequence <sup>b</sup>	$k_{obs}$ [ $10^{-4}\text{s}^{-1}$ ]	stdev	$R^2$	$k_{rel}$	M+nH	m/z
1	10	TPEMPVLENR	n.d.	n.d.	n.d.	n.d.	2	593.3003
11	23	AAQGDITAPGGAR	1.49	0.14	0.85	0.05	2	592.8046
25	34	LTGDQTAALR	0.93	0.15	0.76	0.03	2	523.2855
35	43	DSLSDKPAK	n.d.	n.d.	n.d.	n.d.	2	480.7535
44	62	NIILLIGDGMGMDSEITAAR	9.62	0.81	0.88	0.35	2	980.0144
63	73	NYAEGAGGFFK	3.22	0.24	0.94	0.12	2	580.7722
74	91	GIDALPLTGQYTHYALNK	6.40	0.35	0.97	0.23	3	659.0143
93	114	TGKPDYVTDSAASATAWSTGVK	18.65	1.11	0.94	0.68	3	738.3622
115	127	TYNGALGVDIHEK	4.30	0.09	0.99	0.16	3	472.9088
128	137	DHPTILEMAK	14.92	1.21	0.93	0.54	2	577.7973
138	166	AAGLATGNVSTAELQDATPAAL-	3.82	0.3	0.89	0.14	3	931.4894
		VAHVTSR						
168	177	C[+57]YGPSATSEK	n.d.	n.d.	n.d.	n.d.	2	550.2399
178	185	C[+57]PGNALEK	n.d.	n.d.	n.d.	n.d.	2	444.7158
186	199	GGKGSITEQLLNAR	1.80	0.2	0.87	0.07	3	481.9353
189	199	GSITEQLLNAR	1.65	0.12	0.91	0.06	2	601.3304
200	209	ADVTLGGGAK	1.07	0.09	0.92	0.04	2	444.7429
210	223	TFAETATAGEWQGK	17.84	1.08	0.94	0.65	2	748.8544
224	232	TLREQAQAR	3.30	0.34	0.89	0.12	2	536.7965
233	267	GYQLVSDAASLNSVTEANQQKP-	10.14	0.5	0.97	0.37	4	926.7242
		LLGLFADGNMPVR						
268	272	WLGPK	27.57	1.93	0.95	1.00	2	300.6788
273	292	ATYHGNIDKPAVTC[+57]TPNPQR	12.02	1.6	0.82	0.44	3	747.3674
293	305	NDSVPTLAQMIDK	7.71	0.68	0.91	0.28	2	710.3428
306	315	AIELLSKNEK	1.79	0.21	0.86	0.06	3	382.2239
316	328	GFFLQVEGASIDK	1.41	0.21	0.79	0.05	2	705.8668
329	351	QDHAAANPC[+57]GQIGETVDLDE-	7.53	1.49	0.74	0.27	3	841.7225
		AVQR						
352	357	ALEFAK	0.77	0.06	0.93	0.03	2	339.6947
359	382	EGNTLVIVTADHAHASQIVAPDTK	4.43	0.17	0.97	0.16	3	829.7661
383	393	APGLTQALNTK	1.85	0.3	0.76	0.07	2	557.3168
394	418	DGAVMVMSYGNSEEDSQEHTGS-	10.25	0.51	0.95	0.37	3	909.7256
		QLR						
419	443	IAAYGPHAANVVGLTDQTDLFY-	14.33	0.71	0.96	0.52	3	899.4511
		TMK						
444	449	AALGLK	2.10	0.18	0.92	0.08	2	286.6919

<sup>a</sup> number of the amino acid in the sequence

<sup>b</sup> [+57] refers to an iodacetamide capping of the cysteine (C)

**Table S10.3** Information on glucosidase (GLU) peptides used for the colormap. Table contains sequence information, observed reaction rate constants ( $k_{obs}$ ) with standard deviation (stdev) and  $R^2$ , relative reaction rate constant ( $k_{rel}$ ), most intense charge state (M+nH) and according mass to charge ratio (m/z).

from <sup>a</sup>	to <sup>a</sup>	Sequence <sup>b</sup>	$k_{obs}$ [ $10^{-4}s^{-1}$ ]	stdev	$R^2$	$k_{rel}$	M+nH	m/z
1	15	MTAGYEPC[+57]WLRAYERK	6.69	0.94	0.93	0.41	2	980.4638
16	30	DQYSRLRFEEIVAKR	1.77	0.71	0.61	0.11	3	637.3463
23	30	FEEIVAKR	3.78	0.71	0.88	0.23	1	991.5571
30	44	RTSPIFQAVVEELQK	4.73	0.92	0.87	0.29	3	582.3246
45	47	GLR	4.06	1.21	0.74	0.25	1	345.2245
80	94	PLEGTLVHPEGYVIR	5.84	0.65	0.95	0.35	3	560.6420
95	103	SDVDDGPFR	2.82	0.83	0.74	0.17	2	504.2251
104	109	IYIIGK	n.d.	n.d.	n.d.	n.d.	1	353.7285
110	123	TDAGVLYGVFHFLR	n.d.	n.d.	n.d.	n.d.	2	797.9225
146	159	MINHWDNMDSIER	14.65	2.82	0.87	0.89	3	573.2522
160	164	GYAGR	1.8	0.54	0.74	0.11	1	523.2623
165	175	SIFFVDDQFVK	3.95	0.48	0.94	0.24	3	448.8993
176	179	QNQR	1.99	0.79	0.62	0.12	1	545.2790
180	185	IKDYAR	1.35	0.45	0.69	0.08	1	765.4254
205	231	TETKLITDHFLPDVAEVADIFRTY-	4.15	1.09	0.78	0.25	2	1546.8188
		GIK						
268	295	IYQYIPDFGGFVVKADSEFRPGP-	6.59	2.62	0.61	0.4	4	807.4054
		FTYGR						
282	295	ADSEFRPGPFTYGR	3.46	0.64	0.88	0.21	2	800.3812
319	329	C[+57]FVYNC[+57]QQDWR	2.46	0.40	0.90	0.15	2	788.3270
330	337	DRTTDRAK	3.53	0.66	0.88	0.21	2	481.7543
338	344	AAYDHFK	5.16	1.05	0.86	0.31	2	426.2060
345	351	PLDGQFR	2.26	0.29	0.94	0.14	1	832.4312
352	359	ENVILQIK	n.d.	n.d.	n.d.	n.d.	3	319.5307
381	408	TNQMMEVQITQEYTGQQKHLCF-	10.6	1.99	0.88	0.64	3	1160.5685
		LIPQWK						
399	408	HLC[+57]FLIPQWK	n.d.	n.d.	n.d.	n.d.	3	447.9094
419	436	GKGSEVKKVIDGSLFDYR	3.9	0.65	0.9	0.24	3	666.6933
437	467	YSGIAGVSNIGSDPNWTGHTLAQ-	6.31	2.58	0.6	0.38	2	1612.2814
		ANLYGFGR						
549	555	DPNWTGH	n.d.	n.d.	n.d.	n.d.	3	276.1208
556	597	TVATGTGYTAQYFPENAAMYES-	11.88	1.94	0.93	0.72	3	1621.7547
		LDTG[+57]PDELLLFFFHHVPYTHR						
598	620	LHSGETVIQHIYNTHFEGVEQAK	n.d.	n.d.	n.d.	n.d.	1	2637.3056
621	625	QLR	n.d.	n.d.	n.d.	n.d.	3	139.4254
624	632	KRWEQLKGK	4.7	1.63	0.63	0.28	2	586.8486
633	637	IDEKR	1.21	0.36	0.74	0.07	3	220.7940
638	653	YHDVLERLTIQVEHAK	4.5	0.97	0.84	0.27	3	651.0180
654	666	EWRDVINTYFYRK	3.54	0.42	0.95	0.21	2	895.4547
666	675	KSGIDDQYGR	9.07	1.23	0.93	0.55	2	569.7780
667	675	SGIDDQYGRK	9.08	1.22	0.93	0.55	2	569.7780
677	679	IYR	16.51	1.95	0.97	1	2	226.1368

<sup>a</sup> number of the amino acid in the sequence

<sup>b</sup> [+57] refers to an iodacetamide capping of the cysteine (C)

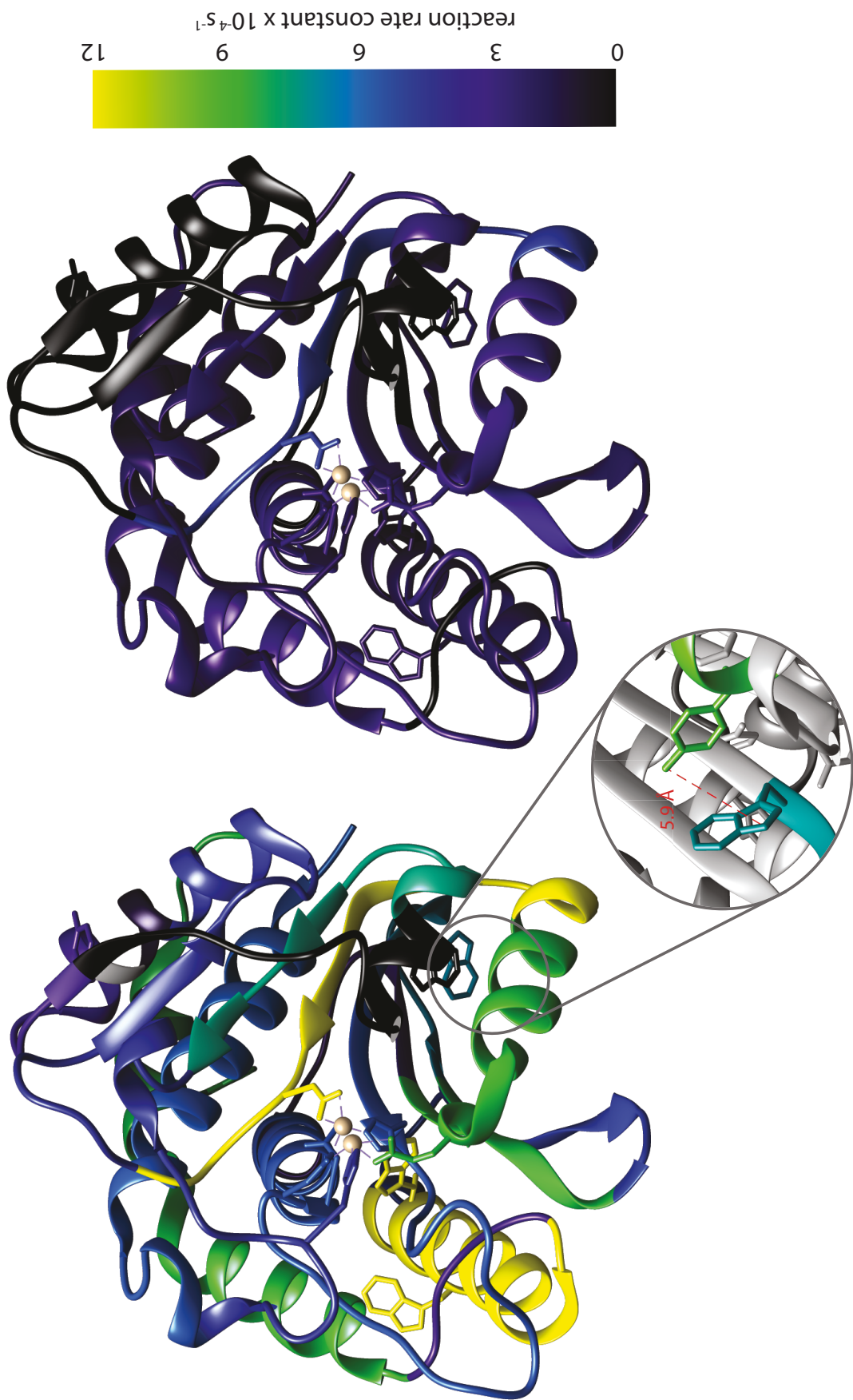


**Figure S10.1** Color maps in viridis color scale illustrating reaction rate constants for *Aeromonas proteolytica* leucine aminopeptidase (BLAP, EC 3.4.11.10, PDB 1RTQ) obtained upon UVB irradiation in absence (left) and presence (right) of 6,7-dihydroxycoumarin. The zoom-in exemplifies the determination of inter-residue distance between the amine nitrogen of Trp91 and the phenol oxygen of Tyr165. This is Figure 3 from the main text in a different color scale.

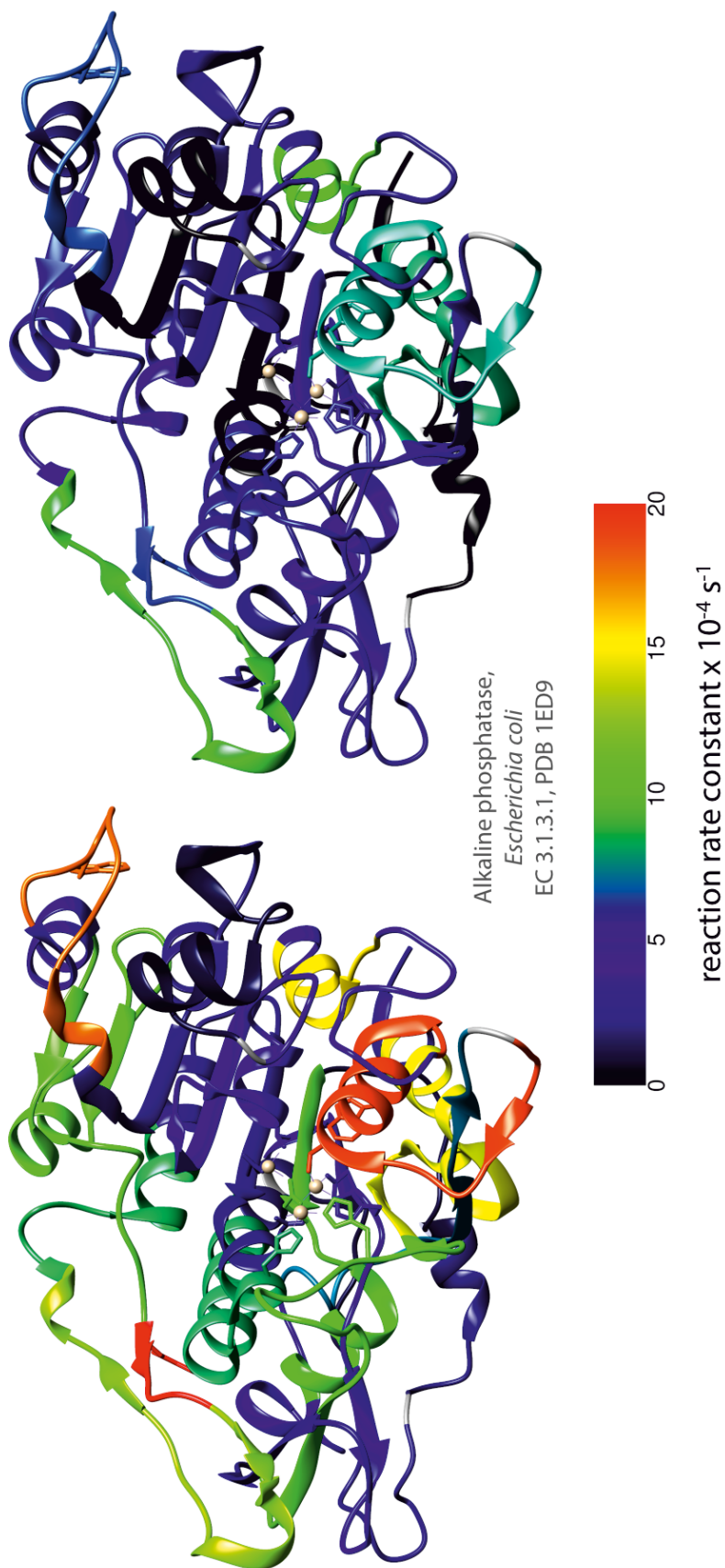


**Figure S10.2** Color maps of *Escherichia coli* alkaline phosphatase structure indicating the range of site-specific reaction rate constants obtained upon UVB irradiation in absence (left) and presence (right) of 6,7-dihydroxycoumarin acting as an antioxidant. Experiment was conducted with 8 UVB bulbs and reaction rate constants were not corrected for the number of bulbs. Grey color indicates non-detectable and black non-reacting peptides.

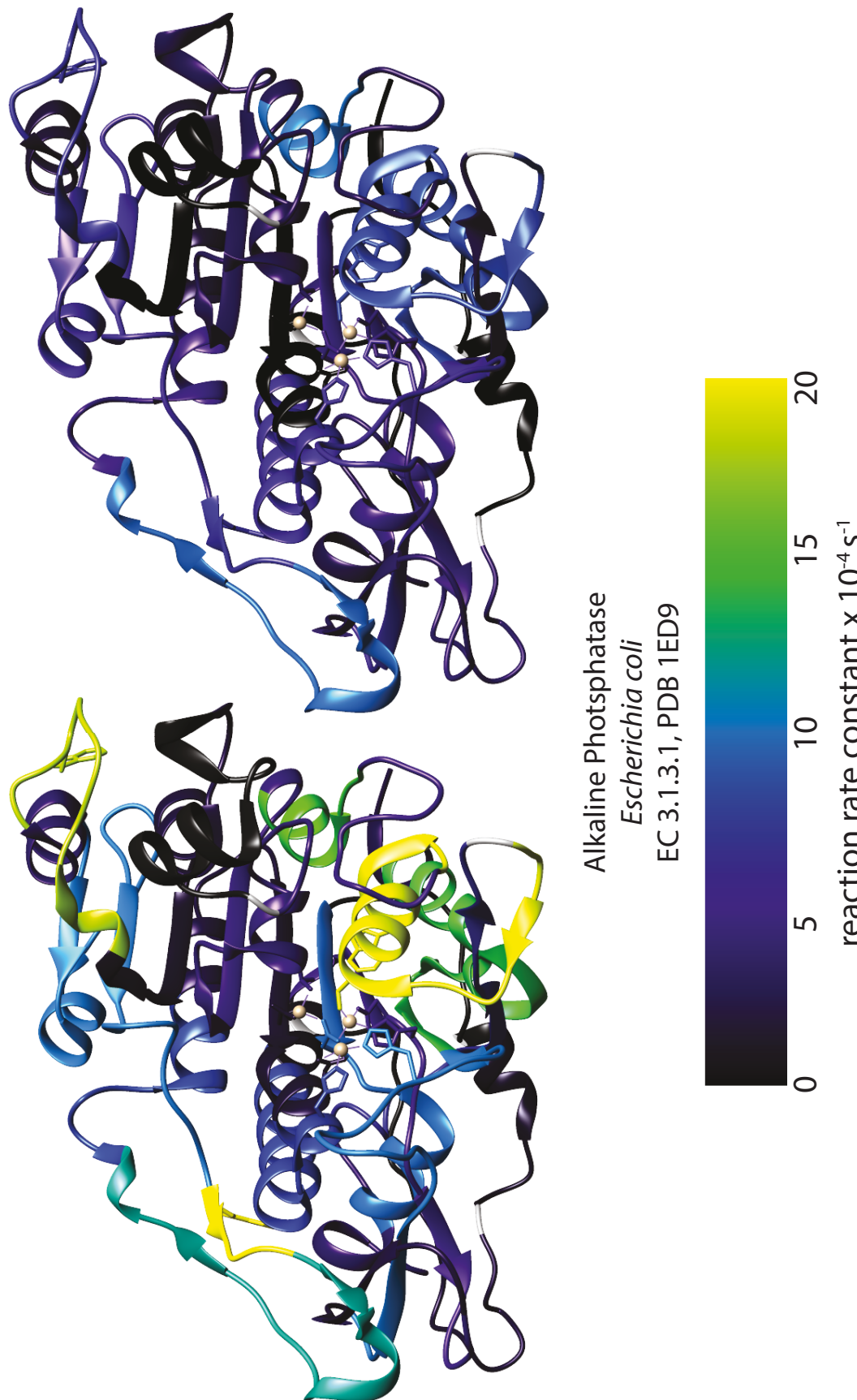
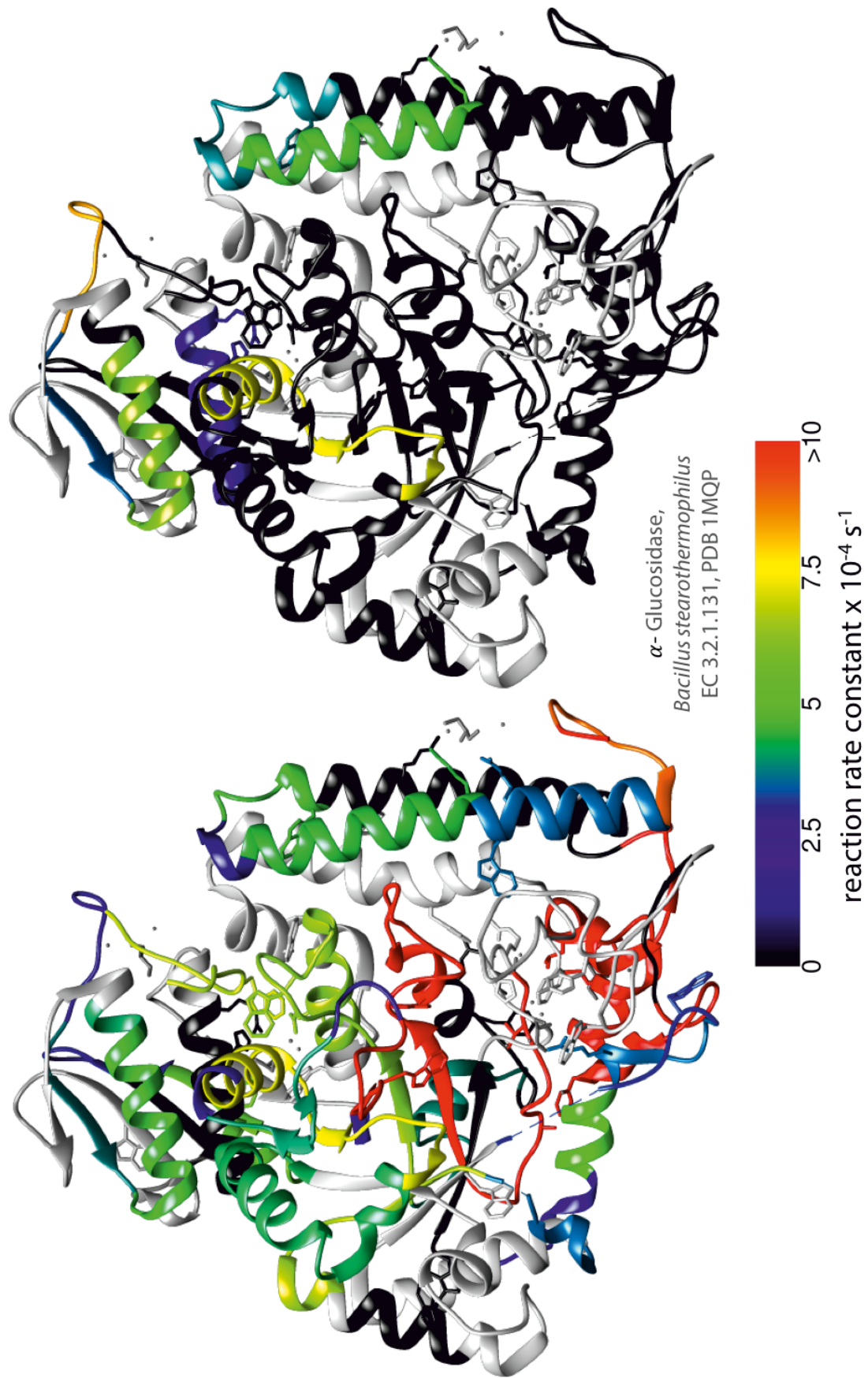


Figure S10.3 Color maps of alkaline phosphatase in viridis color scale (same figure as Figure S10.2)



**Figure S10.4** Resulting color maps of *Bacillus stearothermophilus*  $\alpha$ -glucosidase from direct UVB irradiation (2 UVB bulbs) with site-specific reaction rate constants. In buffered solution (left) and in presence of 6,7-dihydroxycoumarin (right). Grey color indicates non-detectable and black non-reacting peptides.

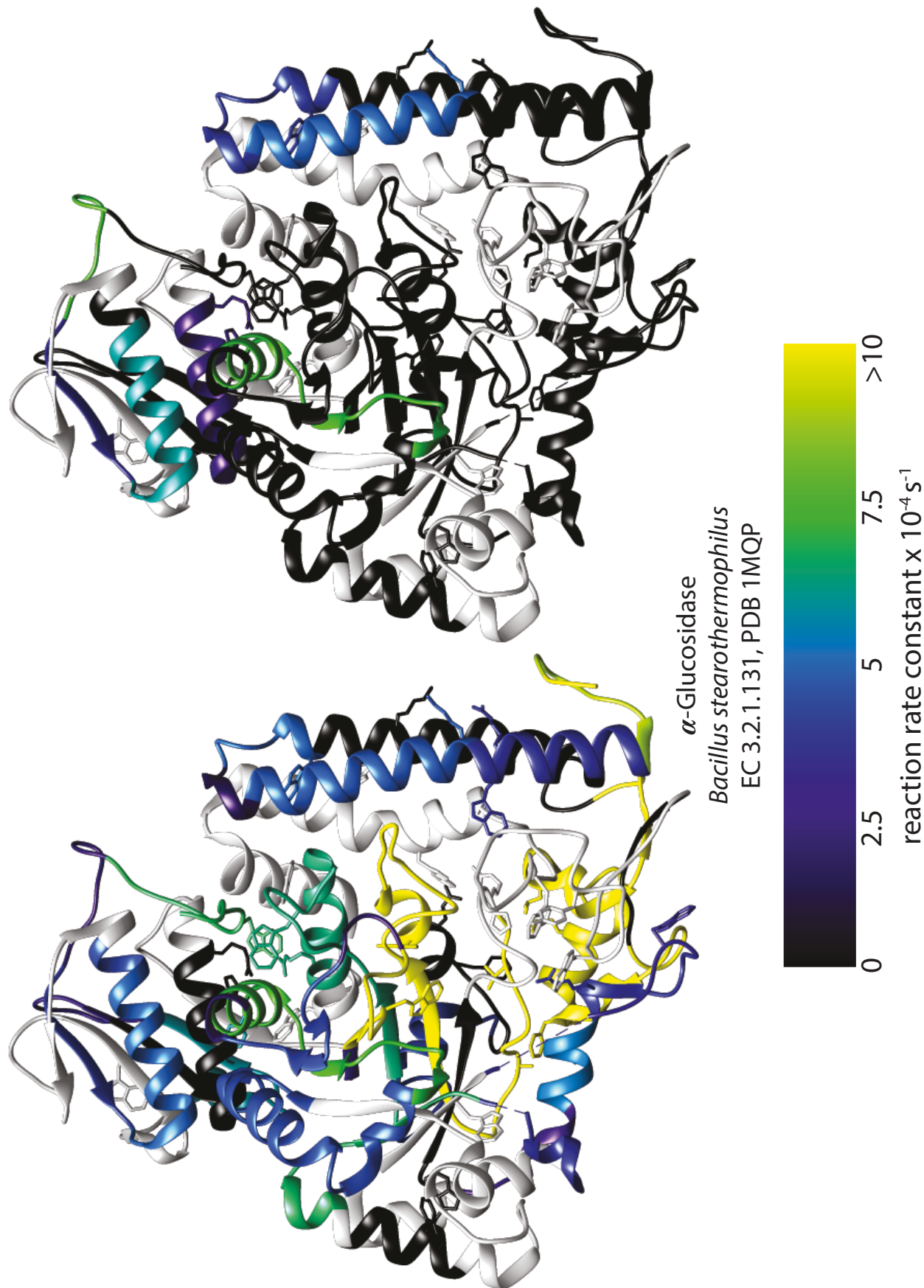
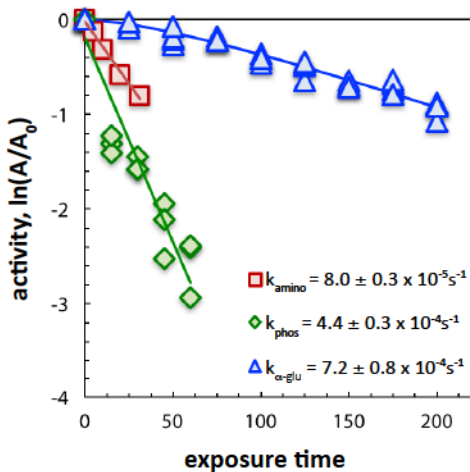
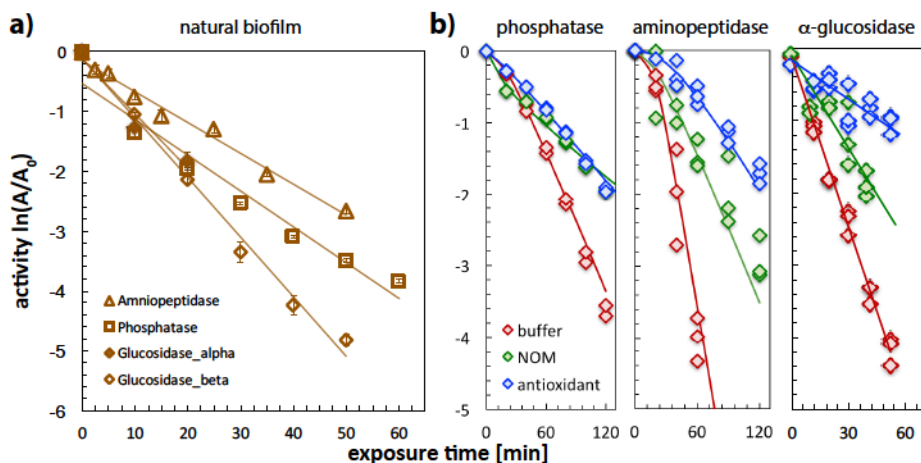


Figure S10.5 Color maps of  $\alpha$ -glucosidase in viridis color scale (same figure as Figure S10.4)

## S11 Loss of Model Enzyme and Biofilm Activities



**Figure S11.1** Photoinactivation of phosphatases from biofilm samples (red squares), model glucosidase (GLU, green diamonds) and model aminopeptidase (BLAP, blue triangles) upon exposure to solar light (simulated sunlight). Indicated are the respective inactivation rates. Activities were measured as described above by the UPLC assays.



**Figure S11.2** Originally measured data of photoinactivated activities in a) biofilm and b) model enzymes upon exposure to UVB light. Inactivation experiments were conducted with 8 UVB bulbs (biofilm) and 6, 8 and 2 UVB bulbs for phosphatase (ECAP), aminopeptidase (BLAP) and glucosidase (GLU), respectively. Figure 2 of the main manuscript shows this data normalized to 6 UVB bulbs.

**Table S11.1** Overview of photoinactivation rate constants for model enzymes. All reaction rate constants were corrected for the fluence rate of 6 UVB bulbs.

enzyme	inactivation in buffer		inactivation with esculetin		inactivation with NOM	
	$k_{\text{direct}}$ [ $10^{-4}\text{s}^{-1}$ ]	$t_{1/2}$ [min]	$k_{\text{Esc}}$ [ $10^{-4}\text{s}^{-1}$ ]	$\Delta^{\text{a}}$ [%]	$k_{\text{NOM}}$ [ $10^{-4}\text{s}^{-1}$ ]	$\Delta^{\text{a}}$ [%]
ECAP	$5.17 \pm 0.21$	22.4	$2.67 \pm 0.08^{\text{b}}$	48.4	$2.54 \pm 0.09^{\text{c}}$	50.8
BLAP	$8.49 \pm 0.87$	13.6	$1.89 \pm 0.12^{\text{b}}$	77.7	$3.13 \pm 0.25^{\text{d}}$	63.1
GLU	$39.36 \pm 0.99$	2.9	$8.99 \pm 1.34^{\text{b}}$	77.2	$21.34 \pm 2.60^{\text{e}}$	45.8

<sup>a</sup> calculated relative to the rate constants measured in buffer      <sup>b</sup> 50  $\mu\text{M}$  Esc  
<sup>c</sup> Waskish Peat, 10  $\text{mgC L}^{-1}$       <sup>d</sup> Aldrich Humic Acid, 10  $\text{mgC L}^{-1}$       <sup>e</sup> Nordic Lake, 10  $\text{mgC L}^{-1}$

## S12 Peptide Degradation and Inactivation

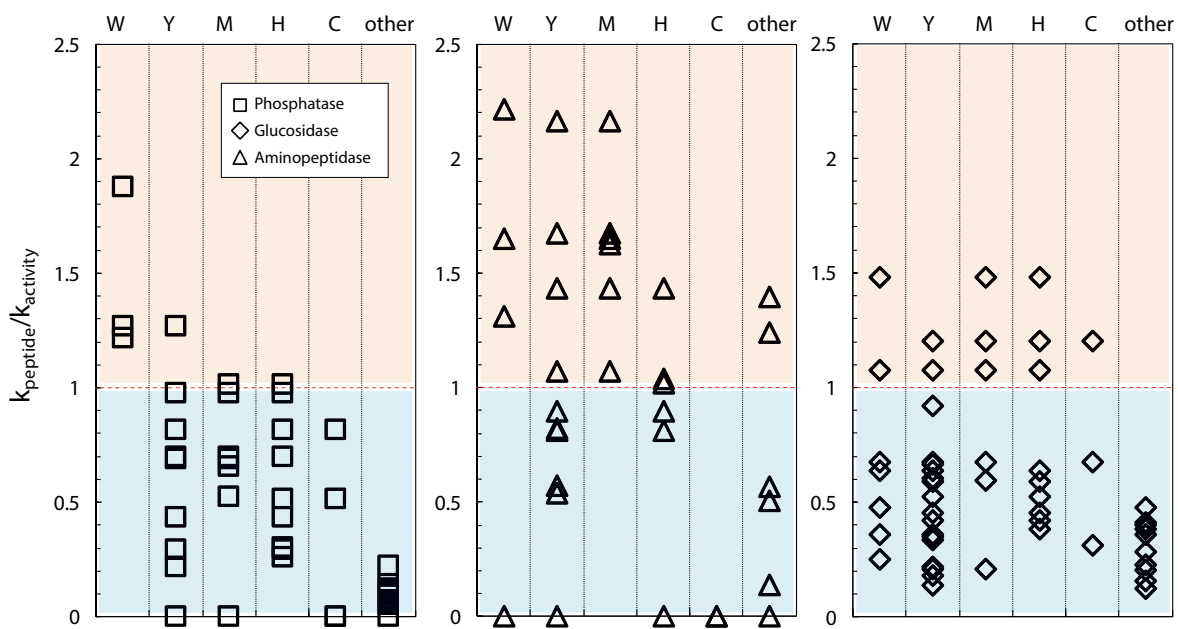


**Figure S12.1** Peptide degradation rate constants normalized with the inactivation rate constant of the respective enzyme and sorted according to the photolabile amino acid on the peptides for phosphatase (left), aminopeptidase (middle) and glucosidase (right). Data of peptides is organized in column based on the presence of photolabile amino acids tryptophan (W), tyrosine (Y), methionine (M), histidine (H), cysteine (C) and other peptides not containing any photolabile amino acids (other). Peptides with  $k_{\text{peptide}}/k_{\text{activity}} < 1$  (blue background) degrade faster than the respective enzyme loses its activity. Inactivation seems not to be driven by one specific amino acid.

## S13 Solvent Accessibility of Trp Residues and external antioxidant effect

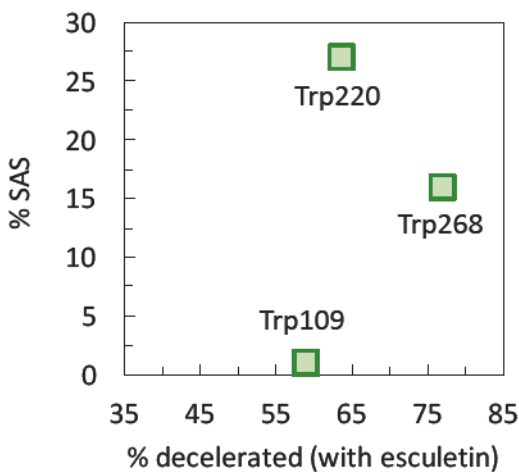


**Figure S13.1** Comparison of the solvent assessable surface area (SAS) of the Trp residues in the phosphatase to the quenching effect of an external antioxidant (esculetin). When phosphatase is exposed to UVB light in presence of an external antioxidant its degradation can be decelerated. This quenching ability is not dependent on the solvent accessibility of the Trp residues.

## S14 Change in Activity Compared to Loss of Trp-like Fluorescence

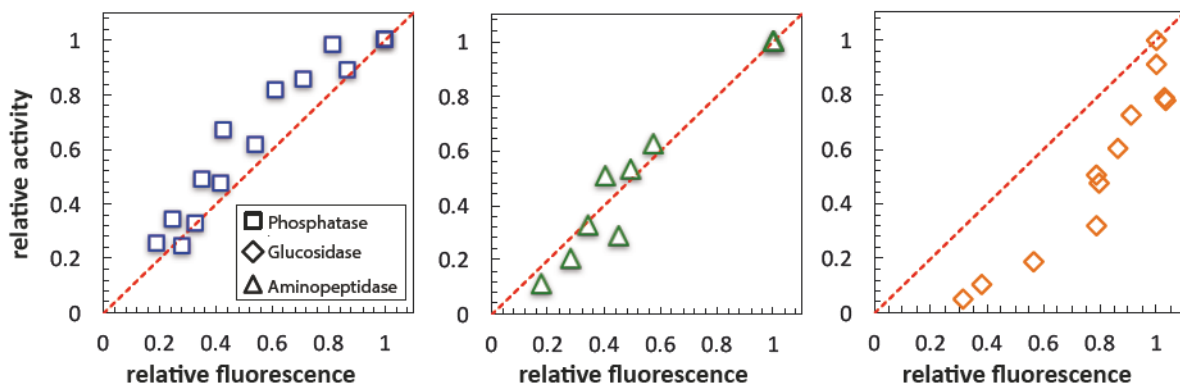


**Figure S14.1** Loss of activity compared to loss in Trp-like fluorescence during UVB exposure of phosphatase (left), aminopeptidase (middle) and glucosidase (right) to initial activity and fluorescence. Fluorescence and activity are expressed relative to values obtained from samples prior to irradiation. Bulk Trp-like fluorescence was measured with a spectrofluorometer (Fluoromax Jobin-Yvon) at 280 nm excitation and 325 nm emission wavelength. Dotted red line indicates a 1:1 ratio of relative activity and relative fluorescence.

## S15 Reactivity of Peptides Containing Photolabile Amino Acids

Data in Figure S15.1 show the relative reaction rate constants for Tyr-containing peptides,  $k_{\text{rel,Tyr}}$ , versus the inter-residue distance to the closest Trp,  $d_{\text{Tyr-O, Trp-N}}$ . Secondary Tyr degradation can be a result of multiple reaction pathways ((PC)ET between  $\text{TrpH}^{\bullet+}$  and  $\text{TyrOH}$ , direct photo-ionization, and oxidation by  ${}^1\text{O}_2$  and triplets<sup>10</sup>) and the overall Tyr degradation shows no clear correlation with proximity to a Trp. Additionally, Table S15.1 shows observed and relative reaction rate constants for Cys-containing peptides as well as for their respective neighbouring Trp-containing peptides,  $k_{\text{obs}}$  and  $k_{\text{rel}}$ . Finally, Figure S15.2 summarizes the relative reaction rate constants across the three model enzymes sorted according to photolabile amino acids on the peptides.

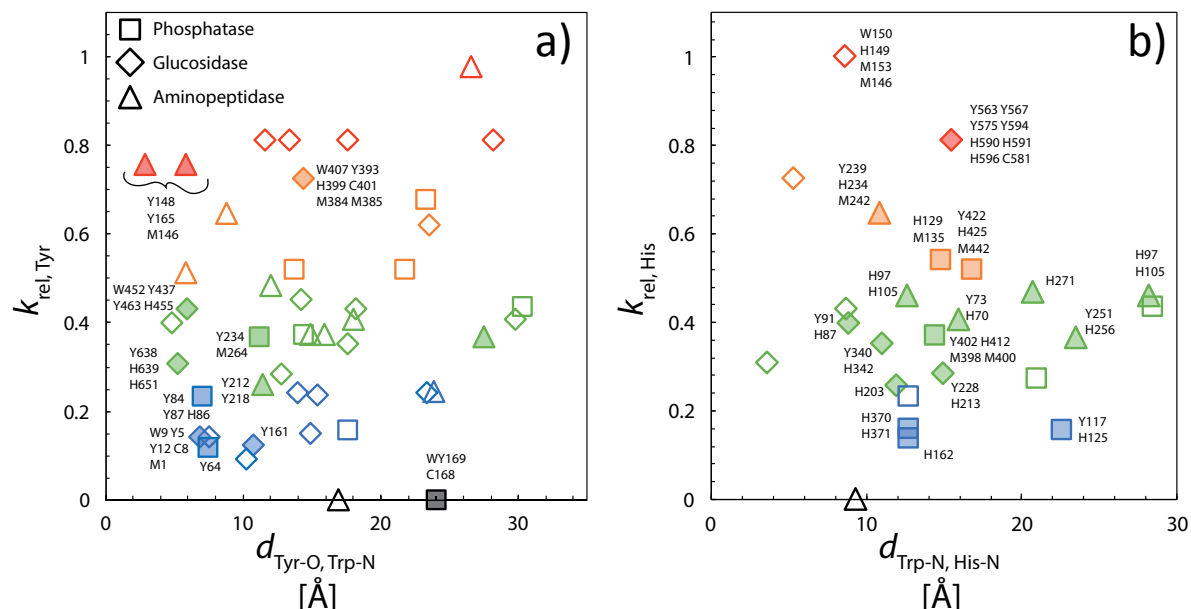
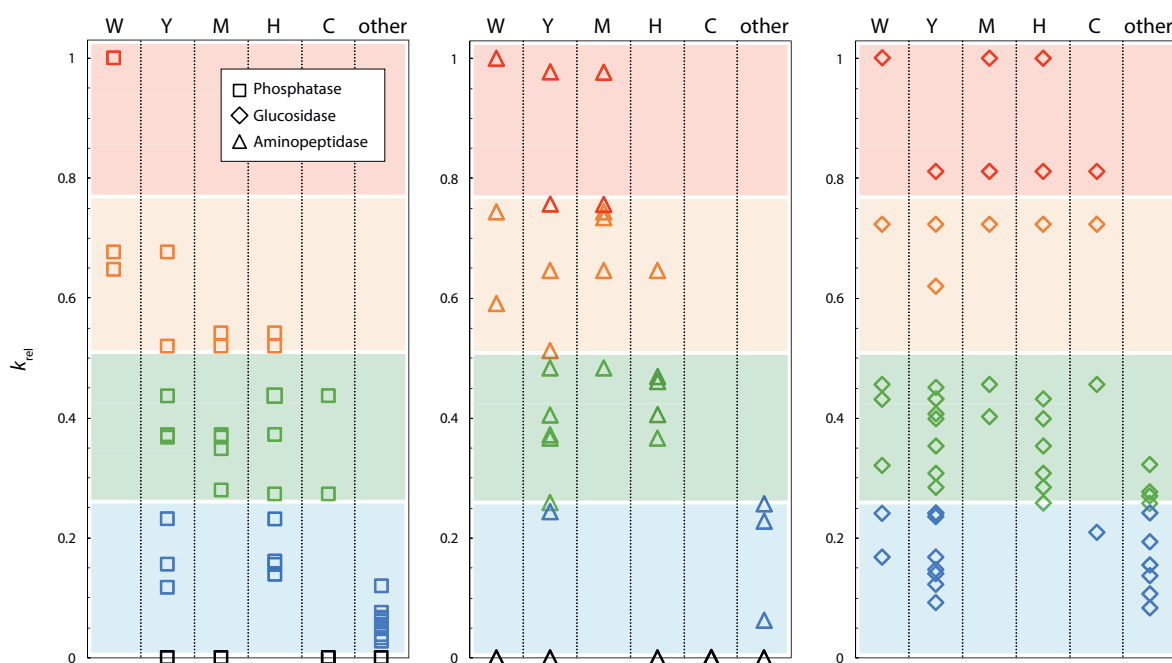


**Figure S15.1** a) Relative reaction rate constant,  $k_{\text{rel}}$ , of the Tyr-containing peptides versus inter-residue distance between Trp and Tyr residues. Filled symbols represent the Tyr-peptides containing the Tyr that build a potential (PC)ET pair with one of the Trp represented in Figure 4 in the main text, the open symbols represent all other Tyr-containing peptides. b) Relative reaction rate constant,  $k_{\text{rel}}$ , of the His-containing peptide versus inter-residue distance between His-N and Trp-N. Filled symbols illustrate peptides with respective sequence numbers of photolabile amino acids and open symbols indicate His-containing peptides that have already been discussed in the context of other reactions.

**Table S15.1** Inter-residue distances and reaction rate constants for Cys- and their neighbouring Trp-containing peptides.

enzyme	#Trp	$k_{\text{obs}, \text{Trp}}$ [ $10^{-4} \text{s}^{-1}$ ]	$k_{\text{rel}, \text{Trp}}^{\text{a}}$	#Cys	$k_{\text{obs}, \text{Cys}}$ [ $10^{-4} \text{s}^{-1}$ ]	$k_{\text{rel}, \text{Cys}}^{\text{a}}$	$d_{\text{Trp-N, Cys-S}}$ [ $\text{\AA}$ ] <sup>b</sup>
ECAP	268	$27.57 \pm 0.19$	1.00	286	$12.02 \pm 0.16$	0.44	6.96
	268	$27.57 \pm 0.19$	1.00	336	$7.53 \pm 1.49$	0.27	8.16
	109	$18.65 \pm 1.11$	0.68	178	$0.00 \pm 0.0$ <sup>c</sup>	0.00	19.75
	109	$18.65 \pm 1.11$	0.68	168	$0.00 \pm 0.0$ <sup>c</sup>	0.00	20.12
BLAP	233	$0.00 \pm 0.0$ <sup>c</sup>	0.00	223	$0.00 \pm 0.00$	0.00	15.13
	233	$0.00 \pm 0.0$ <sup>c</sup>	0.00	227	$0.00 \pm 0.00$	0.00	15.13

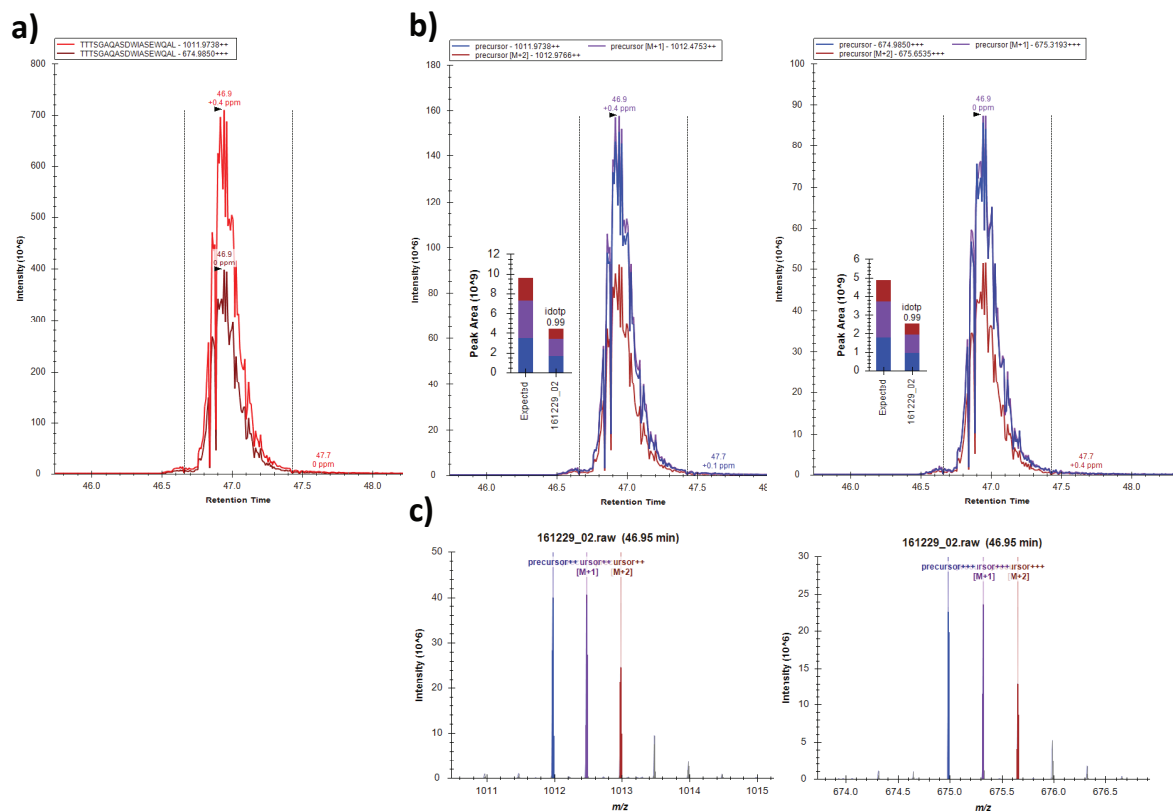
<sup>a</sup>  $k_{\text{rel}}$  is  $k_{\text{obs}}$  divided by  $k_{\text{obs}}$  of the fastest peptide of an enzyme    <sup>b</sup> measured in Chimera from crystal structure data drawn from RCSB Protein Data Base    <sup>c</sup> peptide not degrading



**Figure S15.2** Relative reaction rate constant,  $k_{\text{rel}}$ , of all peptides of the three model enzymes, phosphatase (left), aminopeptidase (middle) and glucosidase (right). Data of peptides is organized in column based on the presence of photolabile amino acids tryptophan (W), tyrosine (Y), methionine (M), histidine (H), cysteine (C) and other peptides not containing any photolabile amino acids (other).

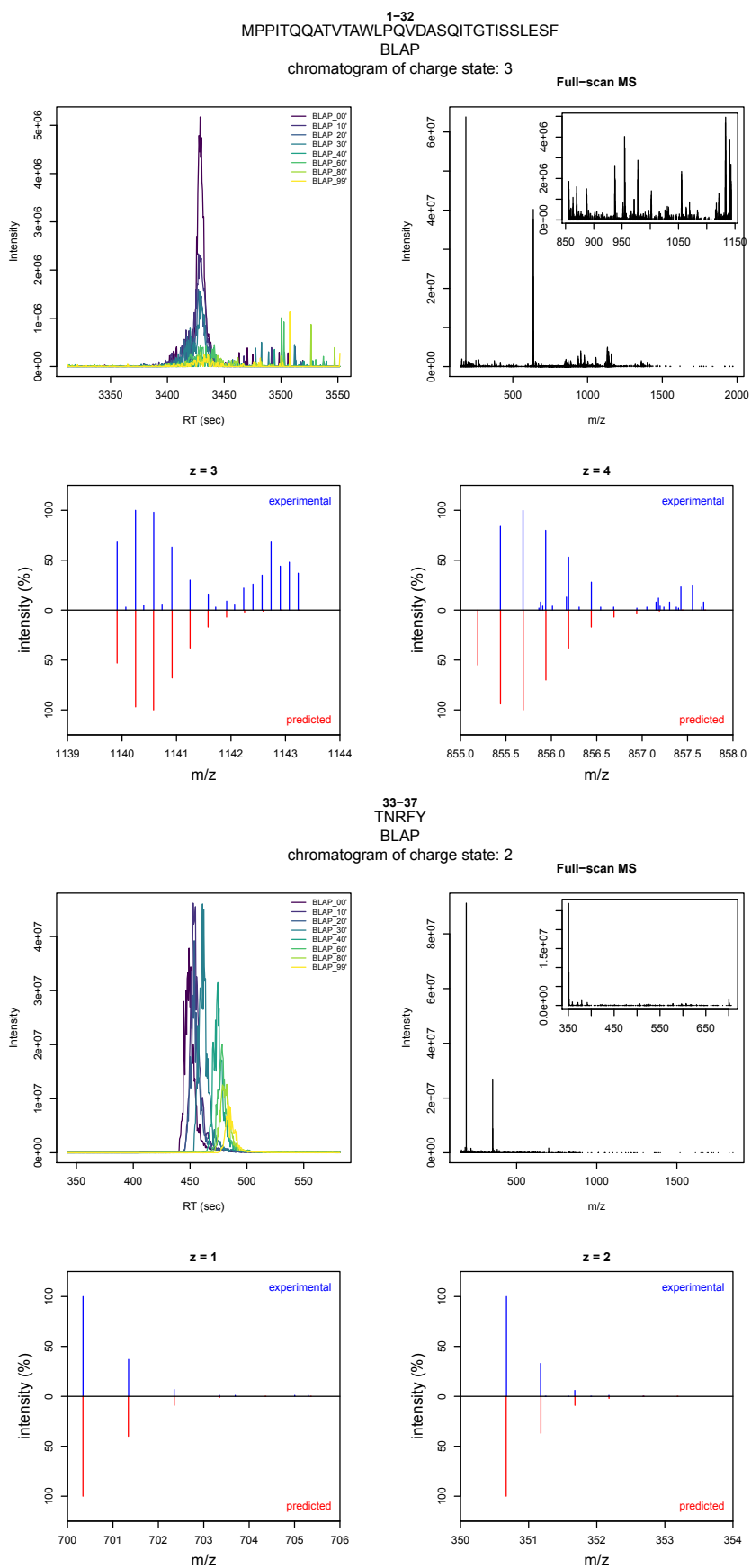
## S16 Chromatograms with Mass Spectra

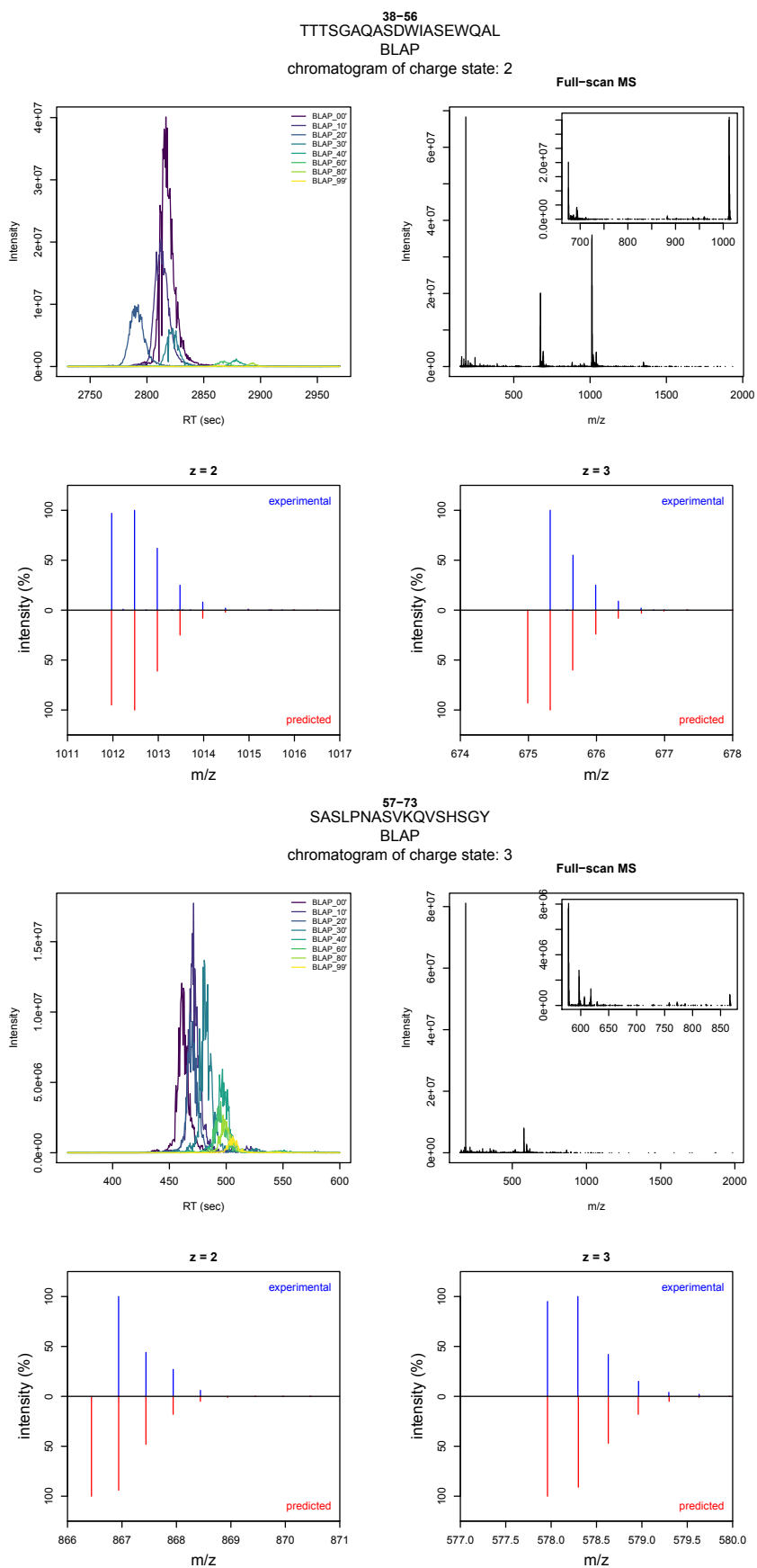
Data analysis was performed with the proteomics software Skyline (v3.5 and v3.6).<sup>33</sup> For the identification of the peptides the presence and shape of the chromatographic traces for three isotopes ( $M$ ,  $M+1$  and  $M+2$ ) of the most intense charge state ( $M+H$ ,  $M+2H$ , ...,  $M+nH$ ), the presence of additional charge states and the comparison with predicted mass distributions was included. An example for the information Skyline provides to support the data analysis can be found in Figure S16.1. Skyline compares the experimental data with the relative distribution of in silico predicted  $m/z$  values, gives a mass deviation in ppm and calculates the idotp value.

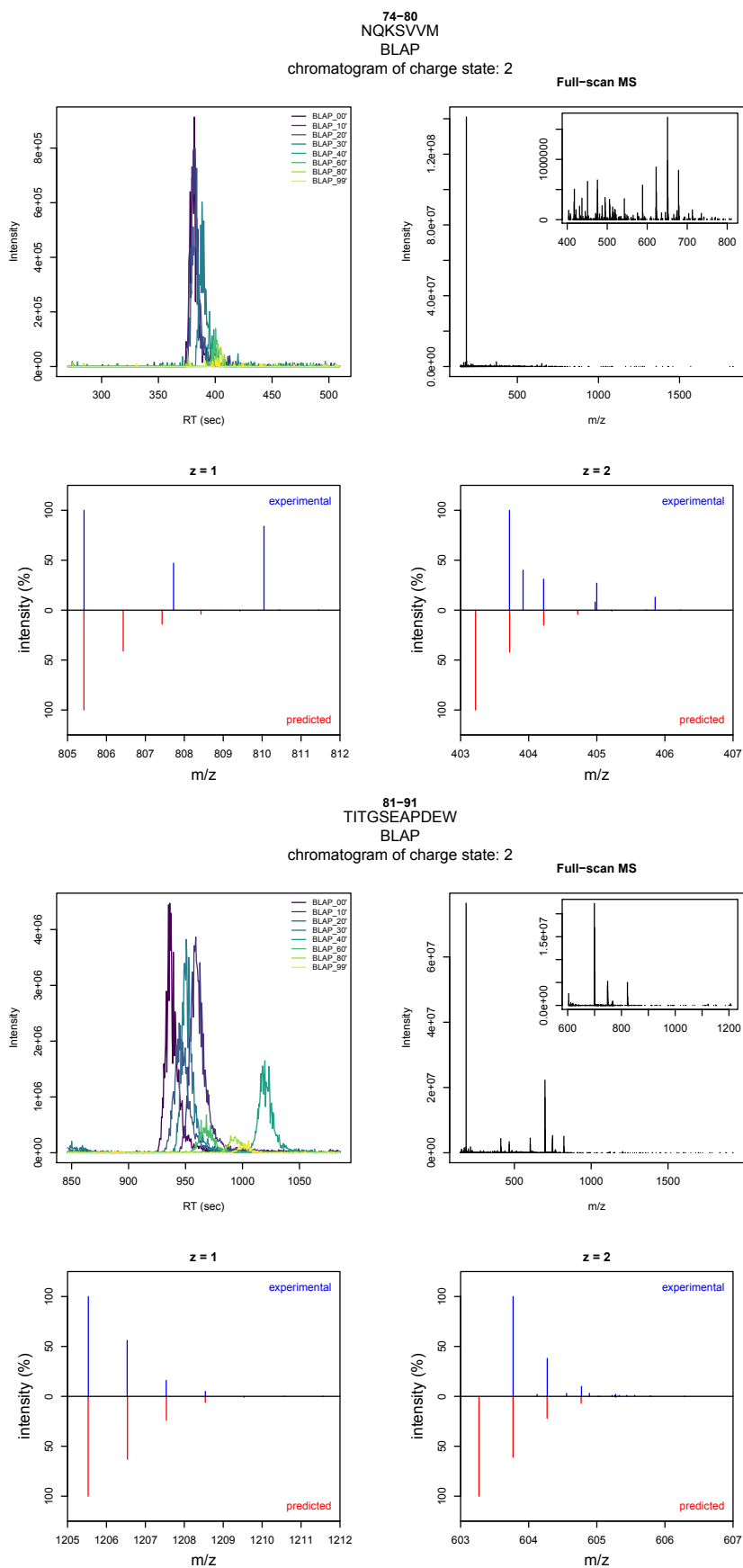


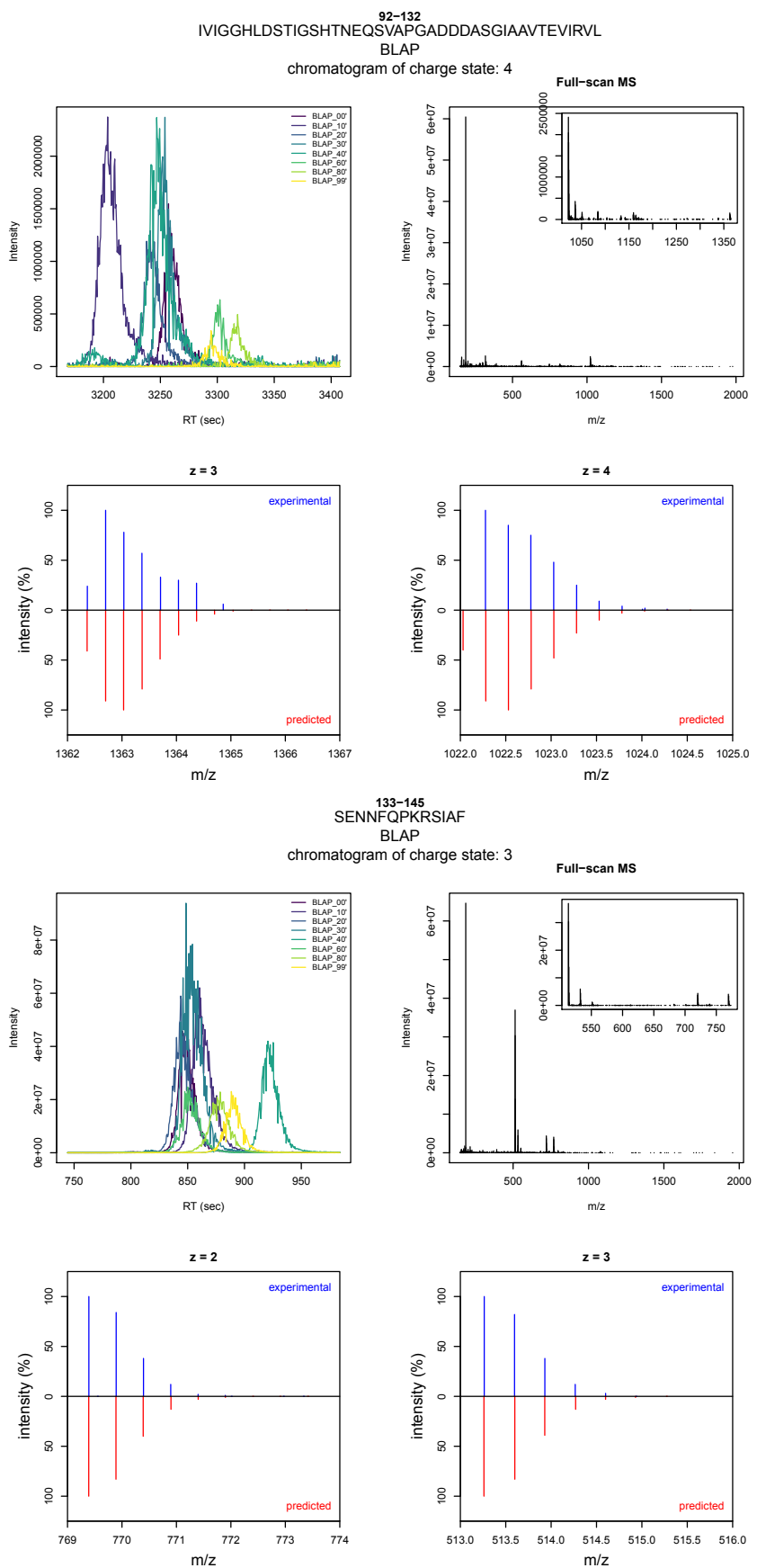
**Figure S16.1** Information and view provided by Skyline for BLAP-peptide TTTSGAQASDWIASEWQAL (38-56). Chromatogram a) shows the overlay of the most intense isotopes of charge state +2 and +3. The peak labels contain the retention time of the peak and the mass deviation compared to the predicted one. Chromatograms b) show the mass traces of the two charge states with the according isotope distribution ( $M$ ,  $M+1$ ,  $M+2$ ). The insert illustrates additional information on the isotope distribution and the calculated idotp value. In spectra c) the measured masses are compared to the predicted masses, indicated with a colored mass range.

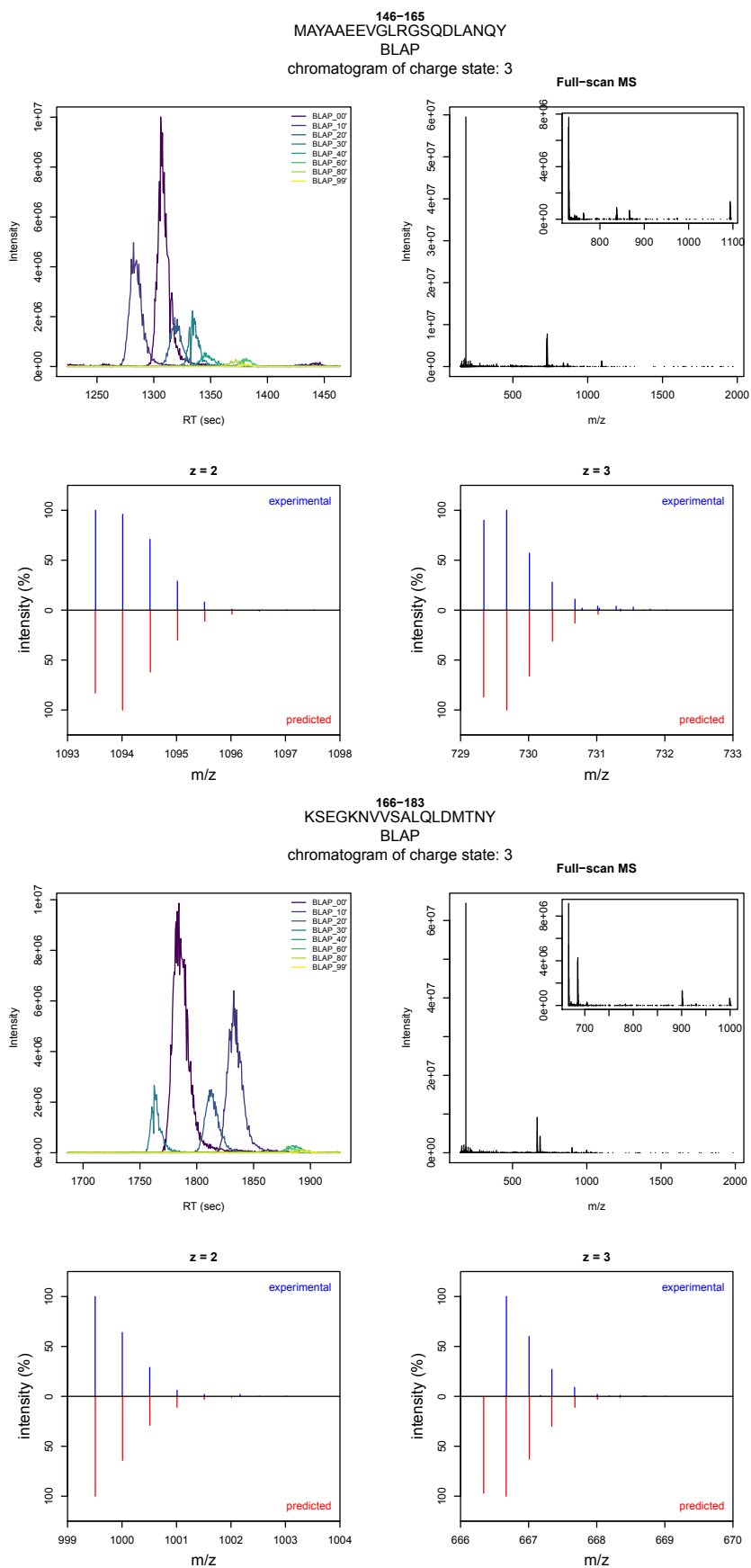
The following section includes chromatograms showing the degradation of the most intense charge state (isotope  $M$ ) for all the studied peptides combined with a total mass spectrum and zoomed in mass spectra for one or two most intense charge states of the zero point peak. The chromatograms were not retention time aligned. The hat of each figure contains the sequence numbers, the peptide name, the name of its enzyme and the charge state in the chromatogram.

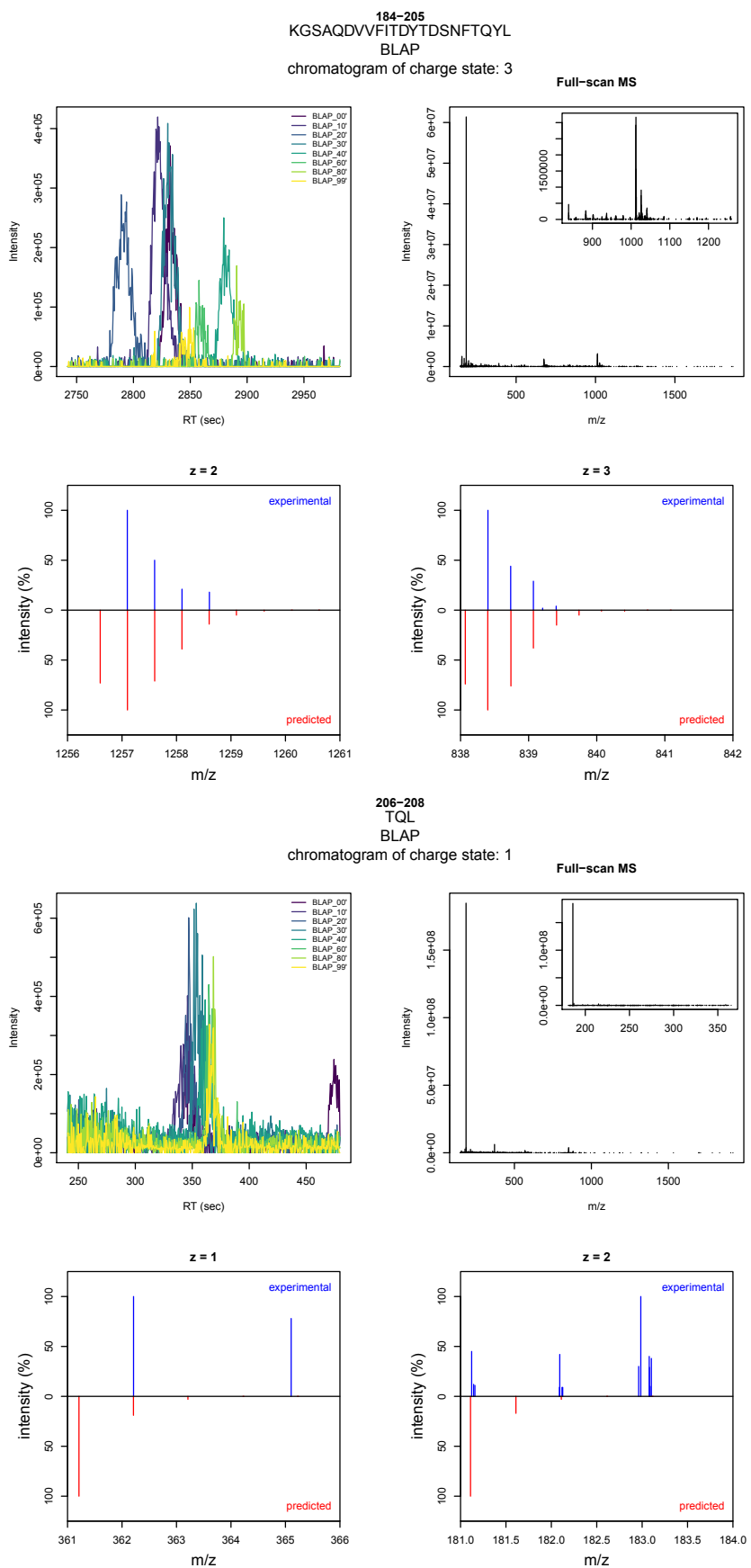


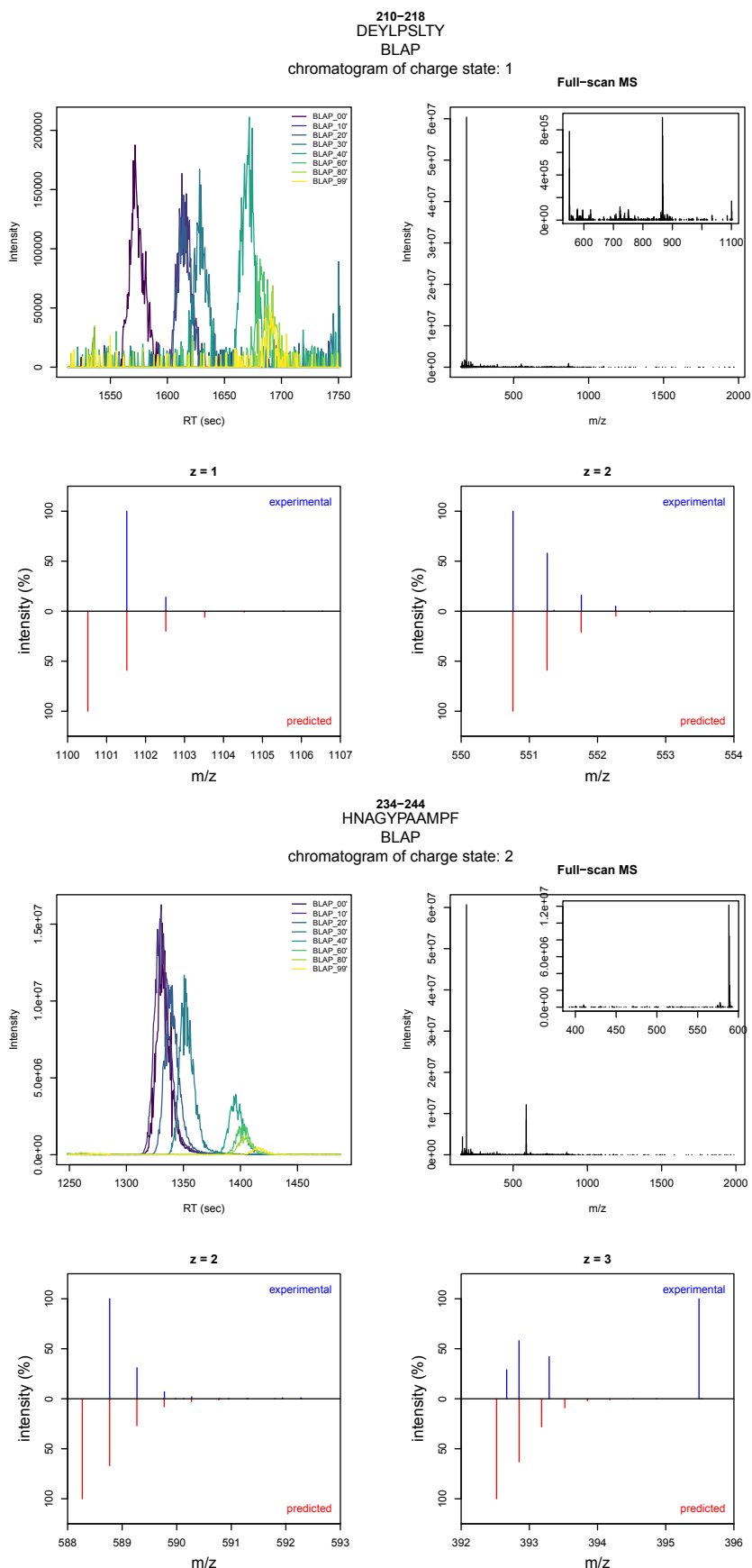


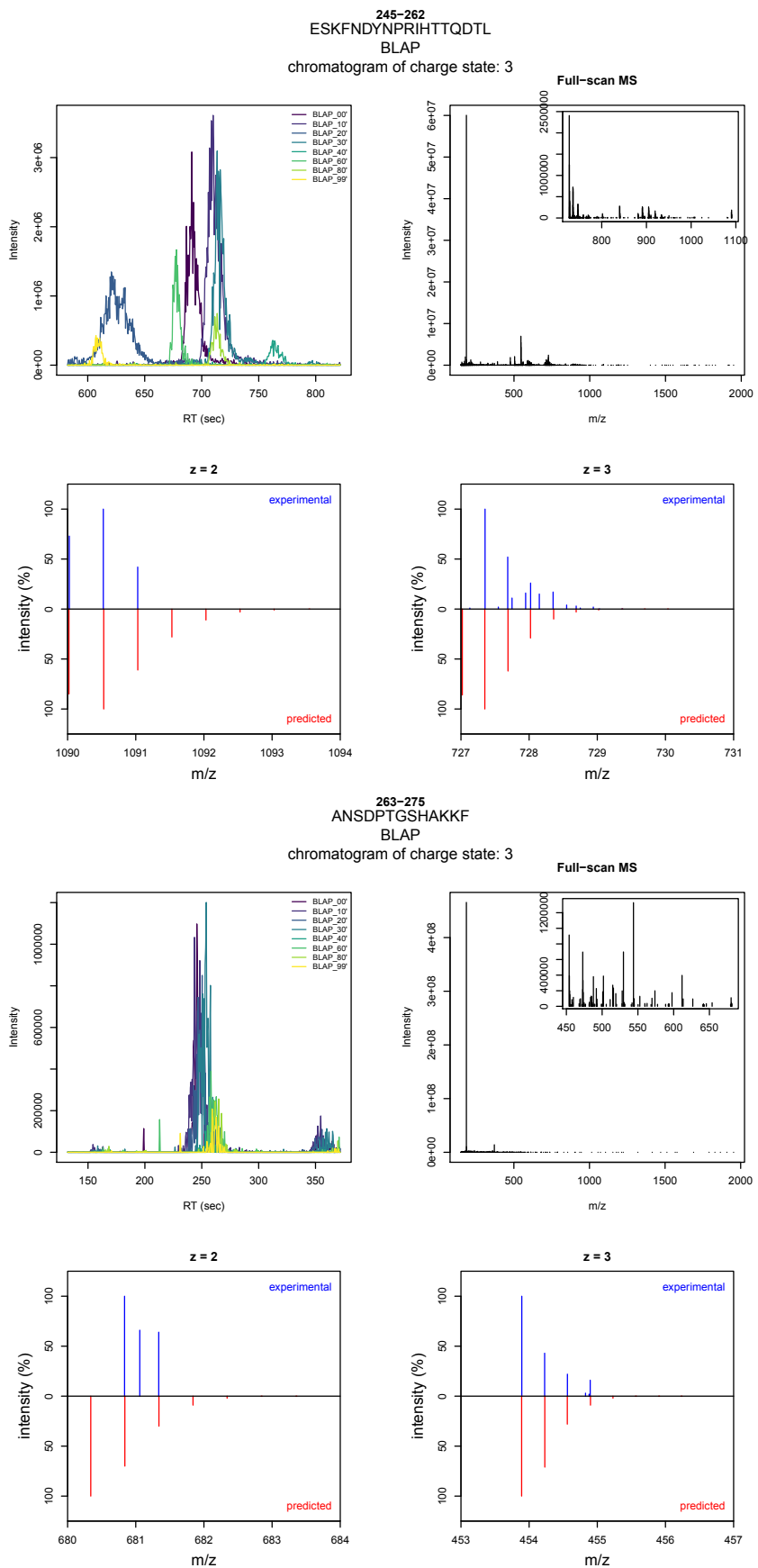


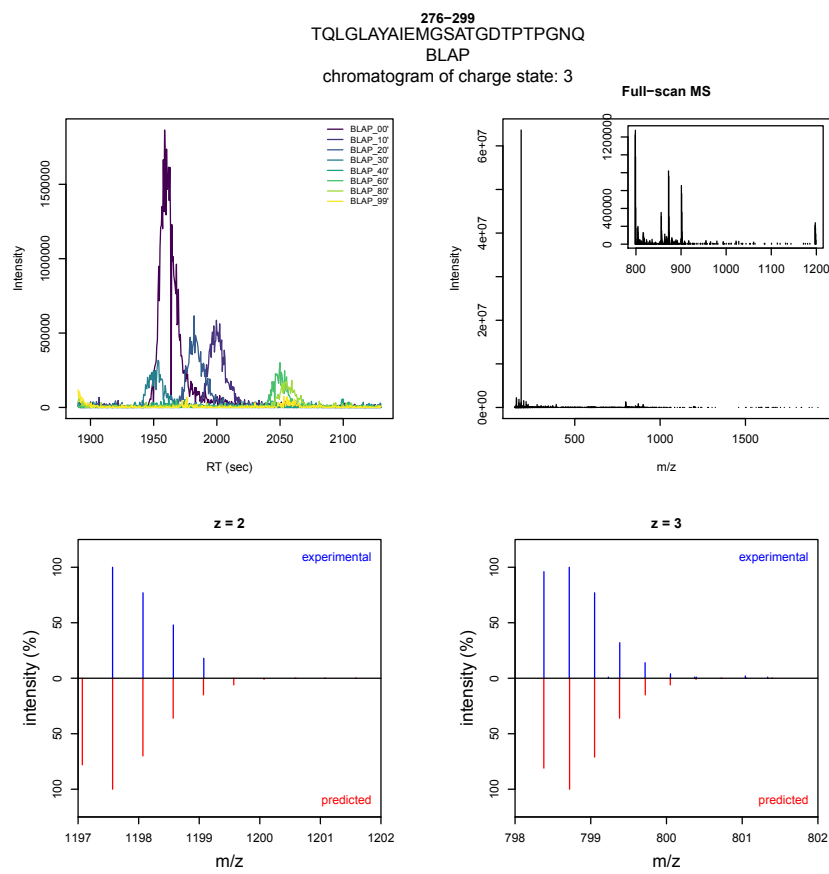


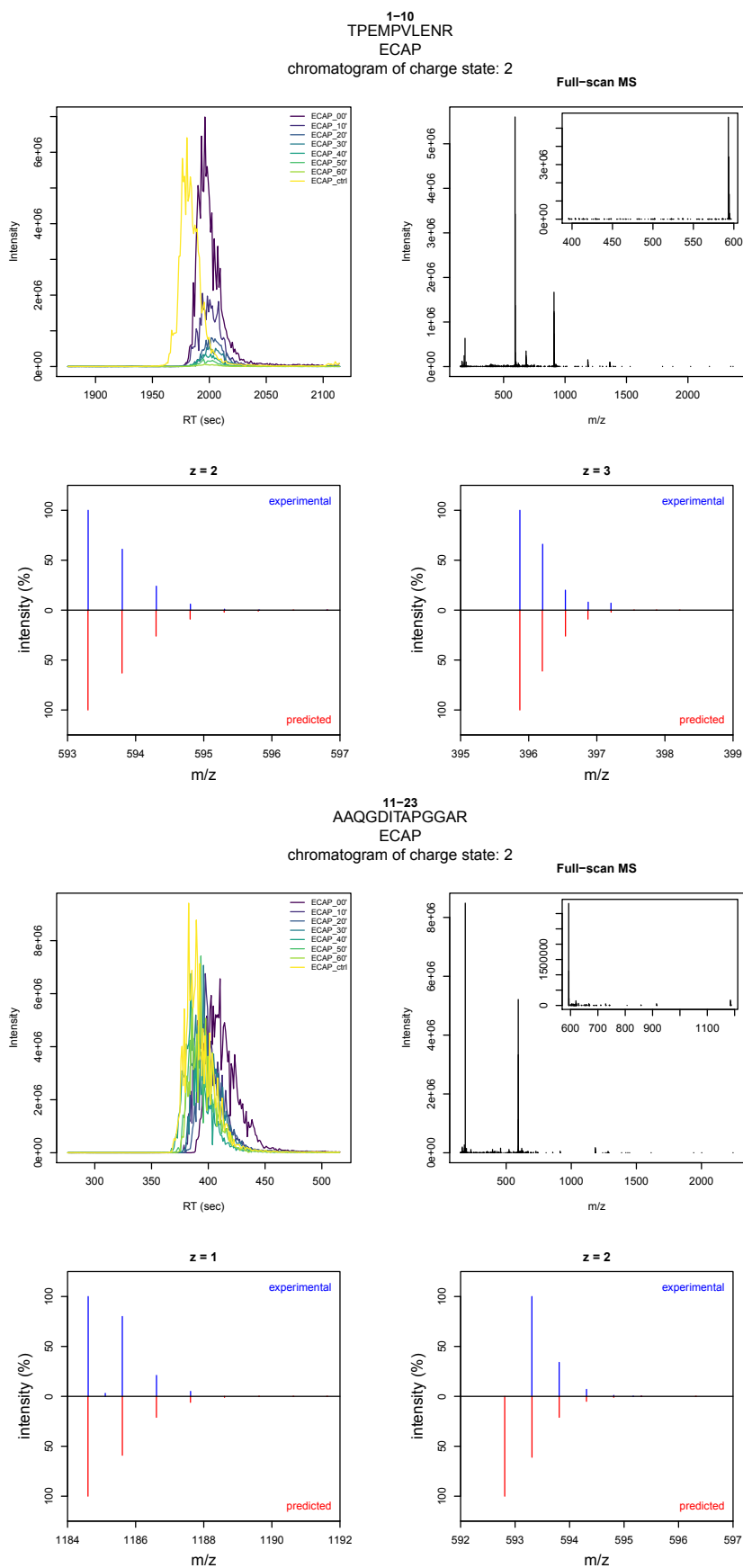


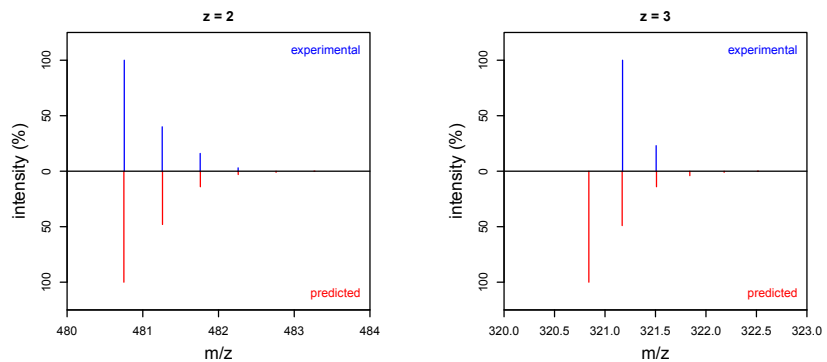
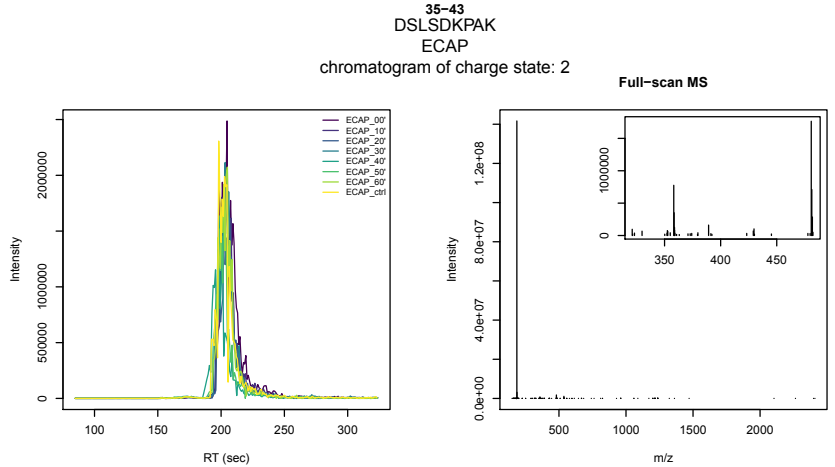
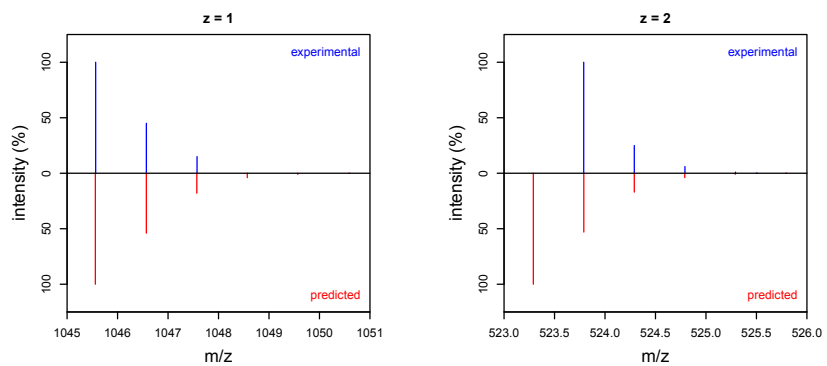
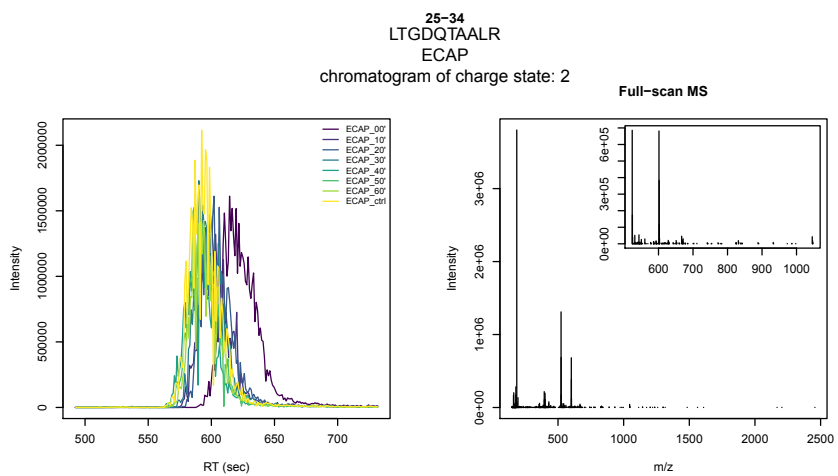


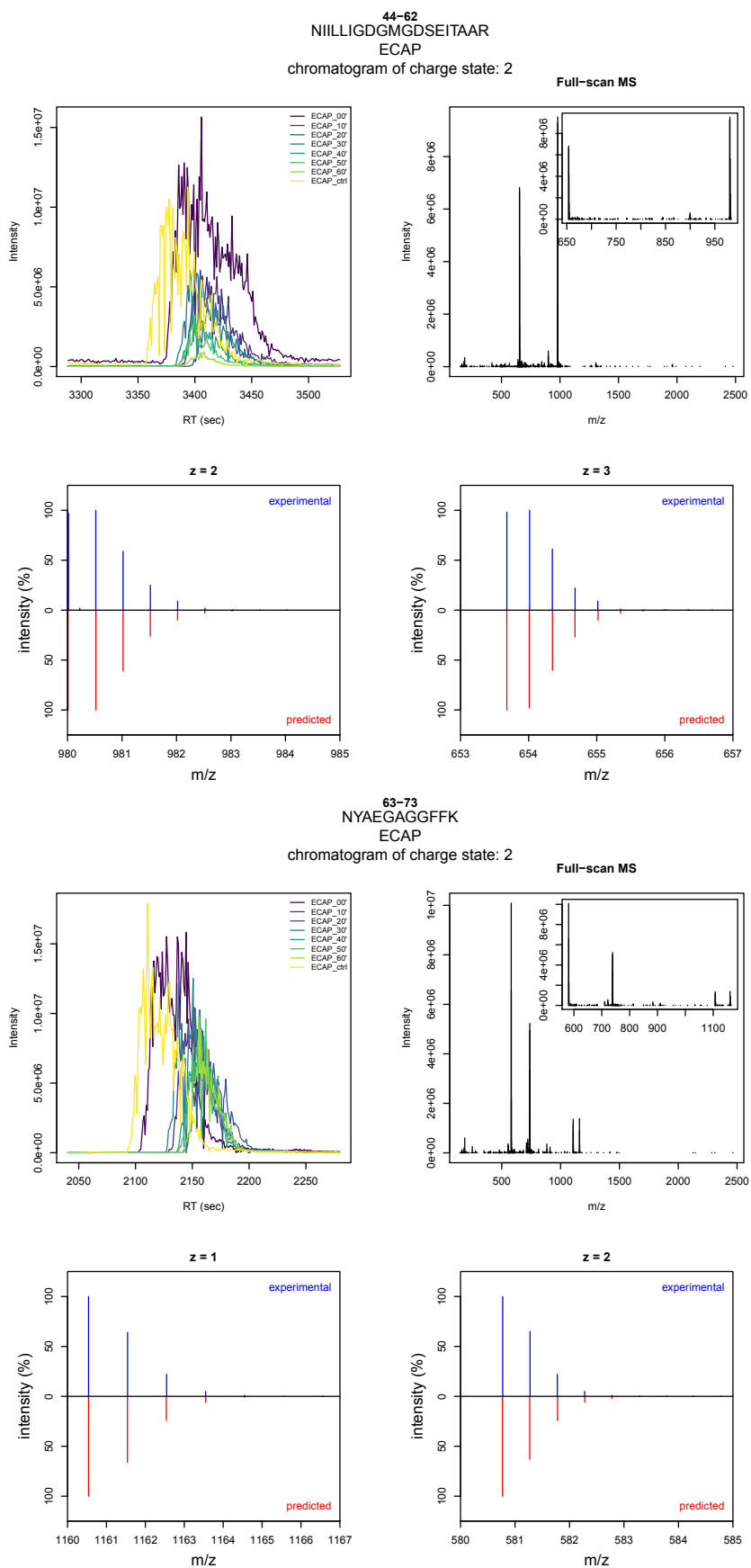


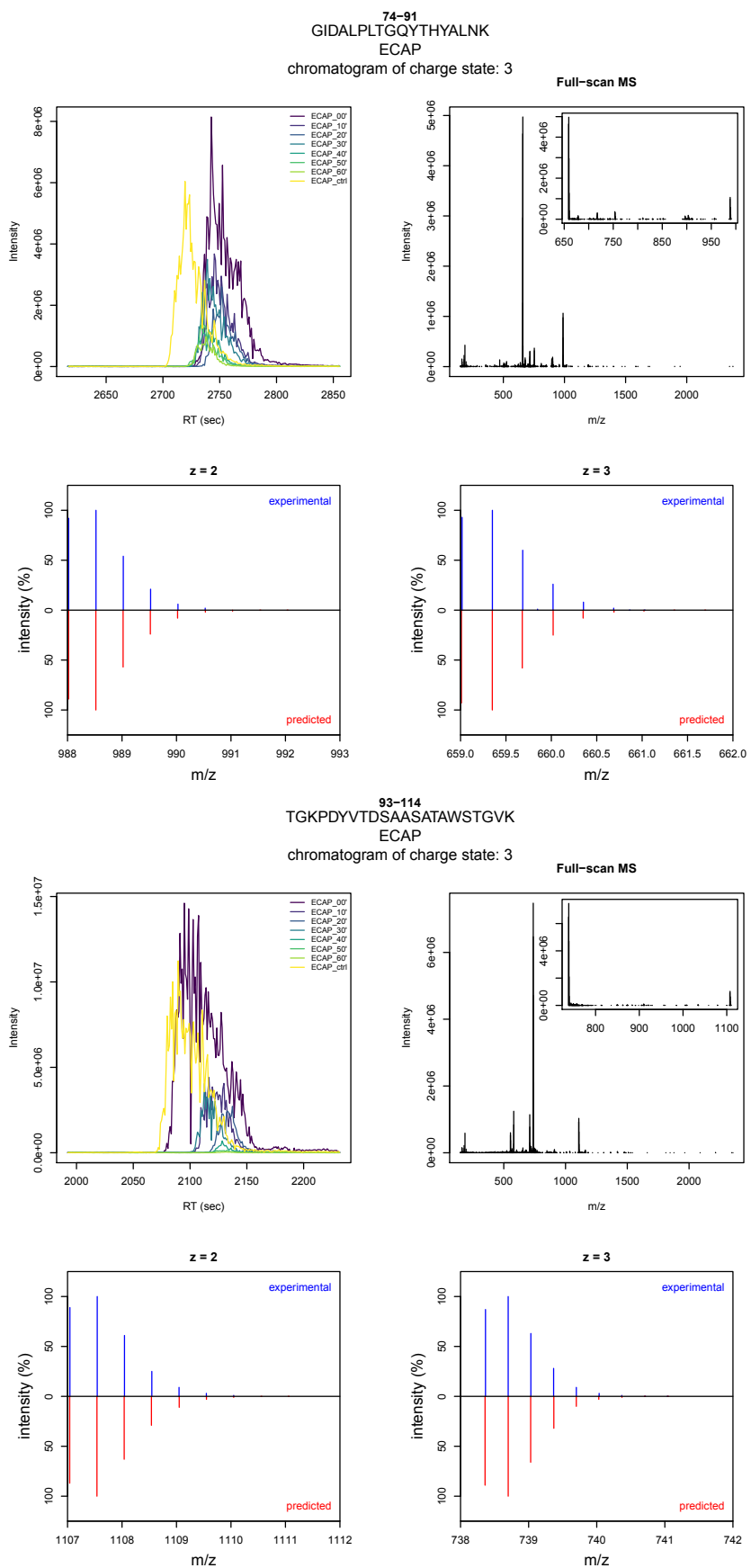


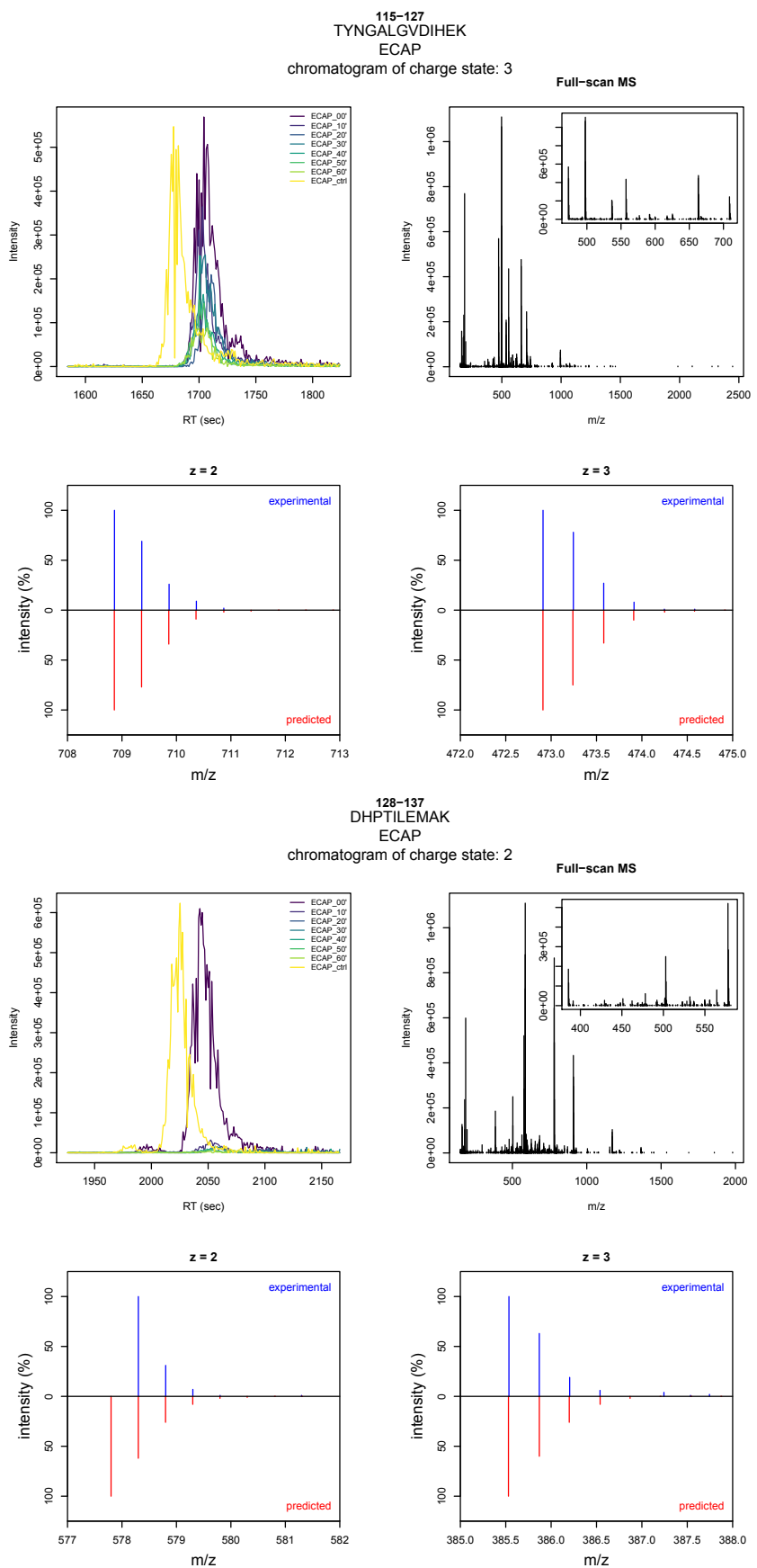


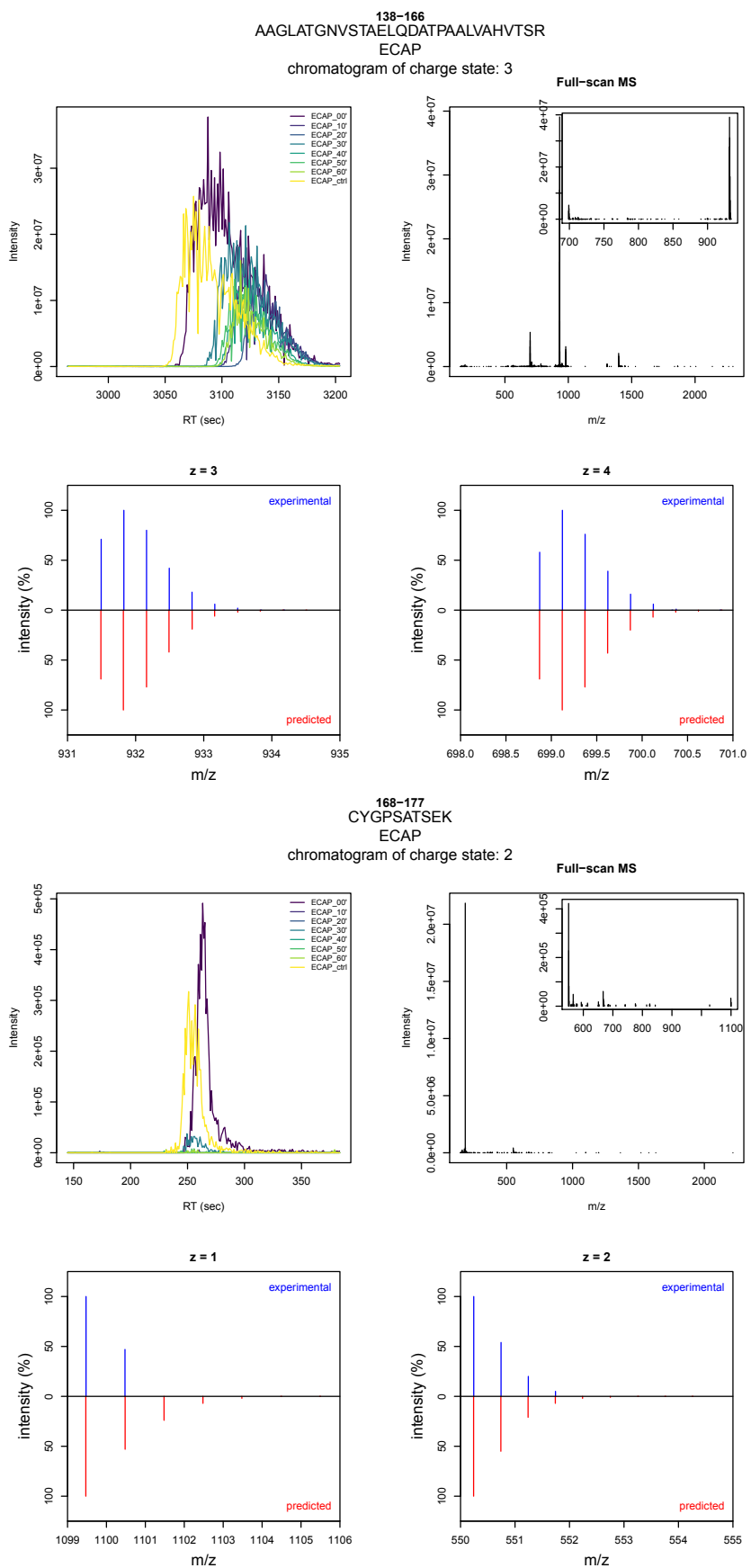


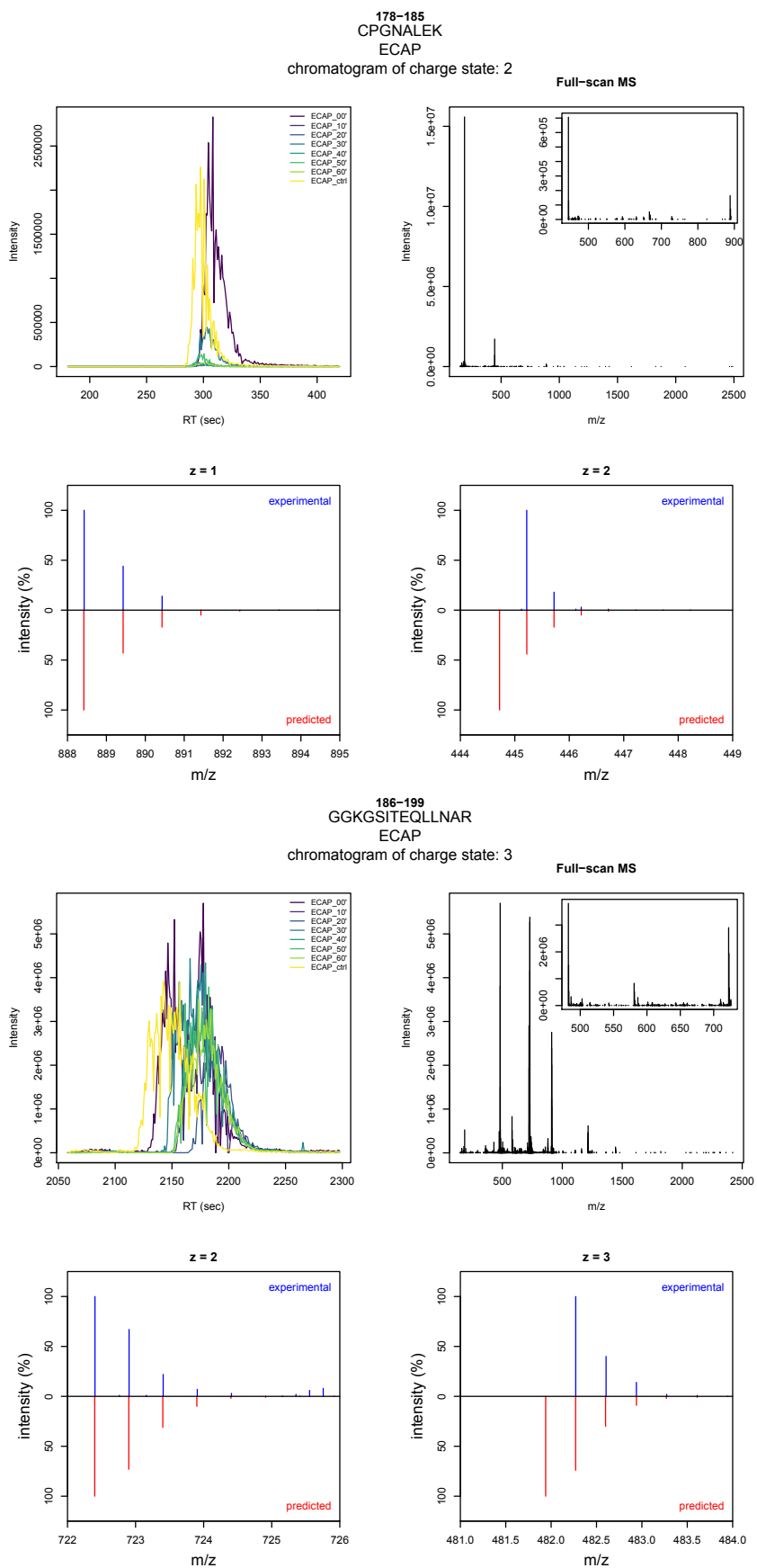


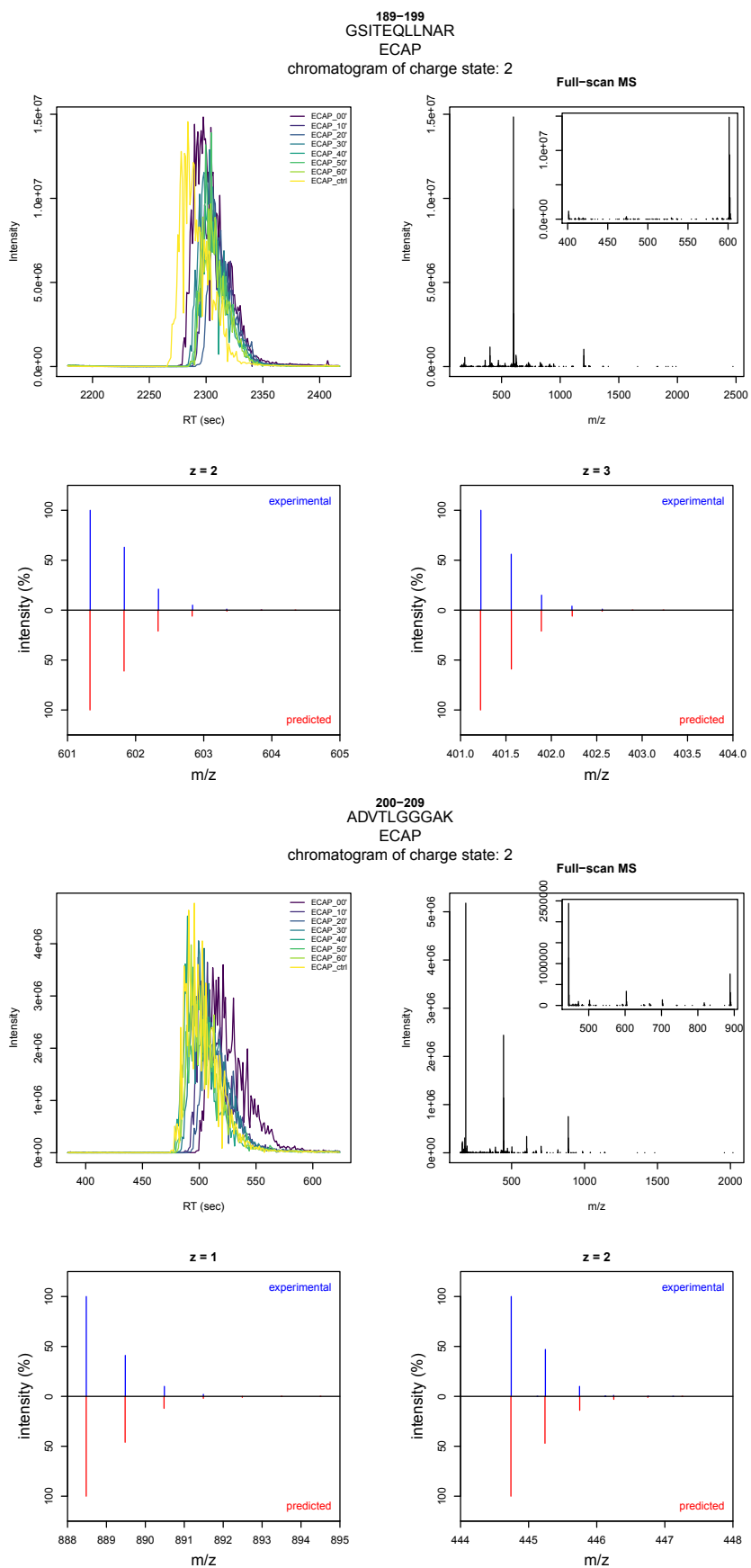


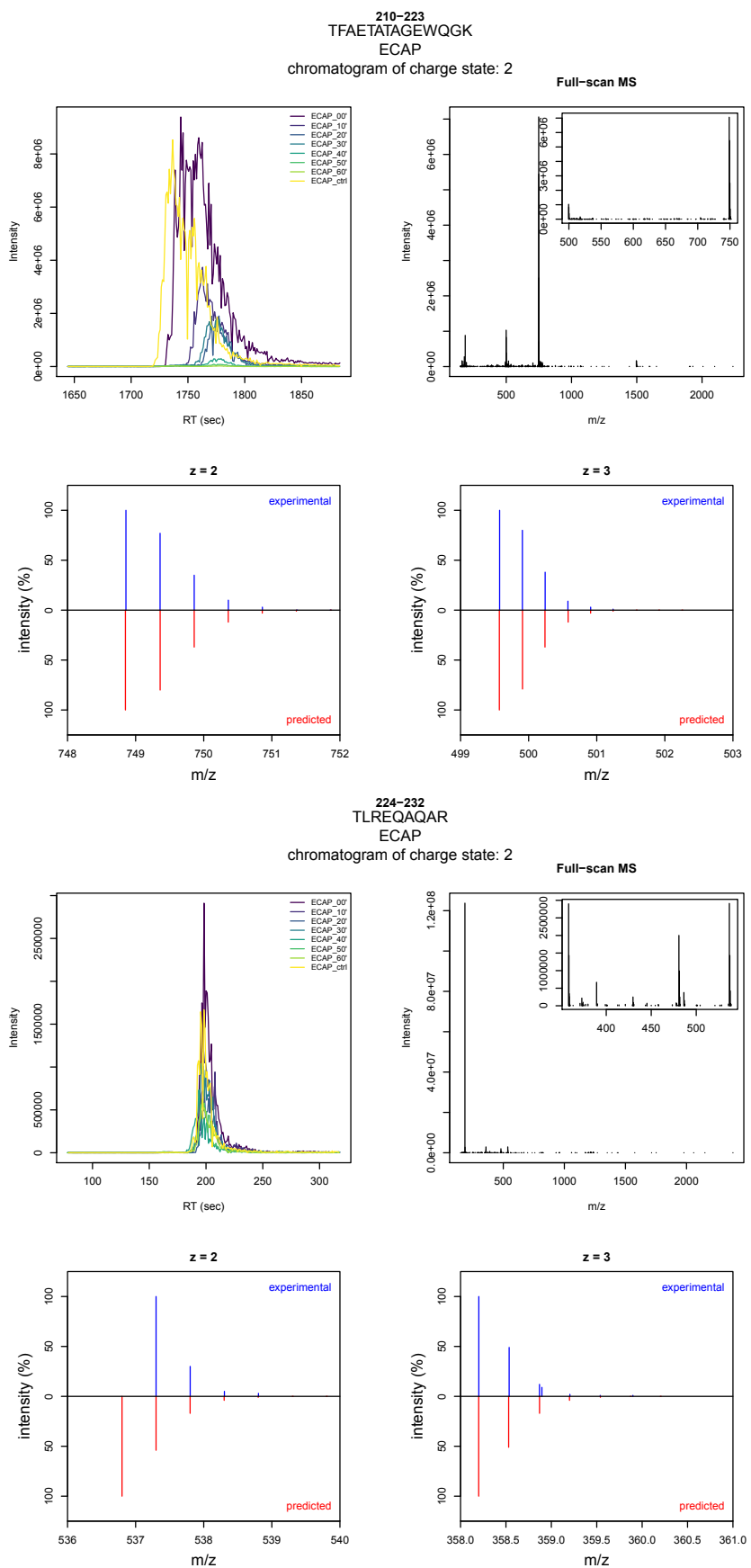


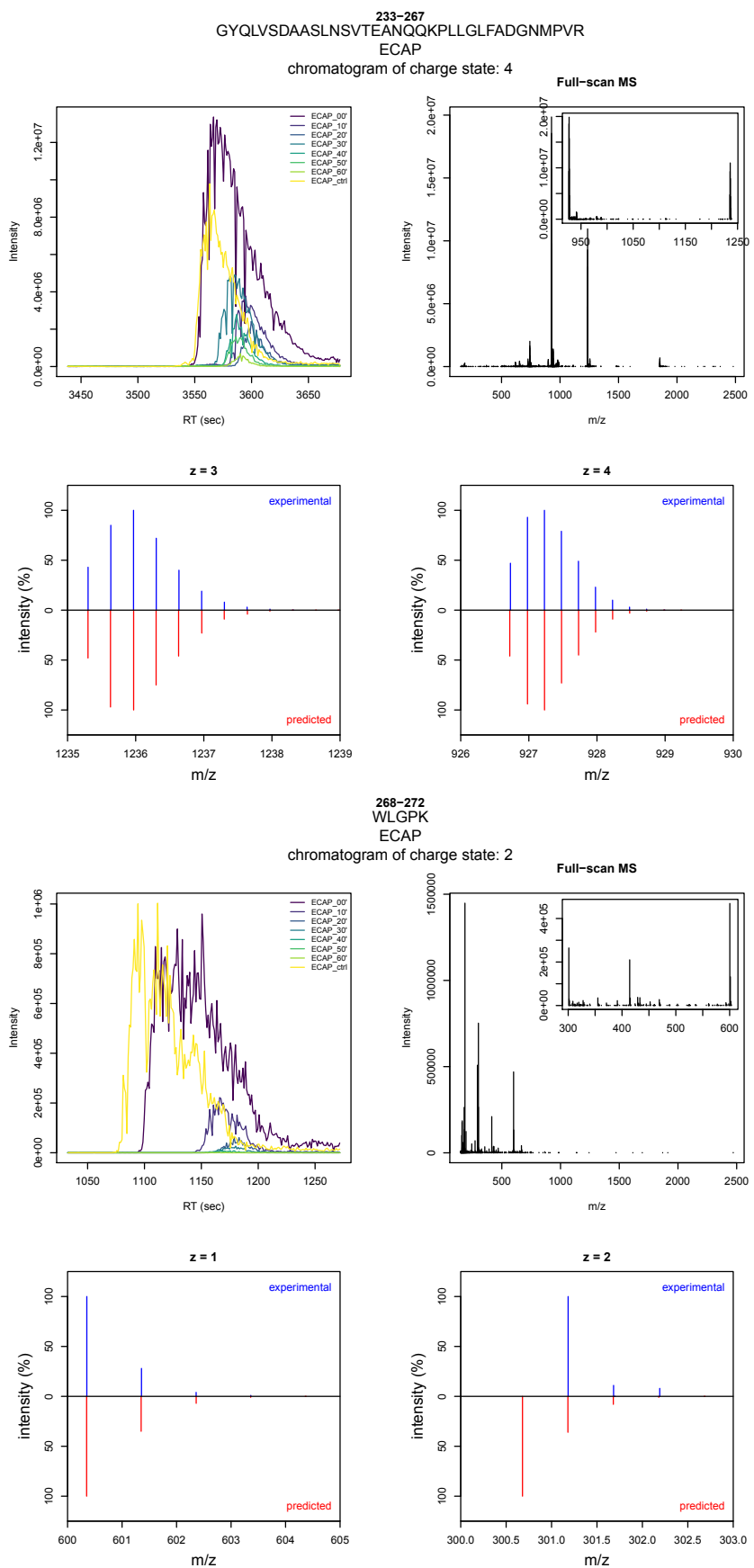


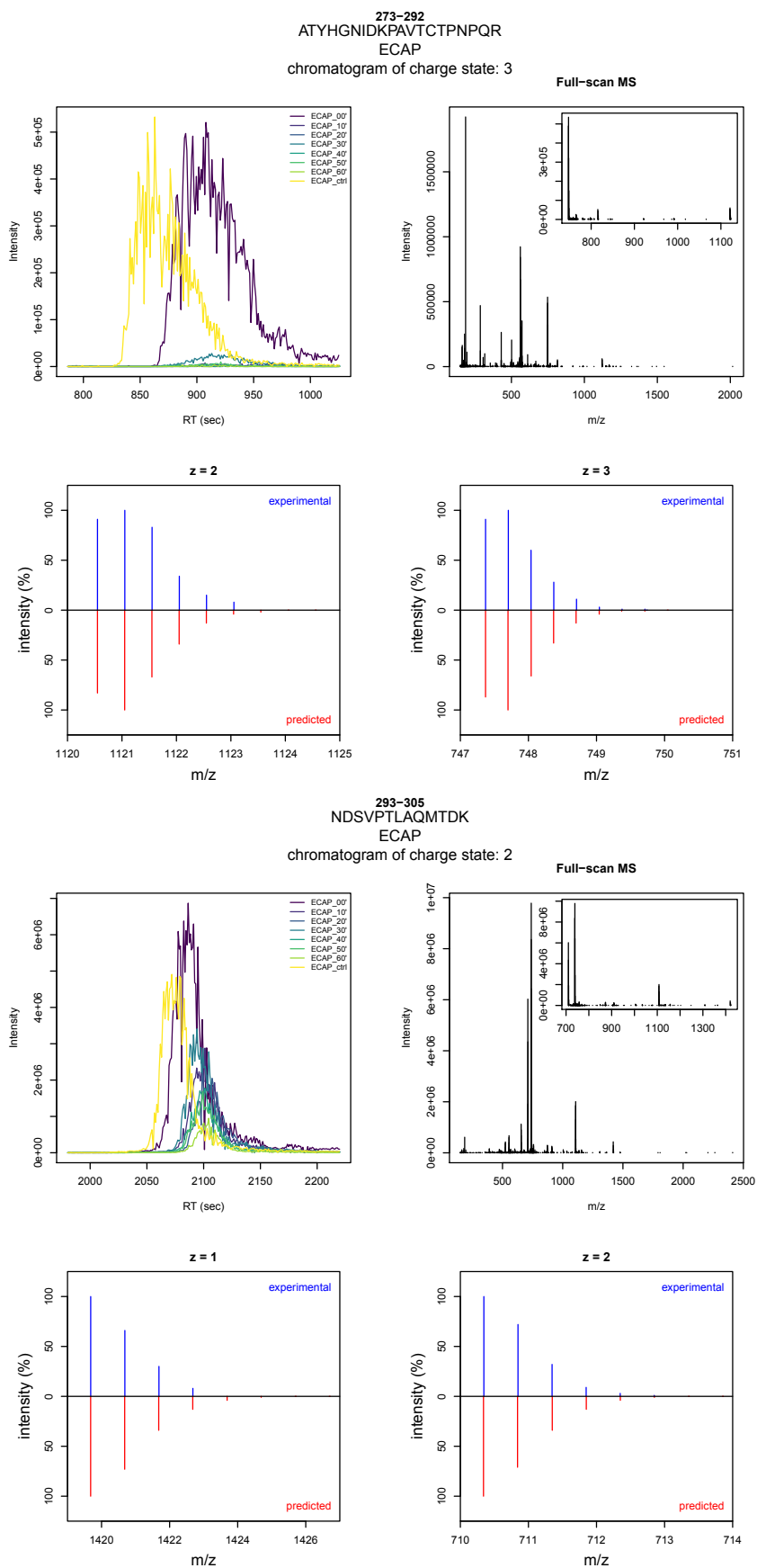


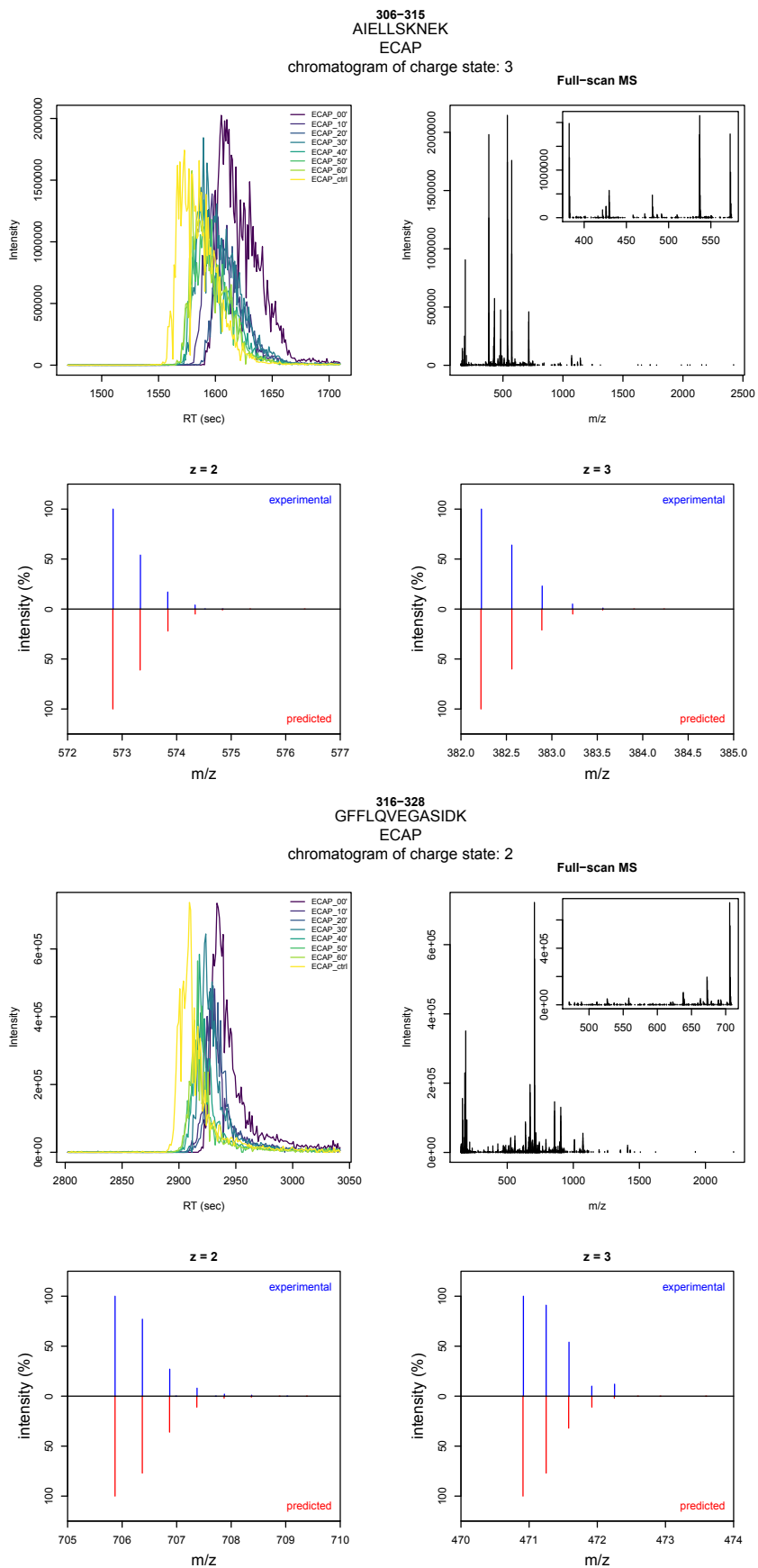


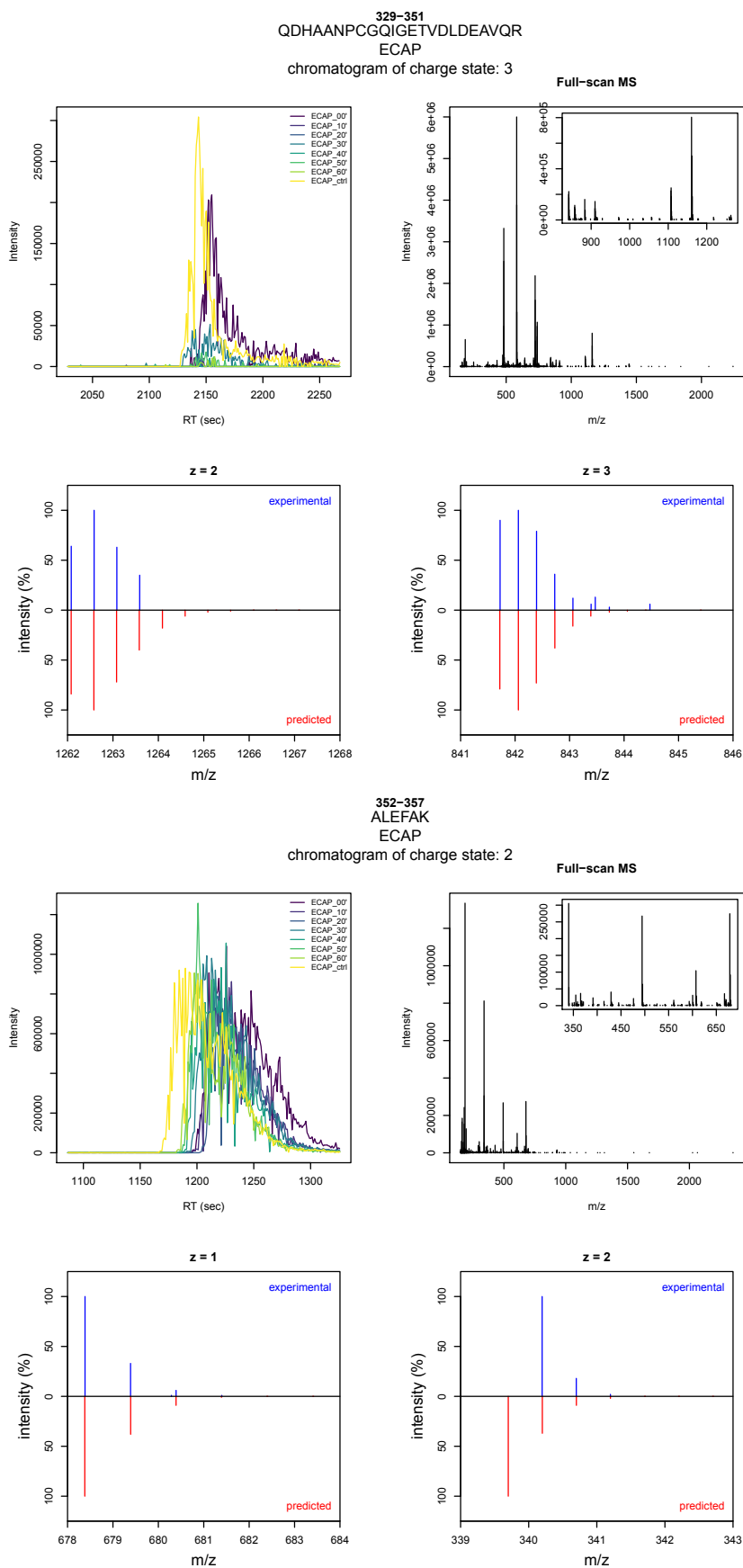


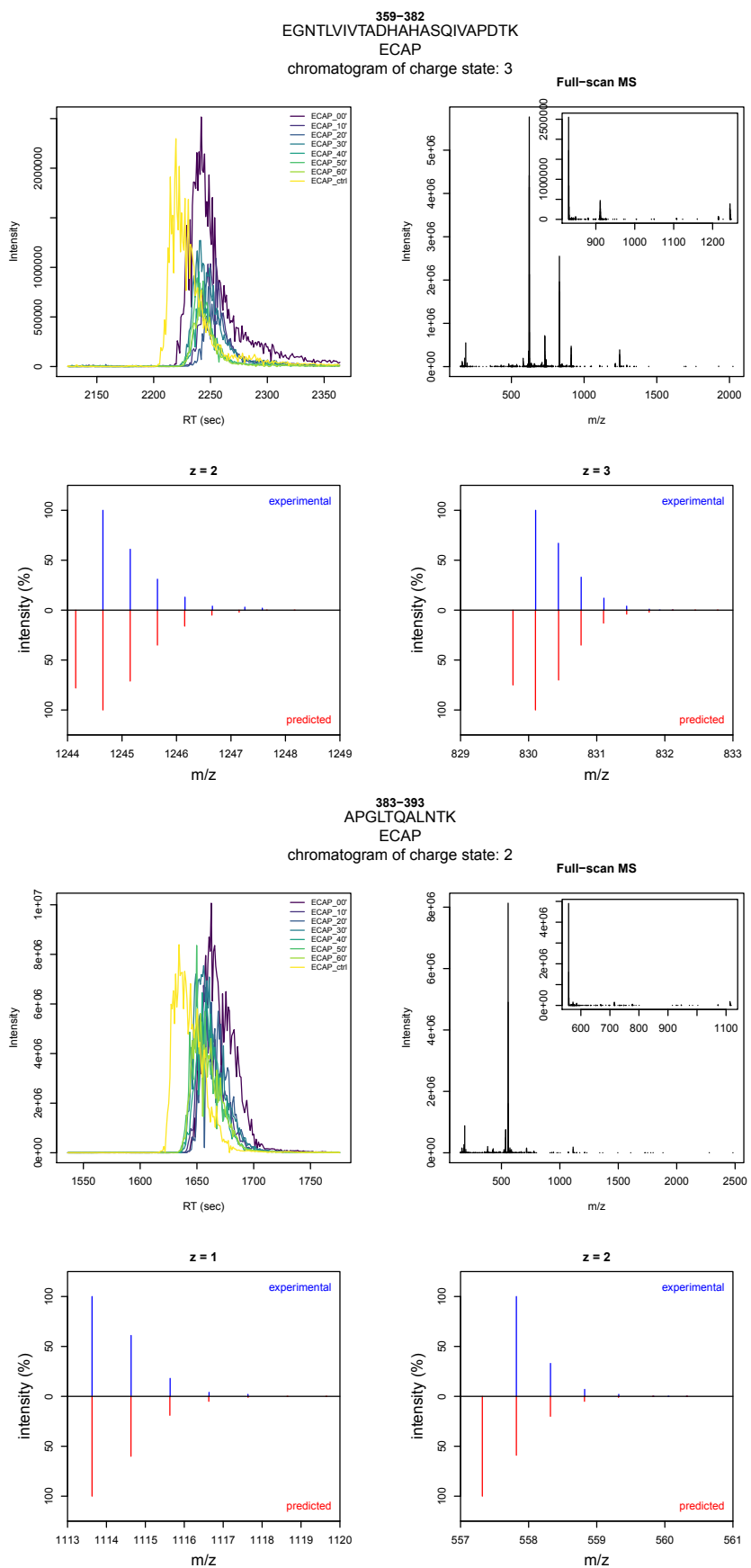


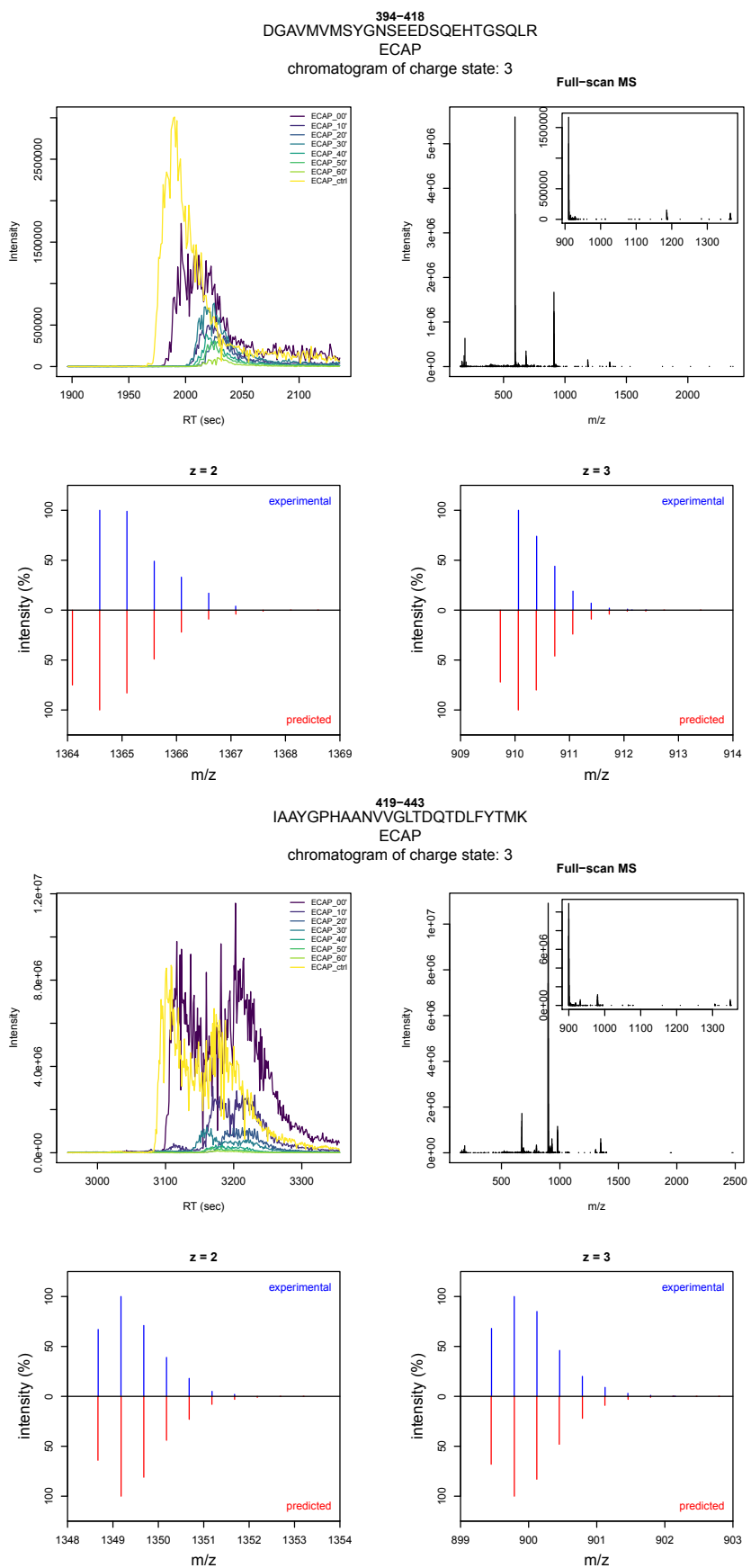


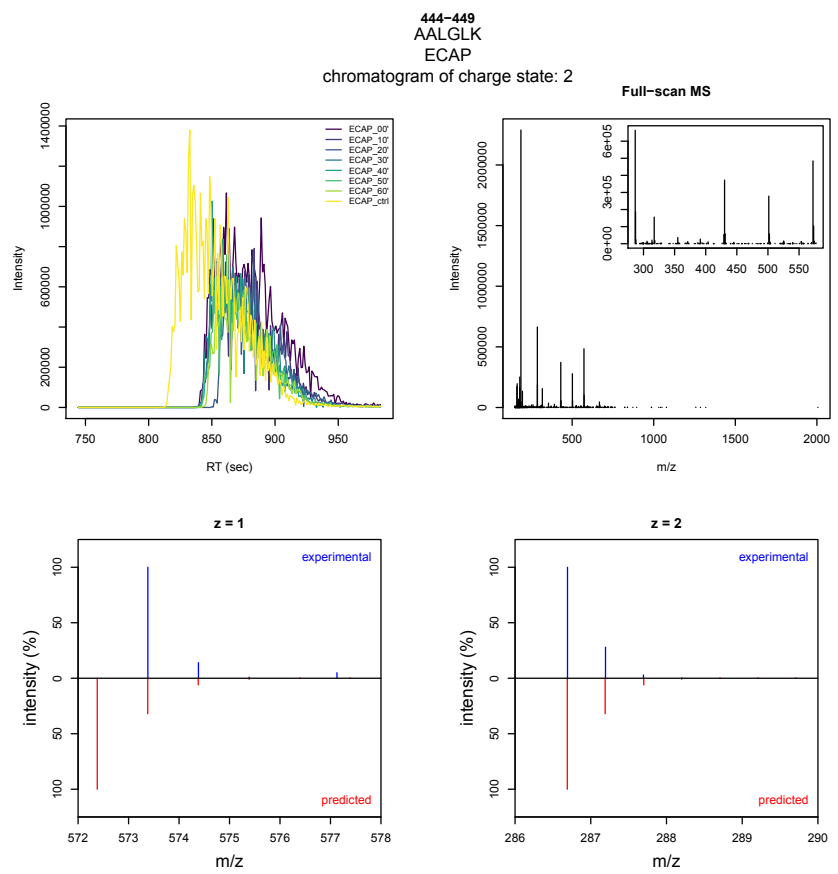


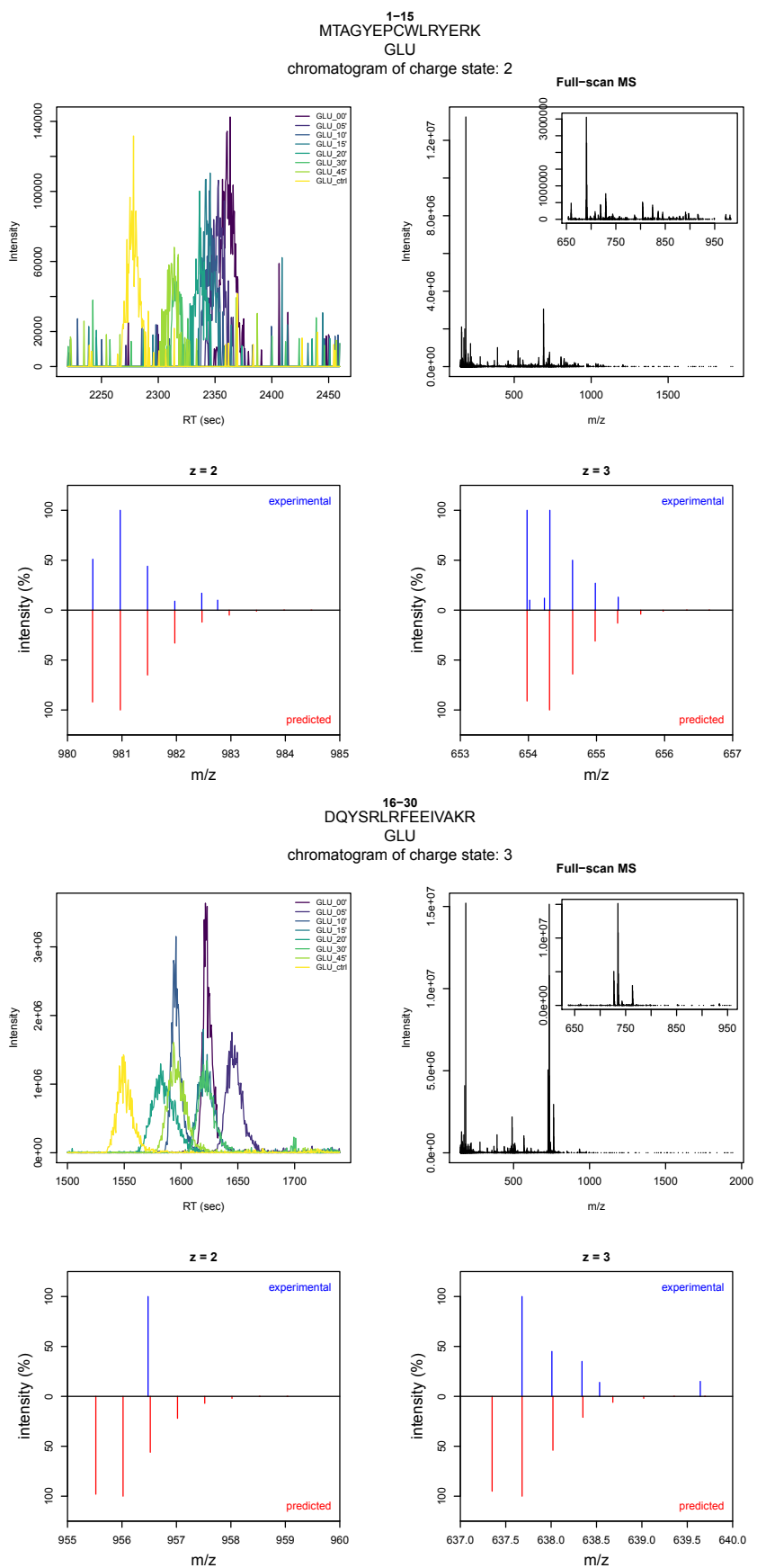


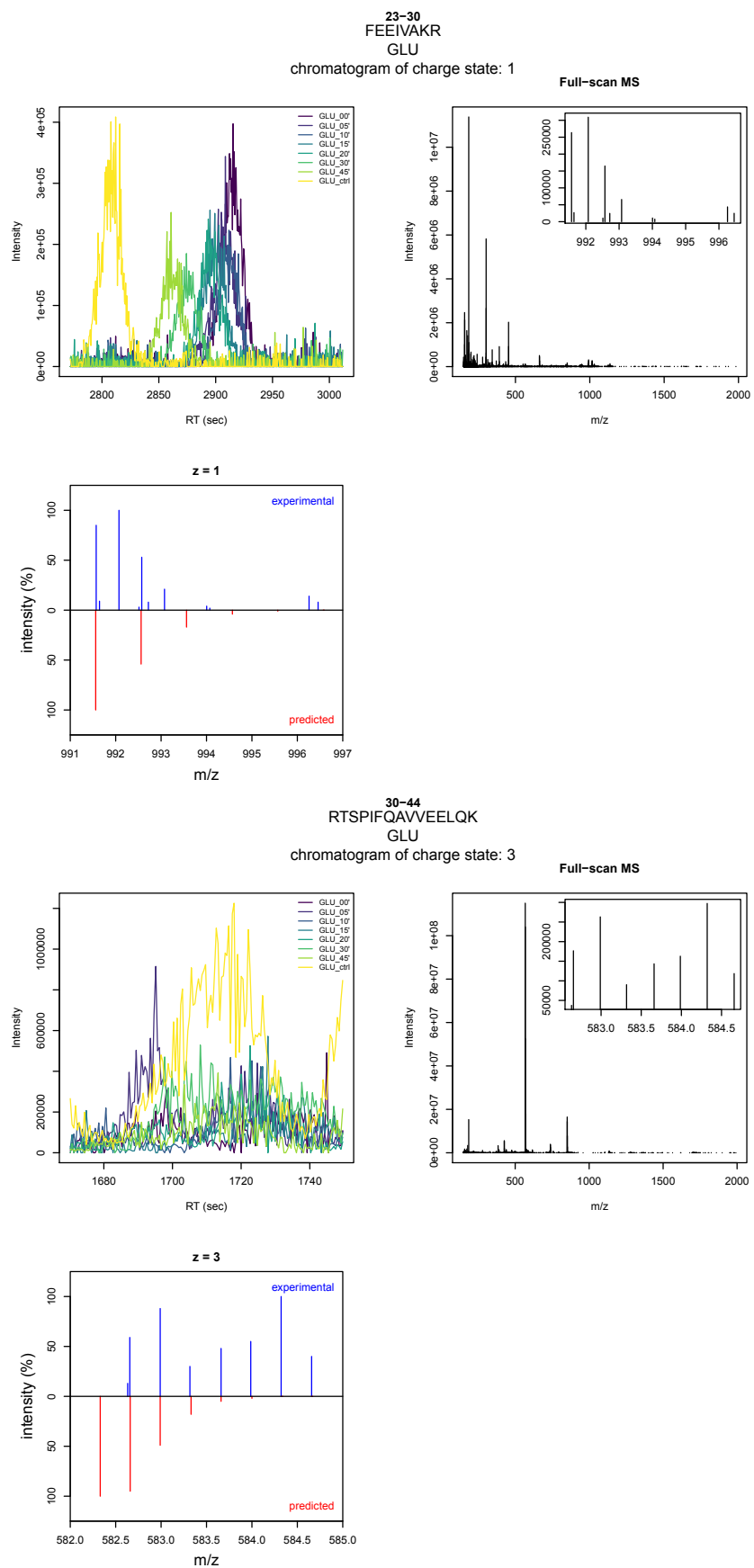


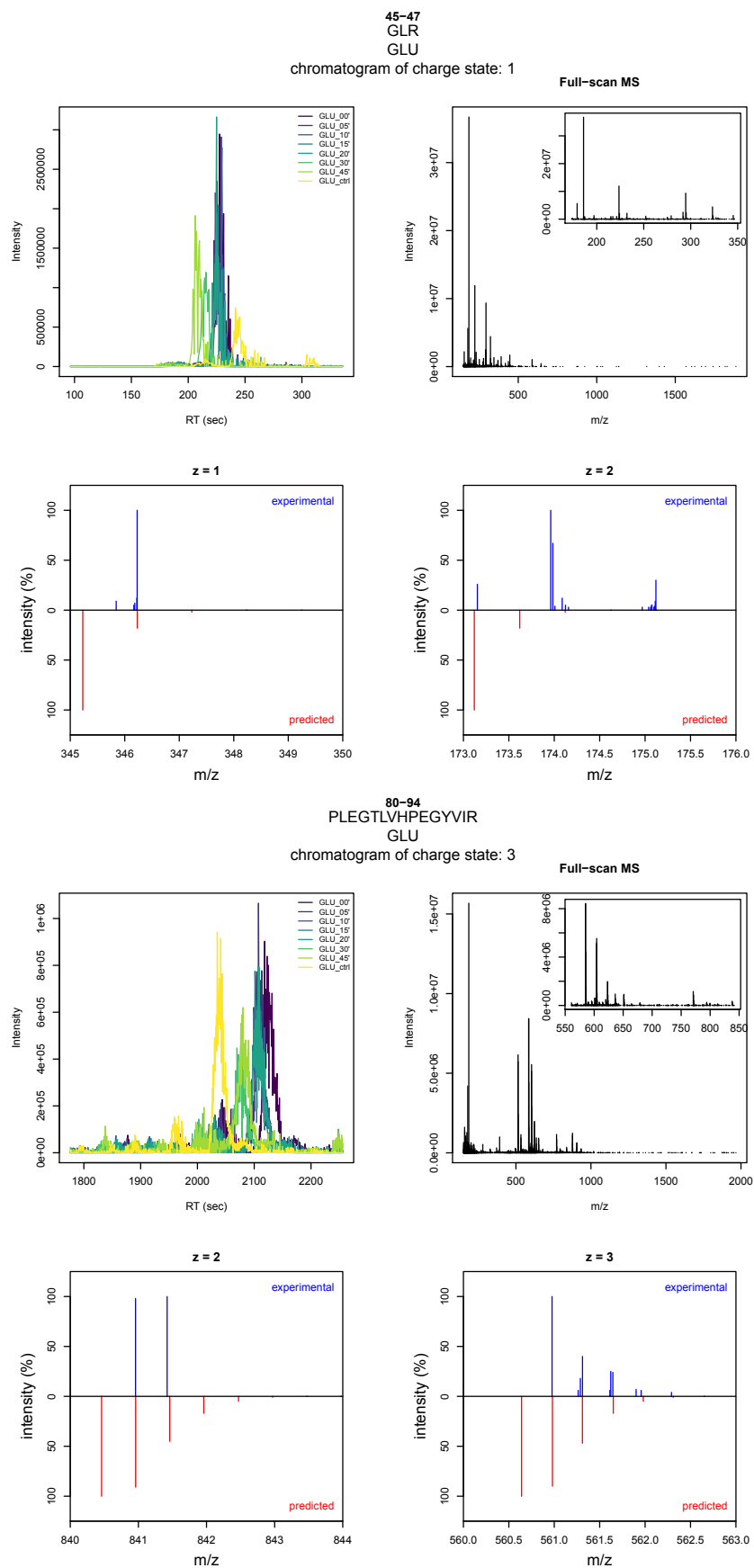


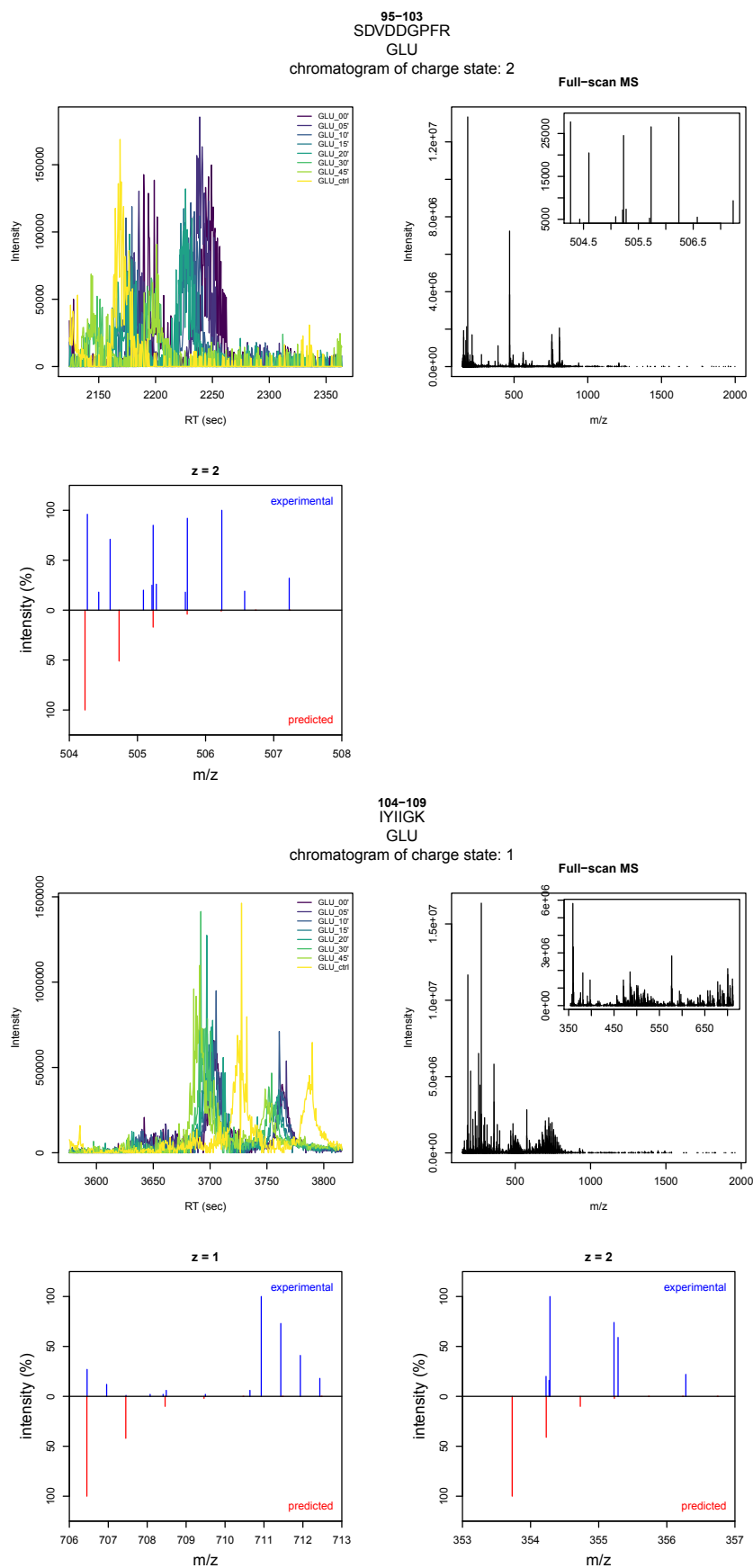


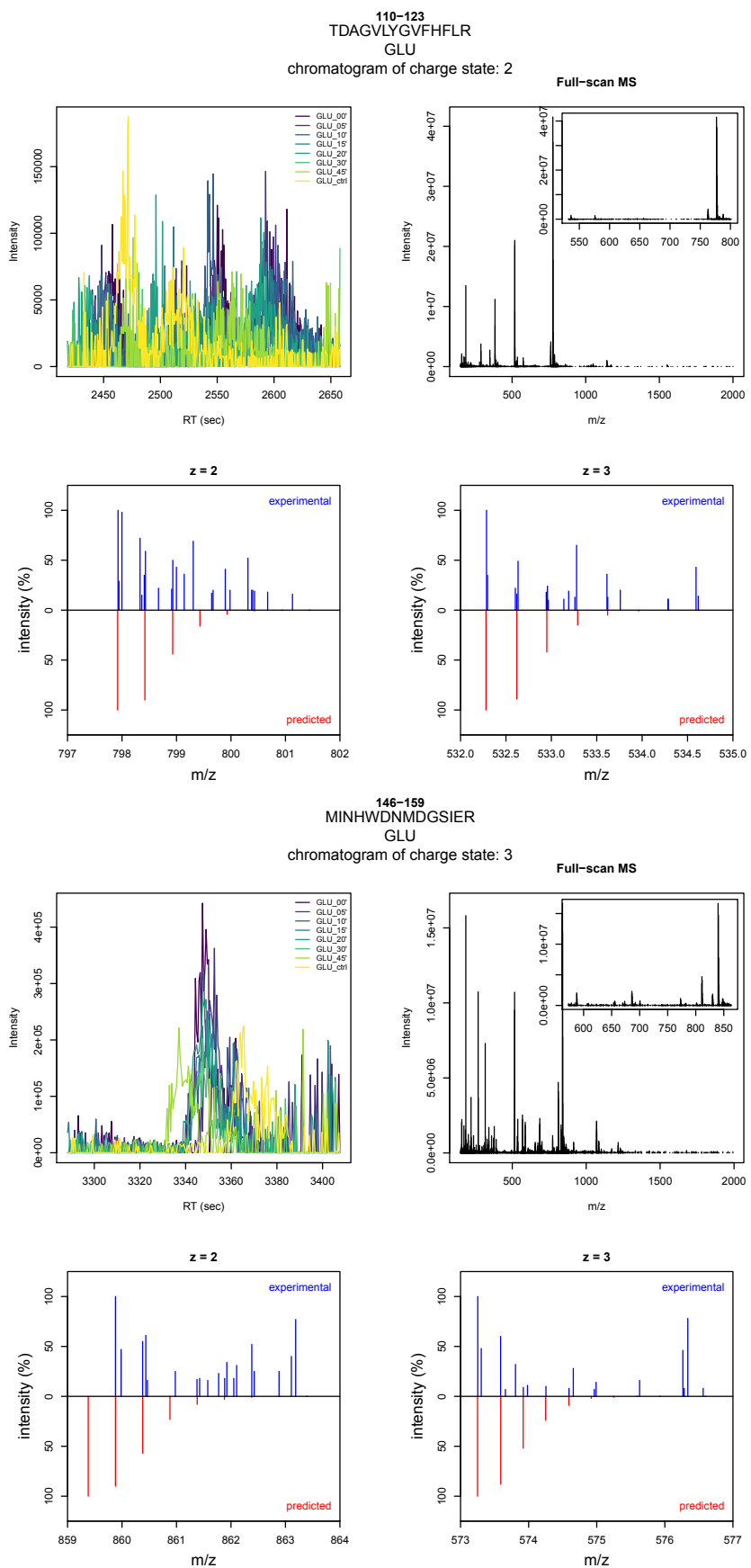


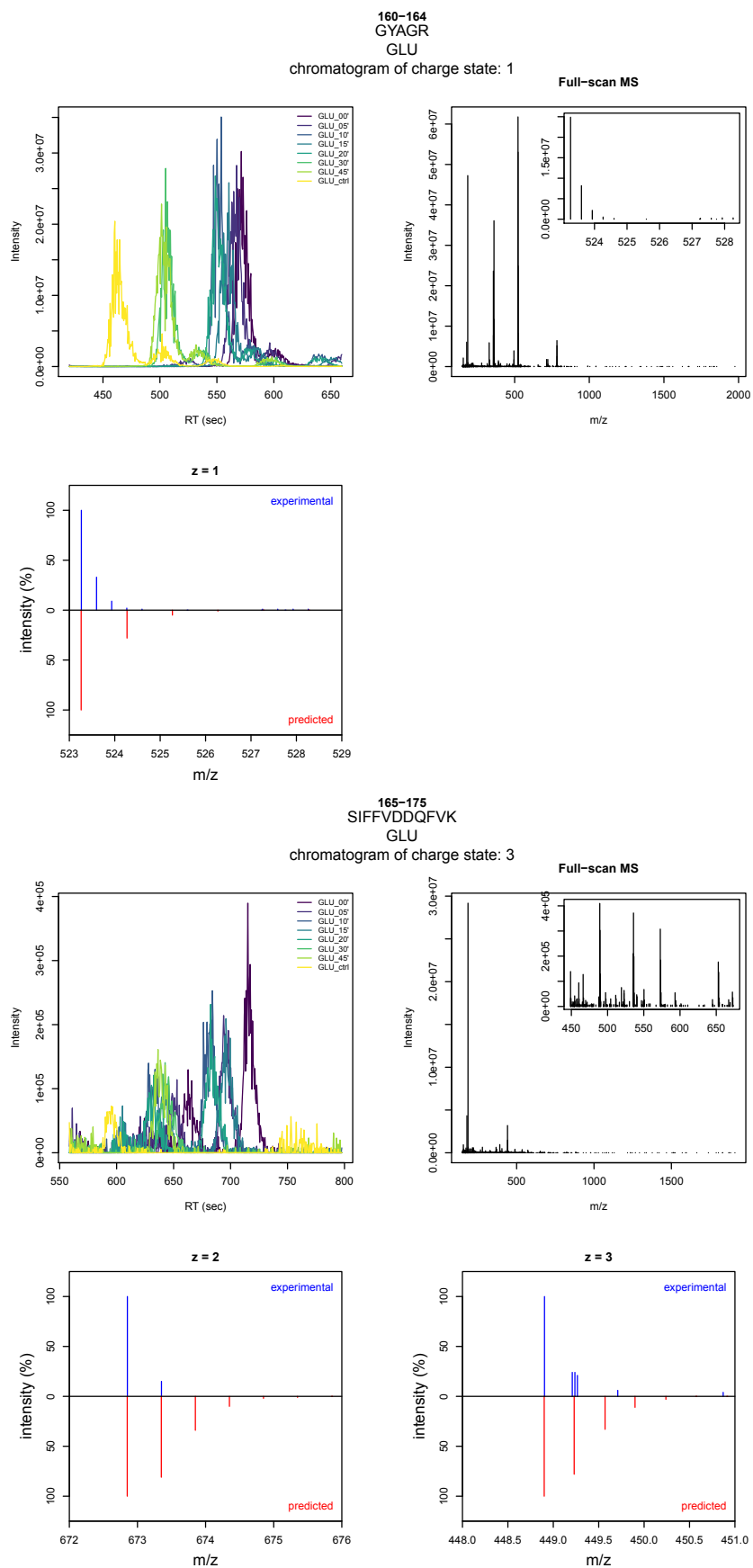


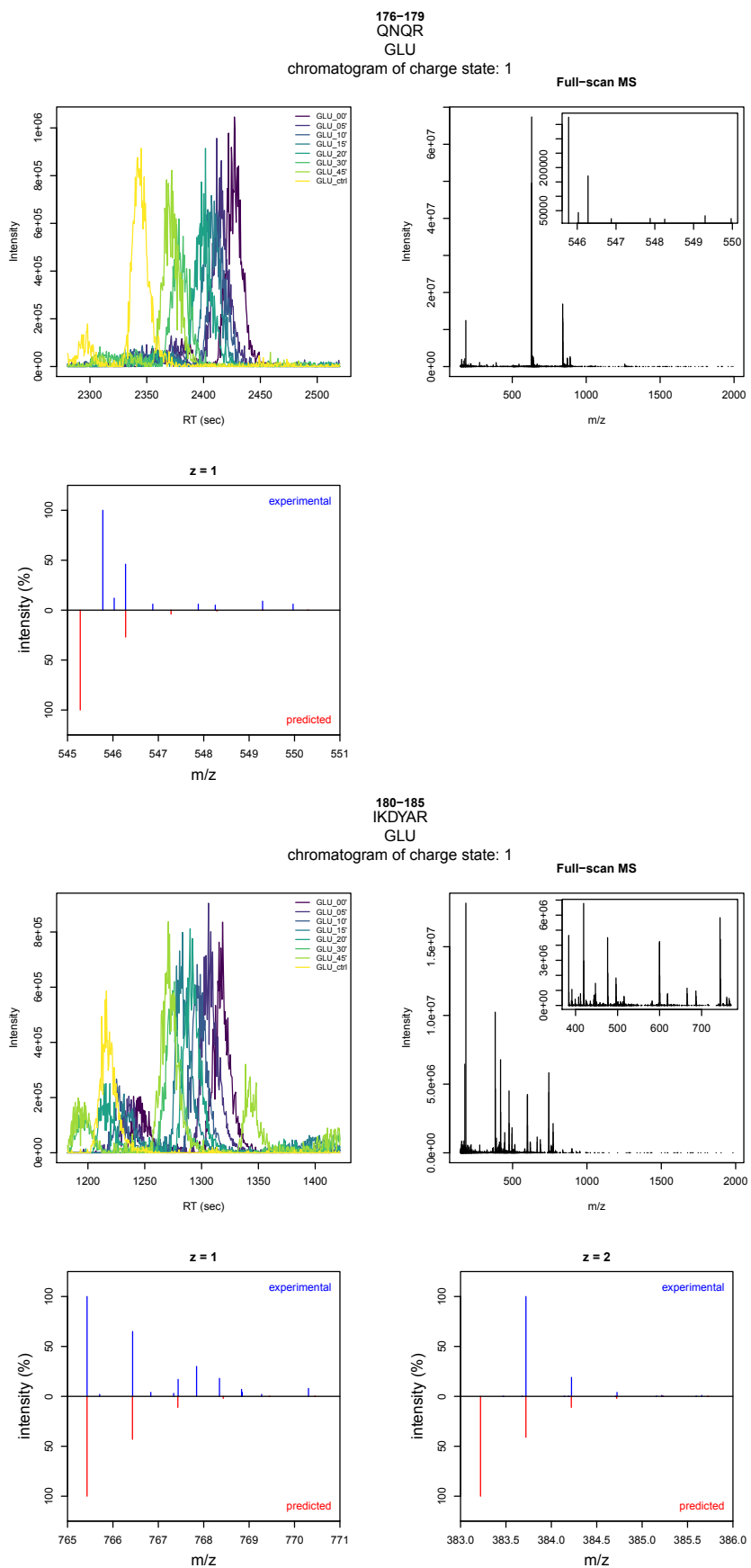


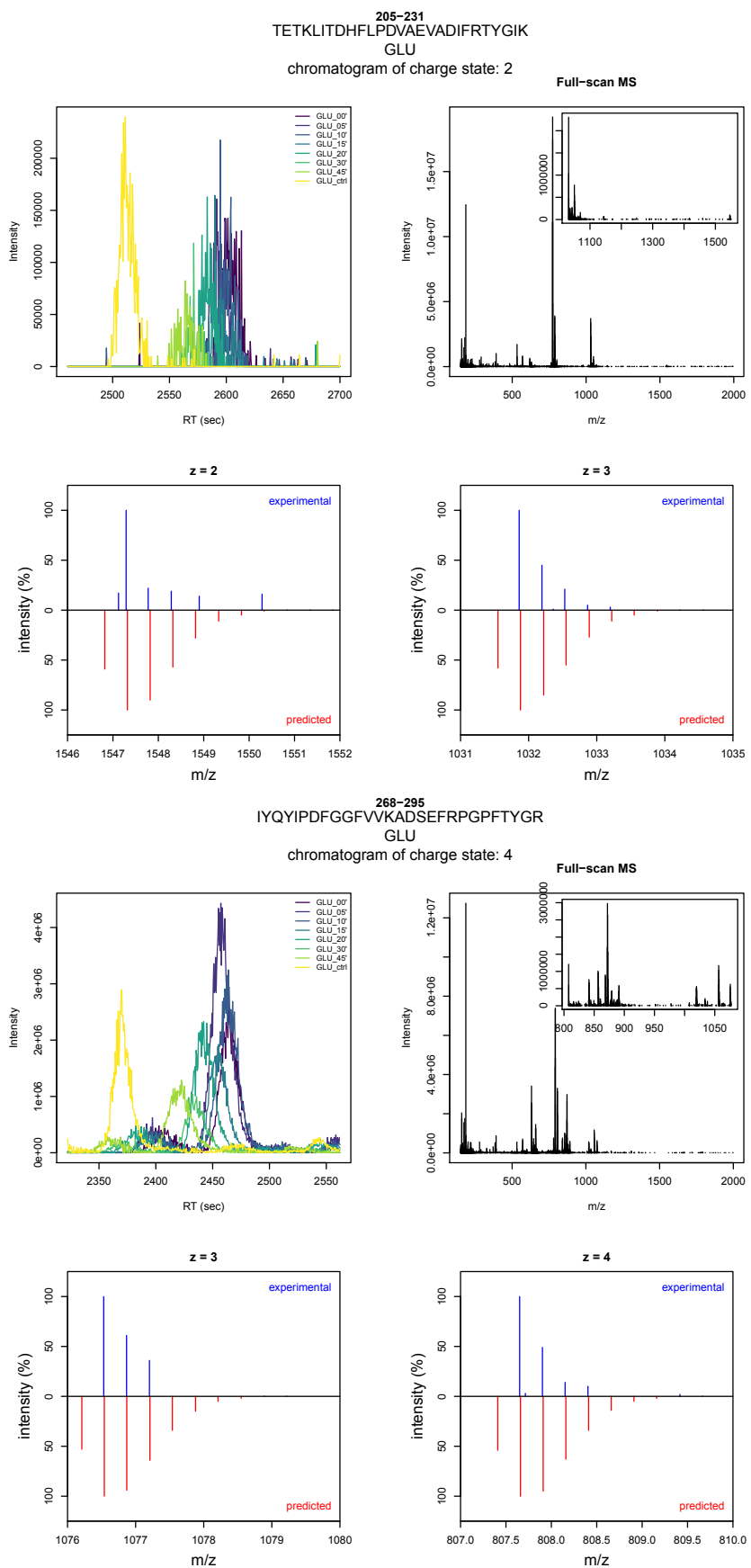


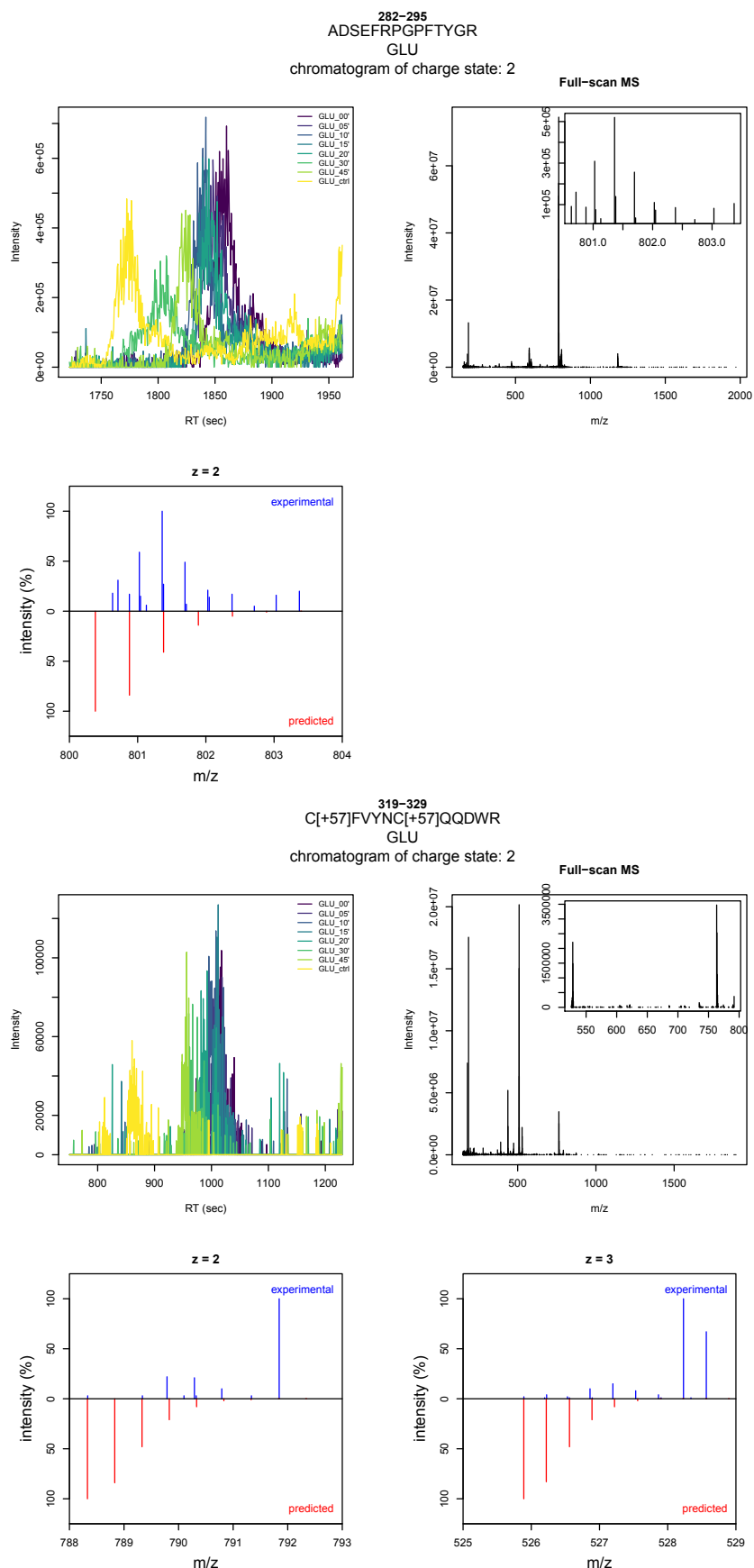


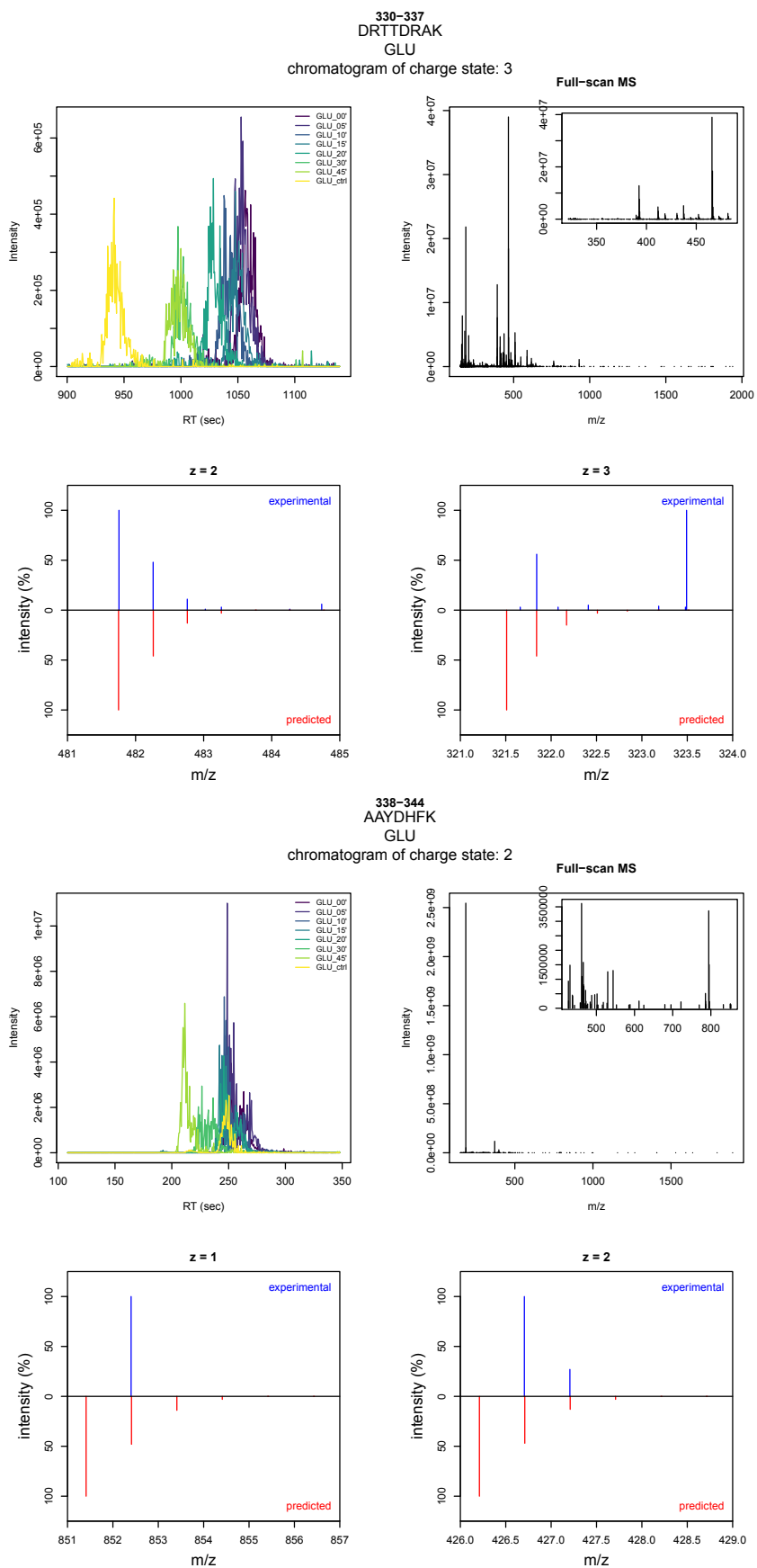


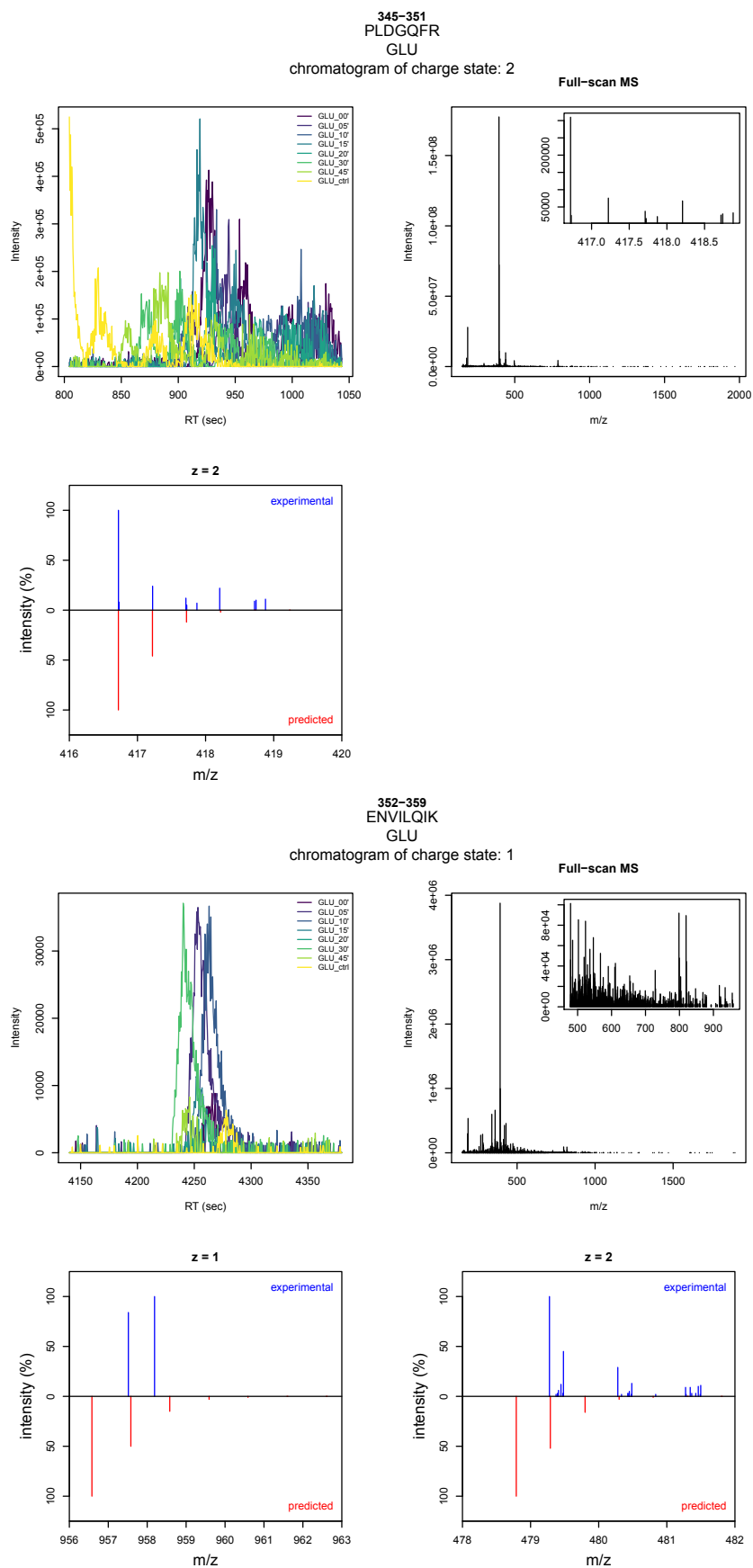


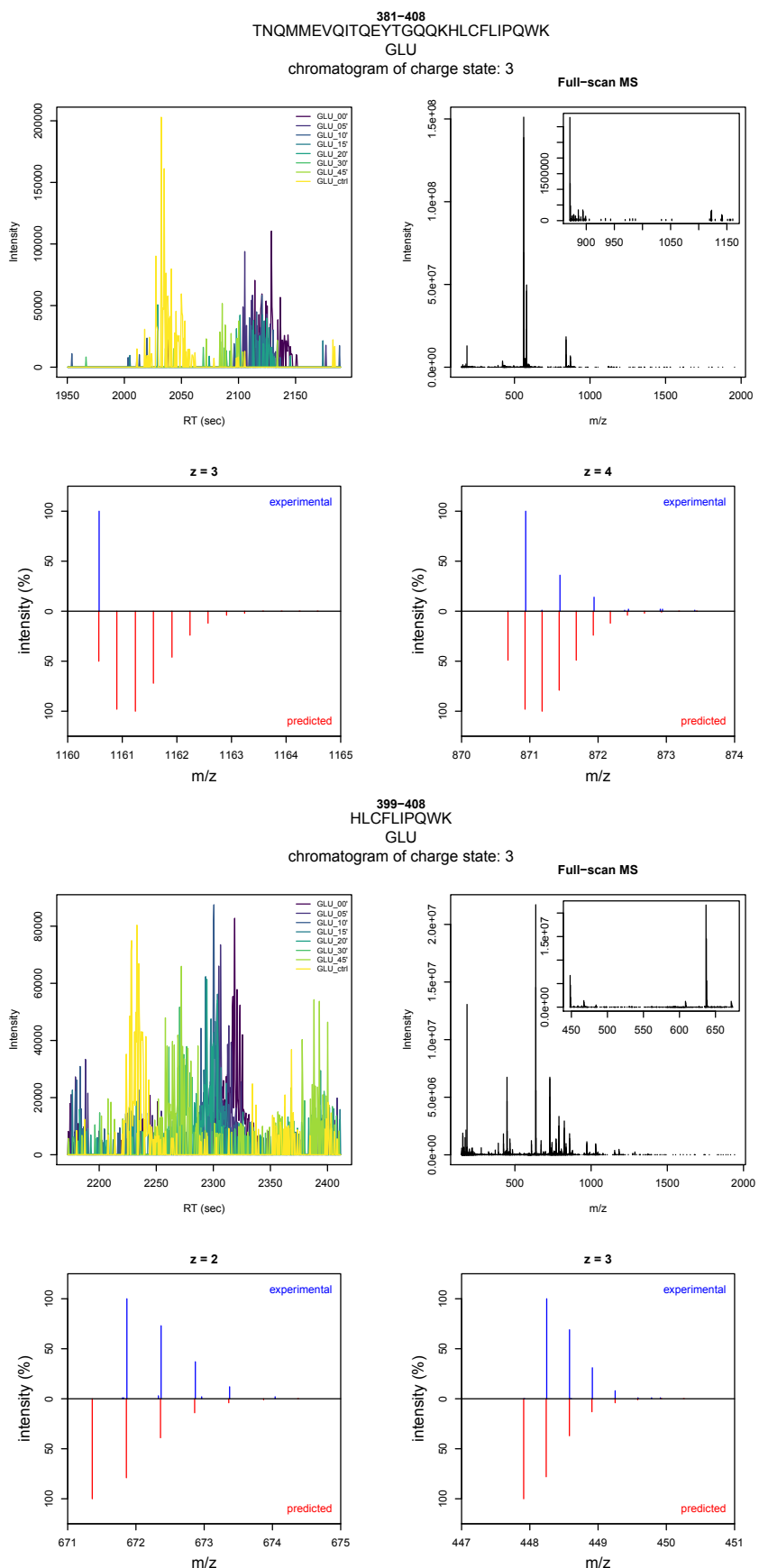


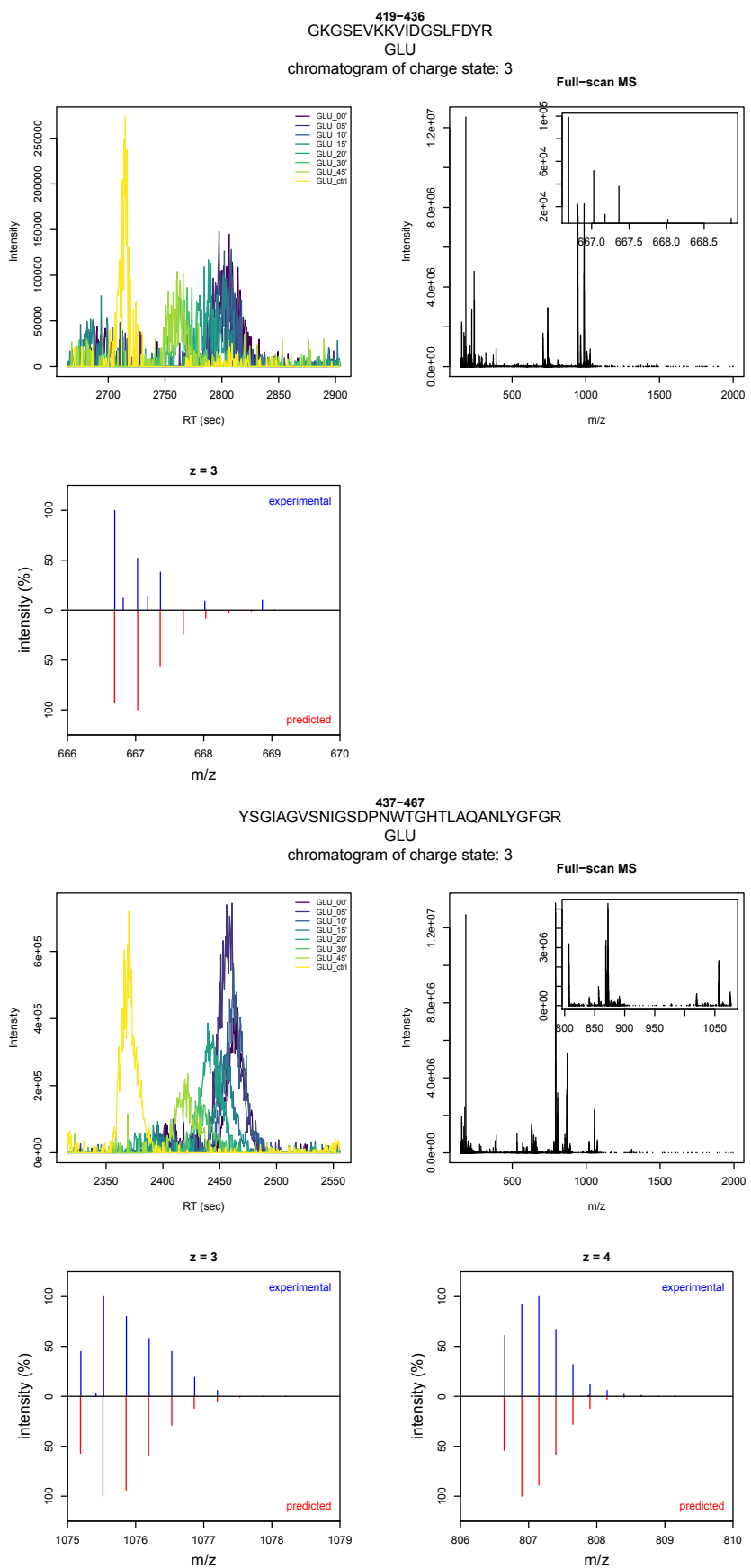


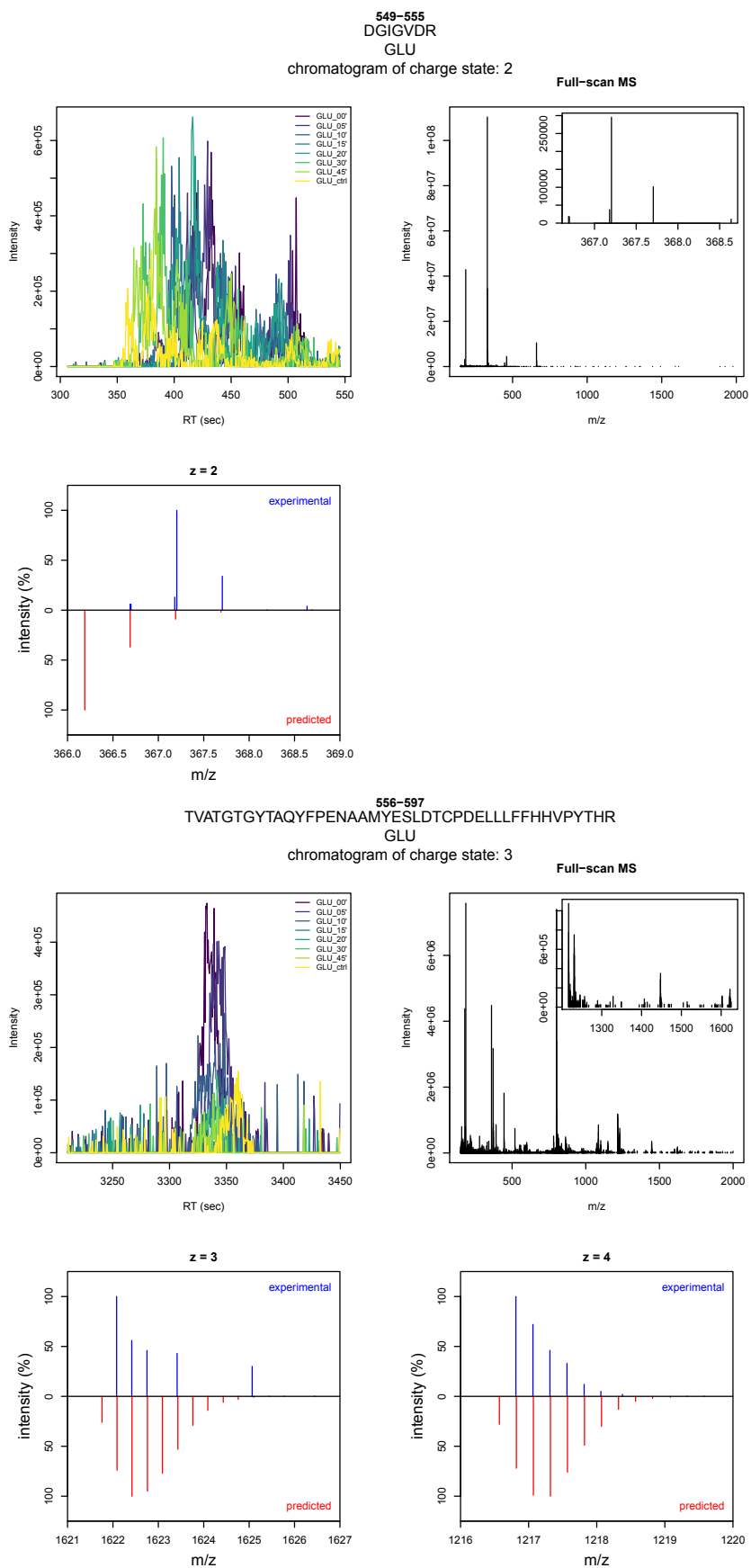


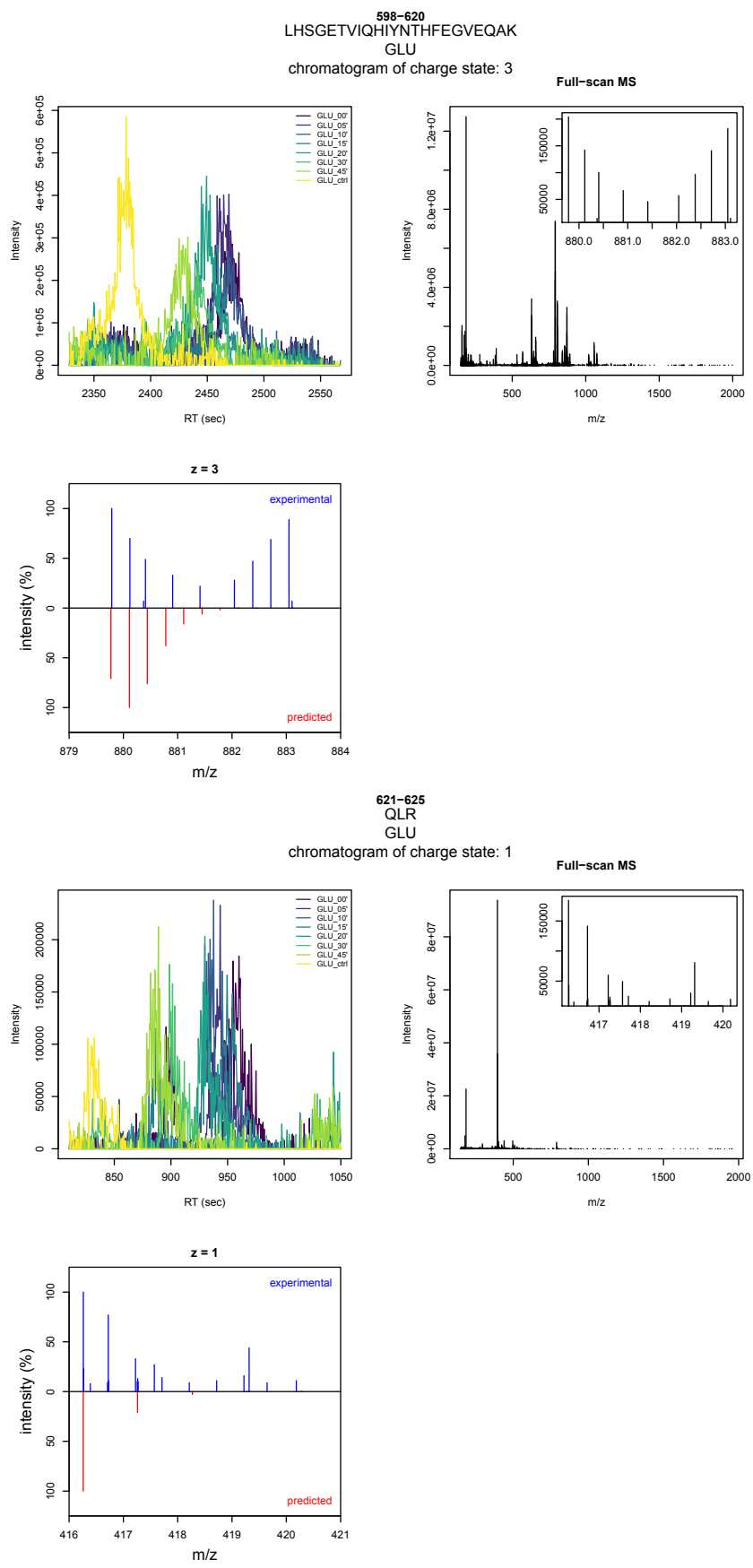


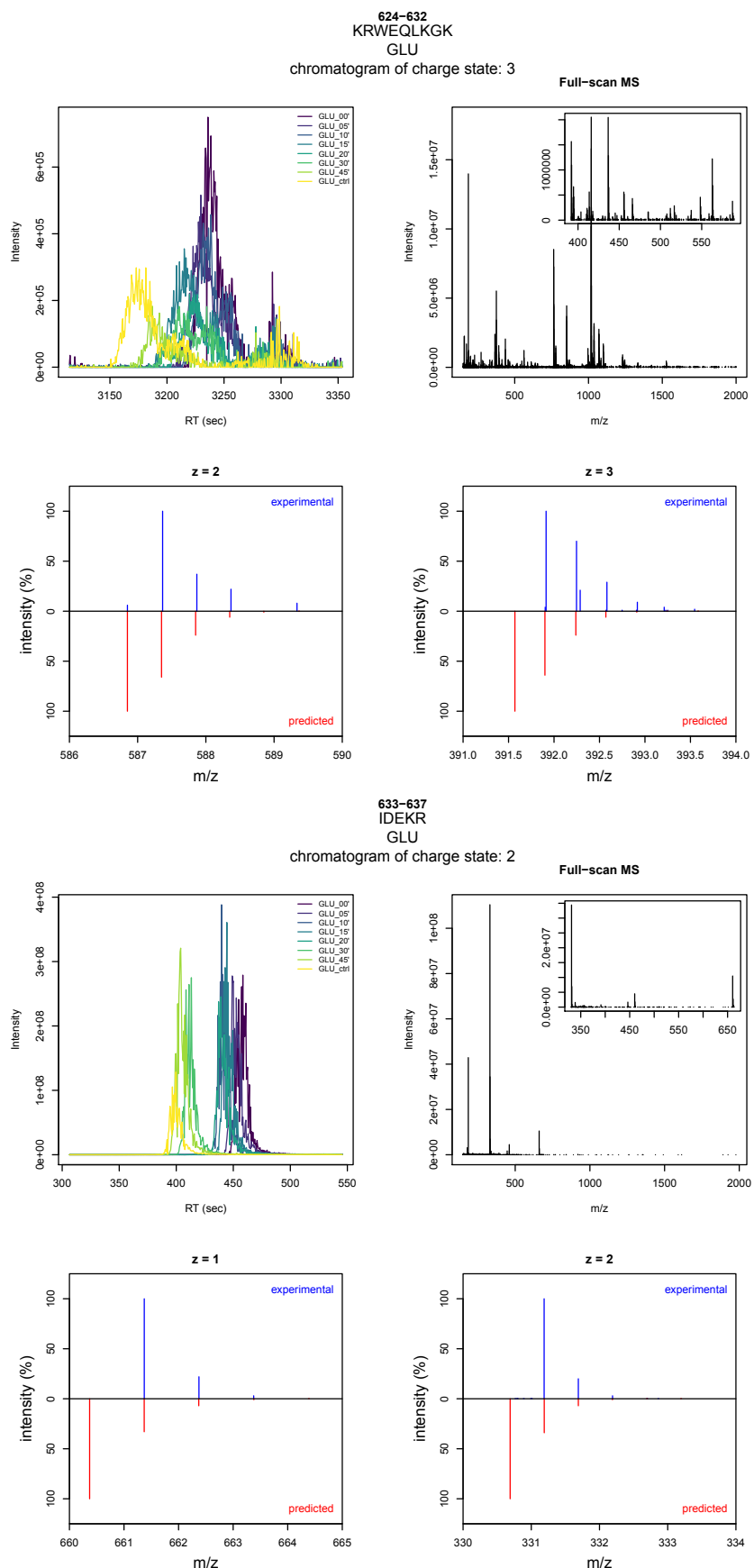


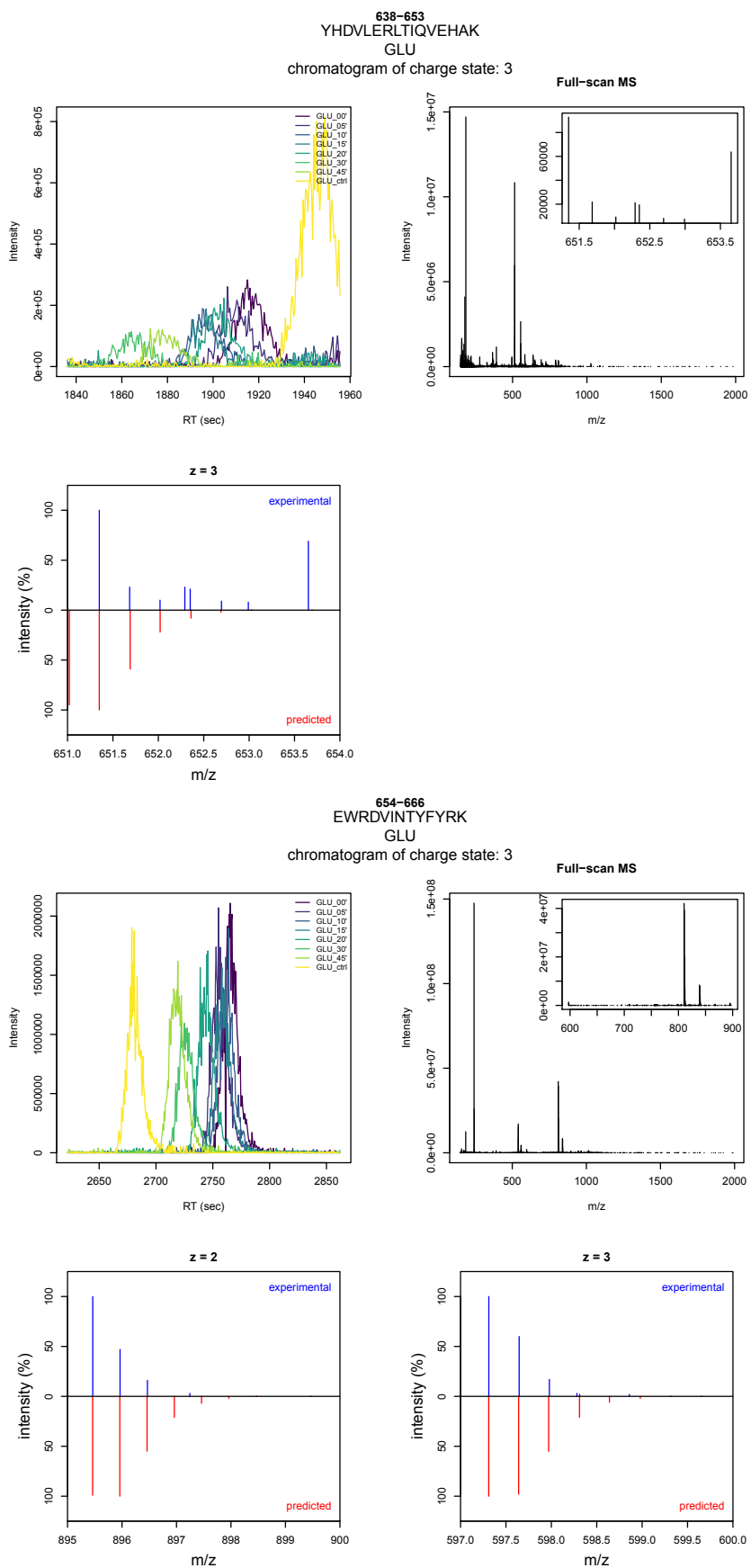


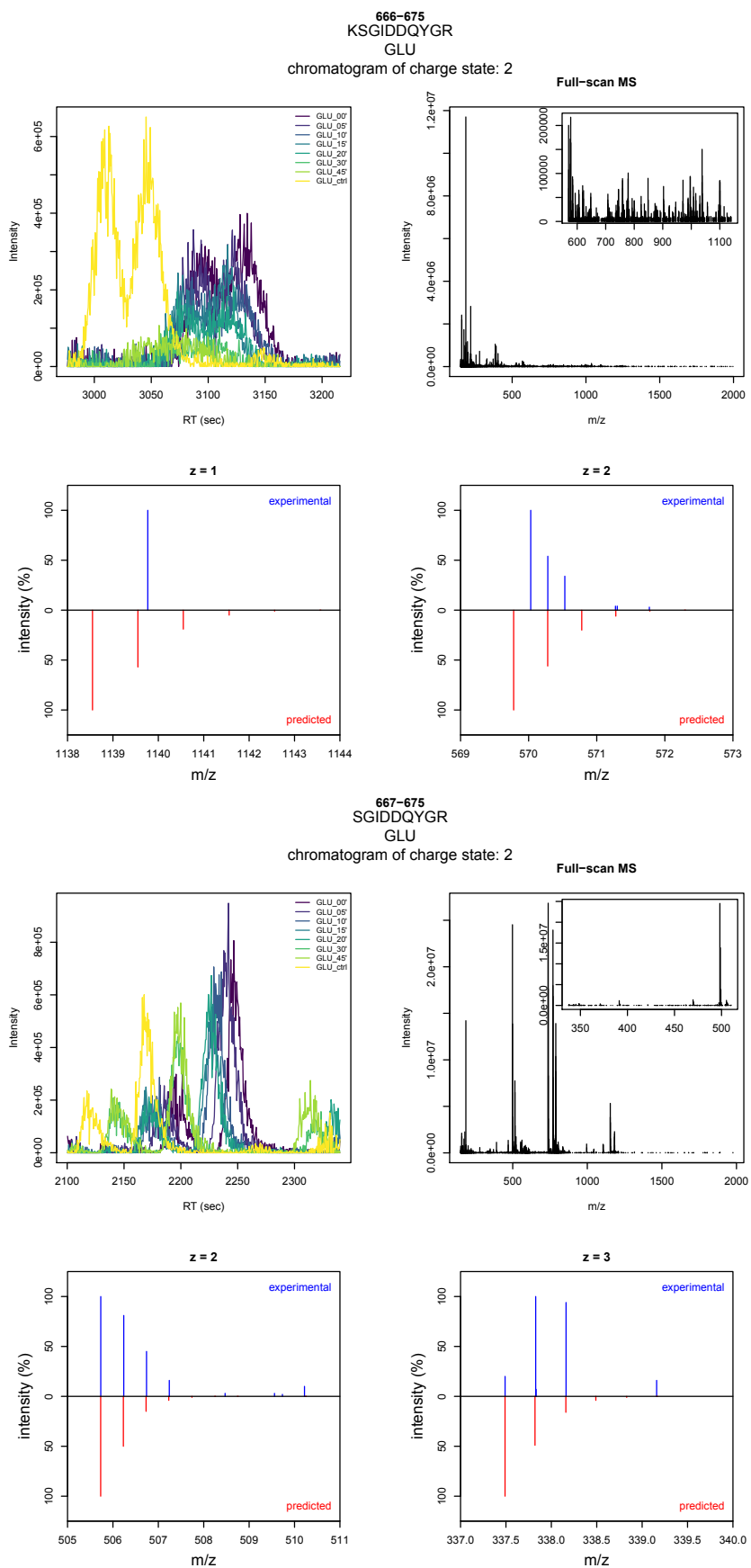


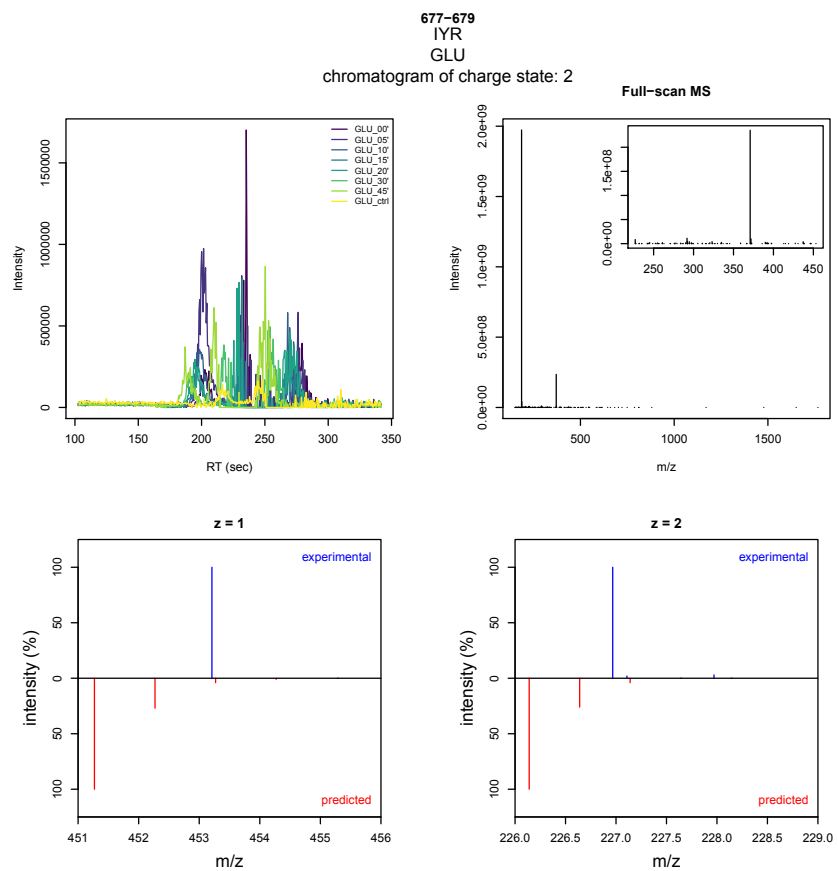












## References

- [1] Baugher, J. F., and Grossweiner, L. I. (1977) Photolysis mechanism of aqueous tryptophan. *J. Phys. Chem.* 81, 1349–1354.
- [2] Bent, D. V., and Hayon, E. (1975) Excited state chemistry of aromatic amino acids and related peptides. III. Tryptophan. *J. Am. Chem. Soc.* 97, 2612–2619.
- [3] Stevenson, K. L., Papadantonakis, G. A., and LeBreton, P. R. (2000) Nanosecond UV laser photoionization of aqueous tryptophan: temperature dependence of quantum yield, mechanism, and kinetics of hydrated electron decay. *J. Photochem. Photobiol. A: Chem.* 133, 159–167.
- [4] Tsentalovich, Y. P., Snytnikova, O. A., and Sagdeev, R. Z. (2004) Properties of excited states of aqueous tryptophan. *J. Photochem. Photobiol. A: Chem.* 162, 371–379.
- [5] Pattison, D. I., Rahmanto, A. S., and Davies, M. J. (2012) Photo-oxidation of proteins. *Photochem. Photobiol. Sci.* 11, 38–53.
- [6] Janssen, E. M. L., Erickson, P. R., and McNeill, K. (2014) Dual roles of dissolved organic matter as sensitizer and quencher in the photooxidation of tryptophan. *Environ. Sci. Technol.* 48, 4916–4924.
- [7] Chen, X., Zhang, L., Zhang, L., Wang, J., Liu, H., and Bu, Y. (2009) Proton-regulated electron transfers from tyrosine to tryptophan in proteins: Through-bond mechanism versus long-range hopping mechanism. *J. Phys. Chem. B* 113, 16681–16688.
- [8] Land, E. J., and Truscott, T. G. (1979) Triplet excited state of coumarin and 4'5' dihydroxydiphenyl: Reaction with nucleic acid bases and amino acids. *Photochem. Photobiol.* 29, 861–866.
- [9] Lu, C.-Y., and Liu, Y.-Y. (2002) Electron transfer oxidation of tryptophan and tyrosine by triplet states and oxidized radicals of flavin sensitizers: a laser flash photolysis study. *Biochim. Biophys. Acta Gen. Subj.* 1571, 71–76.
- [10] Boreen, A. L., Edhlund, B. L., Cotner, J. B., and McNeill, K. (2008) Indirect photodegradation of dissolved free amino acids: The contribution of singlet oxygen and the differential reactivity of DOM from various sources. *Environ. Sci. Technol.* 42, 5492–5498.
- [11] Chin, K. K., Trevithick-Sutton, C. C., McCallum, J., Jockusch, S., Turro, N. J., Scaino, J. C., Foote, C. S., and Garcia-Garibay, M. A. (2008) Quantitative determination of singlet oxygen generated by excited state aromatic amino acids, proteins, and immunoglobulins. *J. Am. Chem. Soc.* 130, 6912–6913.
- [12] Davies, M. J. (2003) Singlet oxygen-mediated damage to proteins and its consequences. *Biochem. Biophys. Res. Commun.* 305, 761–770.

- [13] Davies, M. J., and Truscott, R. J. W. (2001) Photo-oxidation of proteins and its role in cataractogenesis. *J. Photochem. Photobiol. B: Biol.* **63**, 114–125.
- [14] Lundein, R. A., Janssen, E. M. L., Chu, C., and Mcneill, K. (2014) Environmental photochemistry of amino acids, peptides and proteins. *Chimia* **68**, 812–817.
- [15] Hug, G. L., Bobrowski, K., Kozubek, H., and Marciniak, B. (1998) Photooxidation of methionine derivatives by the 4-carboxybenzophenone triplet state in aqueous solution. Intracomplex proton transfer involving the amino group. *Photochem. Photobiol.* **68**, 785–796.
- [16] Castaño, C., Dántola, M. L., Oliveros, E., Thomas, A. H., and Lorente, C. (2013) Oxidation of tyrosine photoinduced by pterin in aqueous solution. *Photochem. Photobiol.* **89**, 1448–1455.
- [17] Dose, K. (1968) The photolysis of free cystine in the presence of aromatic amino acids. *Photochem. Photobiol.* **8**, 331–335.
- [18] Creed, D. (1984) The photophysics and photochemistry of the near-UV absorbing amino acids. – III. Cystine and its simple derivatives. *Photochem. Photobiol.* **39**, 577–583.
- [19] Davies, M. J., Forni, L. G., and Shuter, S. L. (1987) Electron spin resonance and pulse radiolysis studies on the spin trapping of sulphur-centered radicals. *Chem. Biol. Interact.* **61**, 177–188.
- [20] Hawkins, C. L., and Davies, M. J. (2001) Generation and propagation of radical reactions on proteins. *Biochem. Biophys. Acta Bioenerg.* **1504**, 196–219.
- [21] Abaskharon, R. M., and Gai, F. (2016) Direct measurement of the tryptophan-mediated photocleavage kinetics of a protein disulfide bond. *Phys. Chem. Chem. Phys.* **18**, 9602–9607.
- [22] Miller, B. L., Hageman, M. J., Thamann, T. J., Barròn, L. B., and Schöneich, C. (2003) Solid-state photodegradation of bovine somatotropin (bovine growth hormone): Evidence for tryptophan-mediated photooxidation of disulfide bonds. *J. Pharm. Sci.* **92**, 1698–1709.
- [23] Vanhooren, A., Devreese, B., Vanhee, K., Van Beeumen, J., and Hanssens, I. (2002) Photoexcitation of tryptophan groups induces reduction of two disulfide bonds in goat  $\alpha$ -lactalbumin. *Biochemistry* **41**, 11035–11043.
- [24] Permyakov, E. A., Permyakov, S. E., Deikus, G. Y., Morozova-Roche, L. A., Grishchenko, V. M., Kalinichenko, L. P., and Uversky, V. N. (2003) Ultraviolet illumination-induced reduction of  $\alpha$ -lactalbumin disulfide bridges. *Proteins* **51**, 498–503.
- [25] Prompers, J. J., Hilbers, C. W., and Pepermans, H. A. M. (1999) Tryptophan mediated photoreduction of disulfide bond causes unusual fluorescence behaviour of *Fusarium solani* pisi cutinase. *FEBS Lett.* **456**, 409–416.

- [26] Vanhooren, A., De Vriendt, K., Devreese, B., Chedad, A., Sterling, A., Van Dael, H., Van Beeumen, J., and Hanssens, I. (2006) Selectivity of tryptophan residues in mediating photolysis of disulfide bridges in goat  $\alpha$ -lactalbumin. *Biochemistry* *45*, 2085–2093.
- [27] Dulin, D., and Mill, T. (1982) Development and evaluation of sunlight actinometers. *Environ. Sci. Technol.* *16*, 815–820.
- [28] Laszakovits, J. R., Berg, S. M., Anderson, B. G., O'Brien, J. E., Wammer, K. H., and Sharpless, C. M. (2017) p-Nitroanisole/pyridine and p-nitroacetophenone/pyridine actinometers revisited: Quantum yield in comparison to ferrioxalate. *Environ. Sci. Technol. Lett.* *4*, 11–14.
- [29] Appiani, E., Ossola, R., Latch, D., Erickson, P., and McNeill, K. (2017) Aqueous singlet oxygen reaction kinetics of furfuryl alcohol: Effect of temperature, pH, and salt content. *Environ. Sci.: Processes Impacts* *19*, 508–516.
- [30] Janssen, E. M. L., and McNeill, K. (2015) Environmental photoactivation of extracellular phosphatases and the effects of dissolved organic matter. *Environ. Sci. Technol.* *49*, 889–896.
- [31] Geeraerd, A. H., Valdramidis, V. P., and Van Impe, J. F. (2005) GIInaFiT, a freeware tool to assess non-log-linear microbial survivor curves. *Int. J. Food Microbiol.* *102*, 95–105.
- [32] Mattioli, M. C., Sassoubre, L. M., Russell, T. L., and Boehm, A. B. (2017) Decay of sewage-sourced microbial source tracking markers and fecal indicator bacteria in marine waters. *Water Res.* *108*, 106–114.
- [33] MacLean, B., Tomazela, D. M., Shulman, N., Chambers, M., Finney, G. L., Frewen, B., Kern, R., Tabb, D. L., Liebler, D. C., and MacCoss, M. J. (2010) Skyline: an open source document editor for creating and analyzing targeted proteomics experiments. *Bioinformatics* *26*, 966–968.